Engineering Probes and Circuits for Detecting Single Nucleotide Variations in DNA and RNA

Xi Chen

A dissertation submitted in partial fulfillment of the
requirements for the degree of

Doctor of Philosophy

University of Washington

2015

Reading Committee:

Georg Seelig, Chair

Eric Klavins

Barry Lutz

Xiaohu Gao

Program Authorized to Offer Degree:
Electrical Engineering

University of Washington

Abstract

Engineering Probes and Circuits for Detecting
Single Nucleotide Variations in DNA and RNA

Xi Chen

Chair of the Supervisory Committee:
Professor Georg Seelig
Electrical Engineering

Even single nucleotide changes in nucleic acid sequence can result in drastic phenotype differences with significant health impact, such as driver mutations for cancer or antibiotics resistance in pathogens. However, reliable detection and quantitation of single nucleotide variants (SNVs) is challenging when the SNV is at low allele-frequency, due to the physical and chemical similarity of the SNV molecules and their corresponding wildtypes. In the past 30 years, researchers typically empirically optimize assay conditions to temperatures and buffer conditions that are conducive to high specificity hybridization of nucleic acids, but such a process is time-consuming, sensitive to small changes in protocol, and ineffective in multiplexed settings where multiple target SNVs need to be simultaneously analyzed.

This thesis presents a rational design approach to SNV detection and quantitation to overcome the challenges of conventional analysis, by creating probes and circuits that are capable of robustly detecting SNVs at low allele frequencies. These probes and circuits are designed based on the sequence information of target SNVs, and do not require significant empirical optimization for function. Consequently, this approach is amenable to integrating with existing nucleic acid bioanalytic technologies, and I have started working with collaborators at Thermo Fisher (Applied Biosystems) to translate these and other technologies to commercial use.

Four distinct projects are presented herein. The first describes “toehold exchange”

probes for single-stranded DNA and RNA targets that rely on molecular competition by a "protector" oligonucleotide to ensure hybridization specificity; this work enables detection of SNVs across a wide range of temperatures and buffers. The second describes probes for detecting SNVs in double-stranded DNA targets; by utilizing the SNVs present in both the forward and reverse strands of DNA, we are able to significantly improve SNV detection. The third describes construction of reaction networks that use a system's potential energy to circumvent theoretical limitations to hybridization specificity at pre-equilibrium times. The final work describes the use of multiple circuits to implement a linear combination analysis of the concentrations of two distinct RNA species that differ by a single nucleotide.

The recurrent theme of this thesis is that a systematic, engineering-based approach to designing nucleic acid molecules can enable a set of robust behaviors and interactions that is valuable to the field of molecular biology. My work thus far have focused on the single nucleotide variant detection problem, but in principle

ACKNOWLEDGMENTS

Graduating with a bachelor's degree in physics and mathematics, I thought that everything could be explained and predicted based on basic rules and equations. If the equation shows that something should work, it will. So for my Ph.D., I thought I would build something experimentally functional with my analytical expertise, without having to go through the empirical testing and optimization. I thought I would first test the system in reaction buffer, and then move the system to cell culture, and later to mice and to humans, and boom, it just works.

You can imagine how much discouragement I had when I first met the real world of experimental science. Without the great patience, caring, and guidance from my excellent advisor, Georg Seelig, I would not be here presenting you those works. Georg has always been supportive, he helps and encourages me when I am frustrated, and inspires me with his brilliance. With the deepest appreciation, I thank my advisor Georg Seelig.

I thank my committee members, Eric Klavins, Barry Lutz, and Xiaohu Gao. They presented to me challenging questions during my qualification, general, and defense exams, and every time they made me nervous. Behind each question, they inspire me with more possibilities and led me to deeper understanding and broader views of science.

I also thank my lab mates: Yuanjue Chen, Alex Rosenberg, Richard Muscat , Ben Groves, Sergii Pochekailov, Nick Bogard, Gourab Chatterjee, Sumit Mukherjee, Alexander Baryshev, Sifang Chen, Arjun Khakhar, Sundipta Rao, Randolph Lopez, and Tim Strovas, as well as lab members in Klavins group. Lab would not be such a warm and fun place without you.

I thank the National SSF GRDS program for not only providing me nice stipends but also introducing me to a group of interesting and enthusiastic young scientists.

I also thank my husband David Zhang. His love encourages me in the journey of science

and technology.

Finally I would like to thank my family: my mother, father, and brother, for their consistent support and unconditional love. I want to give special thanks to my mom Ruichun. She was diagnosed with breast cancer just several days before my defense exam. Her braveness, optimism will always stay in my heart.

Contents

Chapter 1: Introduction

Thermodynamics and Kinetics

Nucleic acids

Nucleic acids are one of the most important classes of biological molecules, found in all known life. Deoxyribonucleic acid (DNA) is the main hereditary material in most living organisms and many viruses. With the genetic instructions encoded as a nucleotide sequence, DNA passes hereditary information from one generation to the next. In nature, DNA normally exists in a stable double-stranded helix form. Each nucleotide forms a base pair with another nucleotide following the specific Watson-Crick base pairing rules: guanine(G) only pairs with cytosine(C), adenine(A) only pairs with thymine(T). Thus, hereditary information are stored in two copies in each duplex DNA molecule. The deoxyribose sugar and phosphate groups form the helix backbone and protect the base pairing information.

Ribonucleic acid (RNA) plays a more complicated role in nature. Different from DNA, RNA is generally single-stranded but the specific Watson-Crick base pairing still applies (thymine(T) is substituted with Uracil(U)). Messenger RNAs (mRNA) act as the interme-

diary between the DNA information storage and the translated protein product that gives rise to phenotype. However, most RNA molecules do not encode protein information, but instead are non-coding RNAs (ncRNA) that regulate the expression of mRNAs. Because RNA is single-stranded, it readily adopts complex secondary structures. Different types of RNA with different lengths and sequences correspondingly possess different structures.

Although nucleic acids are chemically stable in general, they can be damaged from errors in replication, genetic recombination and etc. Some damages can be repaired through DNA repairing, while the un-repaired damages become mutations. Some mutations result in a different protein product being produced, and result in phenotypic differences. Mutations can either be in the germline, in which case it becomes passed on by heredity to progeny, or it may be somatic, in which it only affects one or a number of cells within the individual.

Mutations may span multiple nucleotides, but many important mutations differ from their corresponding wild types by only a single nucleotide. Although the sequence change is small, it can play an important role in genetic variation, such as responses to the environment, drugs, and other treatment[1]. Mutations affect human health in at least two ways: mutations in human can result in genetic disorders or in cancer [2], and mutations in pathogens such as bacteria can result in drug resistance[3]. Profiling the distribution of mutations within the population may also need to useful insights about the role of different genes in human development and health.

Nucleic acids as engineering material

The stability and predictability of DNA makes it a reliable tool to engineer nanoscale structures[4–6] and logic devices[7, 8]. After Santa Lucia characterized the binding energy of DNA sequences[9], Dirks et al. further analysed the problem for multi-stranded complex and developed a web-based program, NUPACK, to calculate a system's free energy and equilibrium state[10]. The hybridization and stacking of DNA strands can be pro-

grammed to produce desired two-dimensional or three-dimensional nanoconstructions that has potential applications in medical bioengineering[11].

In addition to interesting and reliable equilibrium behaviour, DNA can also be used to build dynamic devices, for example logic circuits, catalytic amplifier and motors [12], because the kinetics of DNA sequence interactions are programmable. Researchers characterized the kinetics of DNA hybridization/dissociation and strand displacement [13, 14]. A web-based program (visual DSD) is developed based on those characterizations to give predictions for DNA-based system[15]. Those programmable nano structures and dynamic devices can be integrated to make more functional structures and localized devices.

Definition of common terms

There are some common terms used in this field to describe a nucleic acid sequence or part of a sequence based on its structure or function.

Domain refers to a continuous region in a nucleic acid strand. Each nucleotide in one domain perform the same function in each and every step of reaction.

Strand is a continuous and linear sequence of nucleotides. Every two adjacent nucleotides are connected by a phosphate bond. Several domains may be connect to form a strand.

Complex is a multistranded DNA molecule held together by Watson-Crick binding.

Toehold, also known as 'Sticky ends', are short domains (normally 1-7 nucleotides) that join strands into complexes for a very short times (normally less than 1 second) to initiate strand displacement reactions.

Hybridization

Nucleic acid sequences that are complementary to each other can hybridize due to Watson-Crick base pairing. Watson-Crick base pairing is very specific on the nucleotide

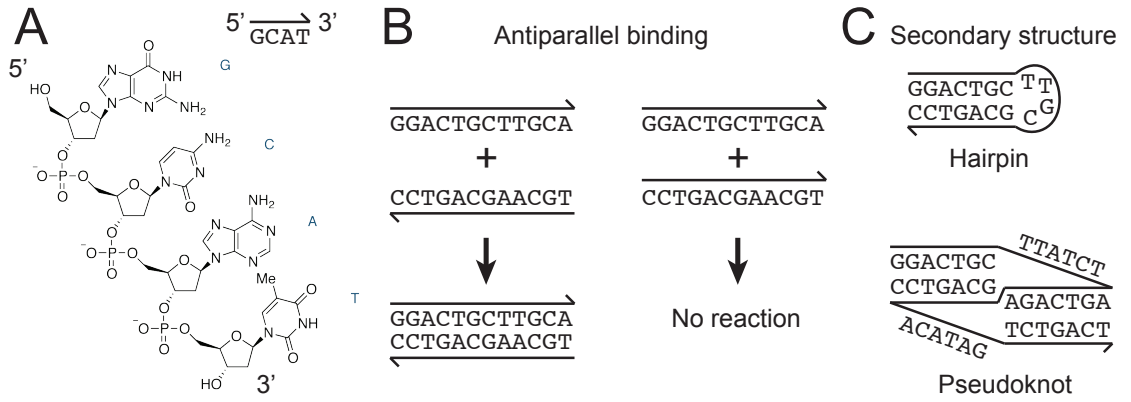

FIG. 1-1: **DNA molecule structures.** **A.** DNA is an asymmetrical molecule. The detailed structure of the sequence CTAGTAG is shown on the left. The structure is normally abbreviated as a line with arrow indicating the direction from 5' end to 3' end. **B.** DNA hybridization. DNA sequences can hybridize to a reverse complement sequence following specific Watson-Crick base pairing rules: guanine (G) only pairs with cytosine (C), and adenine (A) only pairs with thymine (T). **C.** Secondary structure. Hybridization between two domains within the same DNA strand. Hairpins and pseudoknots in DNA and RNA structure are widely observed in nature and often used in nanotechnology.

level: adenines (A) only bind to thymines (T), and guanines (G) only bind to cytosines (C). Nucleic acid sequences are directional, because the phosphate and sugar backbone is asymmetrical. The two ends of a nucleic acid sequence are named three prime end (3') or five prime end (5'). This naming refers to the third and fifth carbon on the backbone sugar is facing. Nucleic acid sequences are written from 5' end to 3' end. In diagrams, an arrow is used to indicate this direction with the arrow head indicating the 3' end (Fig 1a).

Two sequences can only hybridize if they are complementary when aligned in opposite directions (i.e. reverse complements). That is to say, the 5' end of one sequence binds with the 3' end of the other sequence. Two sequences of the same direction can not hybridize even if their base pairs are complementary. For example, GTGGTGTGTGTAT is complementary to ATACACACACCAC rather than CACCACACACATA. (Fig 1b)

A typical hybridization reaction can be written as

$$\text{reactant}_1 + ... + \text{reactant}_n \rightleftharpoons \text{complex}$$

Three or more strands can hybridize together to construct a single complex. For example, hundreds of short DNA strands could hybridize on a long strand and fold the long strand into desired structure. This method developed by Paul Rothemund is widely known as DNA origami. [4] Hybridization could also happen within one nucleic acid strand if the strand contains sequences that are complementary to each other. The base pairs formed between nucleotides bend the strand to form secondary structures (Fig 1c). Secondary structures naturally exist and play important roles in nature. Some RNA secondary structures can be recognized by proteins and processed into functional small RNAs to control gene expression. Simple hairpin shaped DNA are very commonly used in DNA-nanotechnology to make circuits and structures. [7, 16]

During the process of hybridization, the system's free energy is lowered. Although we mentioned a lot about specific base pairing, the hydrogen bonds formed between base pairs contributes only a small portion of the total energy gain from hybridization. Most of the energy comes from π bond stacking of the aromatic rings of the bases. The free energy gain of DNA hybridization can be accurately calculated from nearest neighbour models. It is due to this stacking energy, that two fully double-stranded DNA can be colocalized from the blunt end stacking and even ligated using DNA ligase. Although the total energy of making those bond can be high, each base pair and stacking is not very strong. While the whole structure maintains stable, some bases can be temporarily dissociated, which is referred to as ́breathing. Breathing happens very frequently (especially the end bases of a hybridized sequence) but last for a really short time (microseconds to milliseconds).

Melting Temperature

Nucleic acid hybridization is a reversible reaction. In the reverse reaction, a complex which was made of several strands due to hybridization of complementary sequences is dissociated. This reaction is called melting (or denaturation) of nucleic acid strands.The equilibrium status of this reaction can be calculated from it's standard free energy ΔG°.

$$K_{eq} = e^{-\Delta G^\circ / RT}, \quad \text{and} \quad K_{eq} = \frac{[Complex]_{eq}}{\prod_{i=1}^{n} [Reactanti]_{eq}}$$

Where R is the gas constant, T is the temperature in Kelvin, and integer $n \geq 2$ is the number of strands hybridized in this reaction.

A negative ΔG° indicates that the forward hybridization reaction is favorable; in this case, forming the complex is favoured. A positive ΔG° means that the melting reaction is more favorable and forming the complex is not favored. Using above equations, the amount of complex formed at equilibrium can be calculated if the standard free energy is calculated from sequence via software.

The standard free energy of a reaction relates to the enthalpy change (ΔH°) and entropy change (ΔS°) of the reaction:

$$\Delta G^\circ = \Delta H^\circ - T \cdot \Delta S^\circ$$

In the case of a hybridization reaction, the system gains enthalpy from forming nucleotide base stacking while losing entropy due to co-localization and steric constraint of multiple molecules and chemical bonds. When the temperature raises, the enthalpy gain becomes smaller [9], and the entropy loss becomes more greater, resulting in a more positive reaction standard free energy. Thus, hybridization becomes less favorable and fewer complexes are formed at higher temperatures.

For a defined system with known sequences, concentrations, temperature, and salinity,

the quantity or yield of hybridized complexes formed can be plotted as the function of temperature. At **melting temperature**, half of the limiting strands are hybridized. An example is shown in Figure 2a. Melting temperature is an essential property of a sequence and operating DNA assays near the melting temperature is widely used in PCR, microarray, and sequencing because hybridization at melting temperature is much more specific than at room temperature.

Although hybridization for each nucleotide is specific, hybridization may not be specific for long sequences; misbinding between related sequences [17] often happens at room temperature. A single base mismatch normally causes an energy penalty of about 4 kcal/mol, but the energy gain from hybridizing other base pairs normally overrides this penalty. In the example shown in Figure 2a and 2b, when there is no mismatch, 99.7% of the single strands are hybridized into complexes at room temperature (25^oC); when there is a mismatch, 96.1% of the single strands are hybridized. Hybridization for this sequence is not very specific at room temperature. At the melting temperature (≈ 60°C in this case), when there is no mismatch 50% of the single strands are hybridized into complexes, and about 1% of the single strands are hybridized for the mismatched sequence.

Melting temperature depends on a number of factors in addition to the length and sequence of strands, such as pH, strand concentration, and salinity. Thus, the melting temperature needs to be re-calculated for different experiment conditions, even if the sequences are the same. When several specific hybridization reactions need to be performed together in the same solution (for example for PCR or microarray assays), the primers or probes need to be carefully designed to have the same melting temperature. Because experiments in aqueous solution cannot be performed over at temperatures above 100°C, melting temperature method cannot be used to achieve specific hybridization for very long sequences.

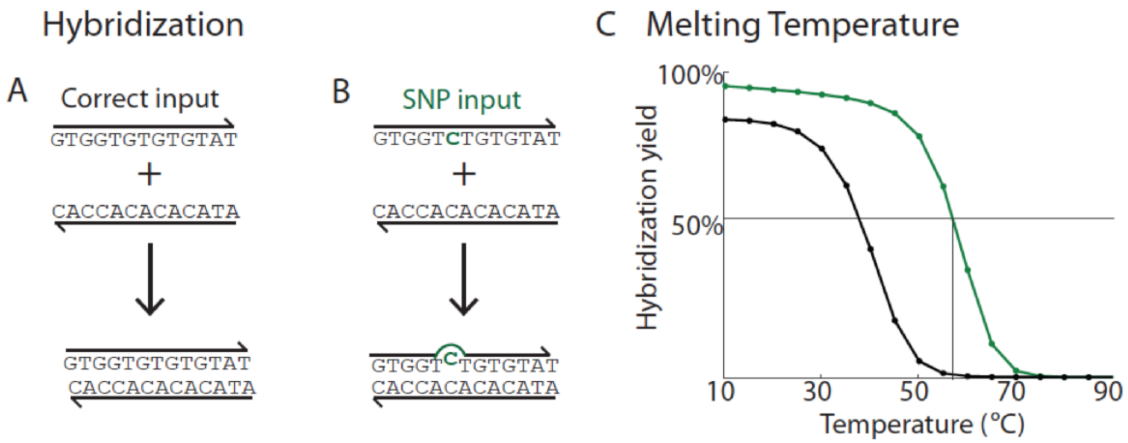

FIG. 1-2: **Hybridization and melting temperature. A.** DNA hybridization of complementary sequences. The base pairs and π bonds formed during hybridization stabilizes the double-stranded structure. **B.** DNA hybridization of sequences with single base mismatch. Due to the mis-binding, a mismatch bubble is formed in the product. The energy gain is smaller than the fully complementary hybridization as shown in panel a. But the total energy gain from other base pairs and π bonds can over ride the penalty of the mismatch bubble. **C.** Melting temperature. At room temperature, hybridization yield for fully complementary and single-base mismatched duplexes are very similar. As the temperature increases, the amount of double-stranded product become smaller. At the melting temperature, of the fully complementary sequences, the hybridization yield of fully complementary sequences is 50% and the hybridization yield of sequences with single base mismatch is less than 1%. Thus, hybridization is sequence specific at melting temperature.

Strand displacement

Like almost all reversible chemical reactions, the equilibrium of nucleic acid hybridization and dissociation is dynamic. By tuning the sequence length and identity, the co-localization time of hybridized strands can be adjusted. When the hybridized sequences is short(1-7 nucleotides), it could dissociate in less than a second, but when the hybridized sequence is long(about 20 nucleotides), it takes months to years to separate the sequences. It is very hard to displace an already hybridized strand by another strand with the same sequence for hybridization.

In a strand displacement reaction, a pre-hybridized strand is displaced by another invading strand after the reaction initiates using a short complementary domain. Hybridization

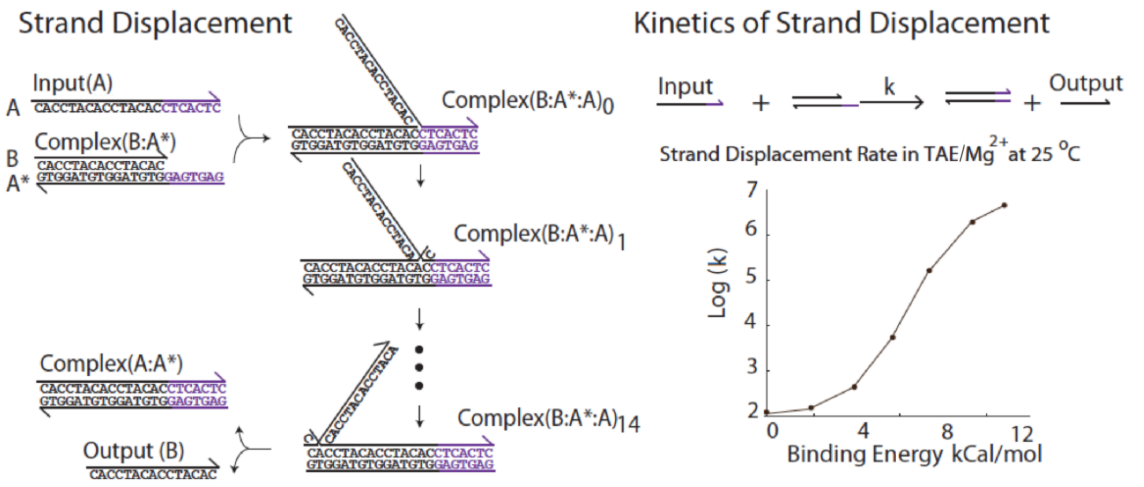

FIG. 1-3: **Strand displacement and Kinetics. A.** Strand Displacement reaction. The reaction starts with the hybridization of toehold (purple), this hybridization provides a short time of co-localization and initiates the branch migration process. When branch migration reaches the end, strand B is no longer bound to strand A* through any Watson-Crick bonds, and thus will be released. Both hybridization and branch migration are reversible, but releasing B is irreversible at the timescale of seconds. **B.** Kinetics of strand displacement reaction input(A)+C(B:A*) $\rightharpoonup$ C(A*:A)+output(B). The kinetics can be modelled as a function of toehold binding energy.[14]

of the short complementary domain creates short colocalization time of the input strand and the pre-hybridized complex. The nucleotide bases by the end of the pre-hybridized region can be temporarily dissociated through base breathing. Because the invading strand has the same sequence in this region, nucleotide on the input has a 50% chance to bind with the complementary sequence. This exchange of nucleotides on different strands is know as **branch migration**. Because the breathing of hybridization happens very frequently (once per 10 μs), branch migration is fast. When branch migration reaches the end, the initially hybridized strand will be displaced and released. The total process of hybridizations, branch migration and releasing is called **strand displacement** and the short domain used for colocalization is referred as **toehold**.

A basic strand displacement reaction is shown in Figure 3a. The reaction can be written

as:

$$\text{input(A)+C(B:A*)} \rightleftharpoons \text{C(B:A*:A)}_0 \rightleftharpoons \text{C(B:A*:A)}_1 \rightleftharpoons ... \rightleftharpoons \text{C(B:A*:A)}_n \rightharpoonup \text{C(A*:A)+output(B)}$$

C is the abbreviation for complex, and means there are bonds formed between the strands. There are n steps in the whole branch migration. Because branch migration is fast, and the three strand complex is not thermodynamically favourable, the concentration of the three stranded intermediate is low. The above reaction are normally abbreviated as:

$$\text{input(A)} + \text{C(B:A*)} \rightharpoonup \text{C(A*:A)} + \text{output(B)}$$

The rate constant of this strand displacement reaction mainly depends on the toehold strength[14]. Using this characterization, reaction kinetics can be well engineered. Figure 3b shows the reaction rate as a function of toehold strength at room temperature in $125mM \quad Mg^{2+}$

The output of the strand displacement reaction can serve as an input for another complex, and the new complex formed may have other open toeholds that could start another strand displacement reaction. In fact, releasing strand B could open toeholds on both B and A*, which means, B can serve as input to complex (A*:A). Toeholds can thus be engineered to be open or closed, and this method is named **toehold exchange** (Figure 4c).

Previous method to detect single base changes

Use of melting temperature to achieve highly specific hybridization is widely used in PCR, microarray and sequencing [18, 19] that require high specificity binding. But not all experiments or testing can be performed at their melting temperature. Over the past decades, many probes are designed to get both high specificity and wider temperature robustness.

Early attempts to improve discrimination of small nucleic acid changes used the sequence-specificity of enzymes such as ligases [20–22] or endonucleases [23, 24] to get high specificity. Although these worked quite well for specificity, the buffer requirements of these enzymes were frequently incompatible with PCR buffers, so to detect polymorphisms from biological samples where amplification is needed, a two-step protocol would be needed. Two-step protocols with an open-tube transfer step risk contamination, and imposes significantly higher burden of labor.

A different approach to improving hybridization specificity uses non-natural nucleic acid probes or primers with modified backbones or nucleoside bases[25, 26], such as locked nucleic acids (LNA) or peptide nucleic acids (PNA). These non-natural nucleic acid oligonucleotides generally bind significantly more strongly per base than DNA or RNA, so a single base mismatch imposes a larger energetic penalty from not forming the base pair. However, these probes are over 30 times more expensive than standard DNA probes, and also require temperature optimization.

The first DNA probe to show improved specificity based on secondary structure is called the molecular beacons [27–29]. A molecular beacon is a nucleic acid strand that is designed with hairpin shaped secondary structure. The loop on the hairpin is about 15-30 nucleotides long and is complementary to the sequence to be detected. The duplex stem of the hairpin is 5-7 nucleotides long. The molecular beacon probe is functionalized with a fluorophore and quencher by the 5' and 3' of the sequence. In the molecular beacon's native (unbound) conformation, the fluorophore and quencher are colocalized and gives little fluorescence signal.

The molecular beacon produces a fluorescent signal upon binding to its designed target sequence, because the stem duplex is forced apart. The energy from hybridization of the loop domain overcomes the energy needed to break the hybridization of stem. In the reaction with a mismatched target, the loop hybridization provides less energy and may

not be enough to break the stem. Because molecular beacon have non-zero free energy, the reaction between the probe and correct target gains little energy. The energy penalty caused by mismatch becomes more significant, resulting in higher specificity at lower temperatures.

Molecular beacon hybridization is still temperature and concentration dependent, because the number of reactants and products are not the same and entropy change is significant. To achieve high specificity, detection needs to be performed under optimized temperature and buffer conditions specific to the target and molecular beacon sequence and concentration. To make the specificity of the hybridization reaction more robust to temperature and buffer, the number of reactant and product molecules should be the same.

Probes with equal number of reactants and products were designed by Li in 2002, based on strand displacement reactions[30]. Those probes can be further fixed on DNA nano structures [6, 31], so that signals can be observed using fluorescence or atomic force microscopy. The energy change before and after the reaction comes from the hybridization of toehold which is small, but it is normally larger than the energy penalty caused by one base mismatch. Although the sensitivity at equilibrium is not very high, the kinetics (ex, reaction rate) of strand displacement significantly changes due to the energy penalty of mismatch. Taking advantage of this kinetics difference, specificity at equilibrium can be further increased by adding competitive probes designed for possible inputs [30] if the sequence for all correct and mismatched target are known.

To achieve high specificity at equilibrium while maintain the robustness to temperature and concentration, the net free energy and entropy change need to be close to 0. Such condition can be satisfied by toehold exchange reaction shown in figure 4c. The toehold exchange probe produces high specificity and functions robustly from a large range of temperature, nucleic acid concentrations and salinities.[32]

Overview of Thesis

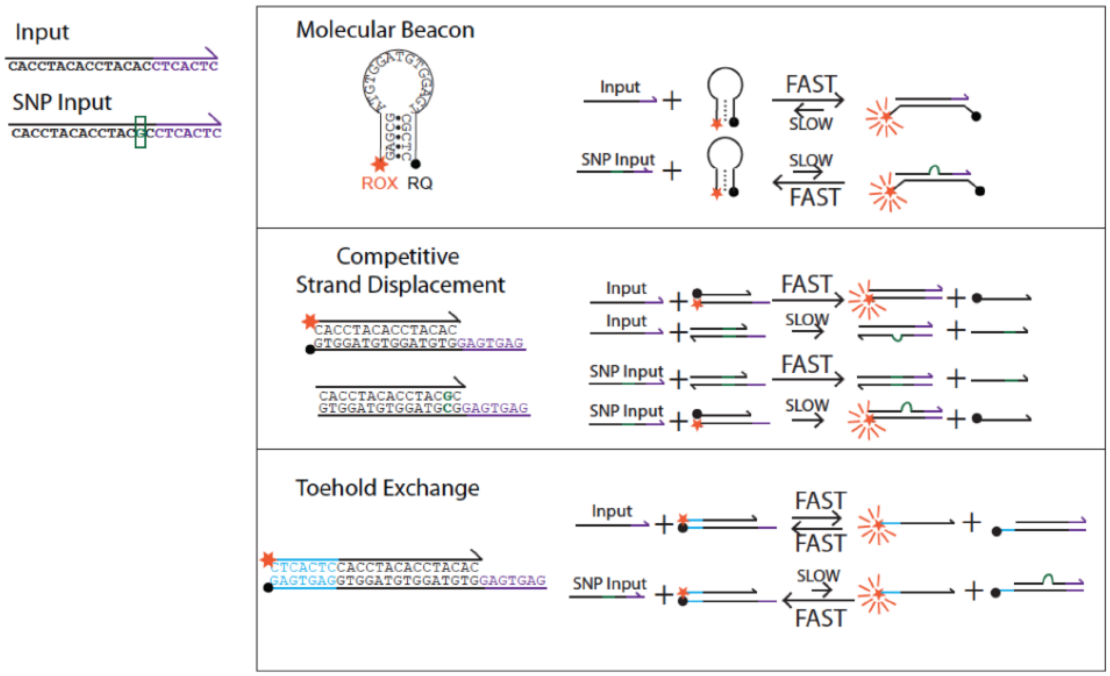

FIG. 1-4: **Previous method to detect single base changes.** An example of input and a SNP input is shown on the top left corner (mutation from A to G) For each method discussed, a probe is designed, and the reactions for both correct input and SNP input is shown in the box. **A.** Molecular Beacon **B.** Competitive Strand Displacement **C.** Toehold Exchange Probe

In this thesis, I present four separate works on design of toehold exchange DNA probe systems that provide high single nucleotide discrimination power across wide ranges of temperatures and buffer conditions. I started with initial proof-of-concept work on synthetic DNA and RNA oligonucleotide targets, but then moved on to detect antibiotic-resistance mutations in DNA extracted from bacteria. Different approaches are presented for detecting sequence variation at low allele frequencies in single- and double-stranded DNA. Additionally, sequence specificity is improved through constructing a cascaded reaction network. Finally, the lessons I learned in probe design for sequence discrimination are used to construct a reaction network that linearly classifies nucleic acid samples based on the relative concentrations of multiple sequences.

[1] Calin, G. A. Human microRNA genes are frequently located at fragile sites and genomic regions involved in cancers*Proc. Nat. Acad. Sci.* **101,** 2999 3004 (2004).

[2] Engle1,L. J. , Simpson,C. L. , & Landers, J. E . Using high-throughput SNP technologies to study cancer *Oncogene***25** 1594 1601 (2006).

[3] Bang, H. , Park, S. , Hwang, J. & Lee1, H . Improved rapid molecular diagnosis of multidrug-resistant tuberculosis using a new reverse hybridization assay, REBA MTB-MDR. *Journal of Medical Microbiology* **60,** 1447 1454 (2011).

[4] Rothemund,P.W.K. Folding DNA to create nanoscale shapes and patterns. *Nature* **440,** 297-302 (2005).

[5] Pinheiro, A.V., Han,D. , Shih W.M. & Yan, H. Challenges and opportunities for structural DNA nanotechnology. *Nature Nanotechnology* **6,** 763772 (2011).

[6] Subramanian, H. K. K., Chakraborty, B., Sha, R. & Seeman, N. C. The label-free unambiguous detection and symbolic display of single nucleotide polymorphisms on DNA origami. *Nano Letters* **11,** 910-913 (2010).

[7] Seelig, G., Soloveichik, D., Zhang, D.Y. & Winfree, E. Enzyme-free nucleic acid logic circuits. *Science* **314,** 1585-1588 (2006).

[8] Qian, L. & Winfree, E. Scaling up digital circuit computation with DNA strand displacement cascades. *Science* **332,** 1196-1201 (2011).

[9] SantaLucia, J. & Hicks, D. The Thermodynamics of DNA Structural Motifs. *Ann. Rev. Biochem.* **33,** 415-440 (2004).

[10] Dirks, R.M. , Lin, M. , Winfree, E. , Pierce, N.A. Paradigms for computational nucleic acid design.*Nucl. Acids Res.* **32,** 1392-1403 (2004).

[11] Douglas, S.M. , Bachelet,I. & Church, G.M. A Logic-Gated Nanorobot for Targeted Transport of Molecular Payloads.*Science* **335,** 831-834 (2012).

[12] Zhang, D. Y. & Seelig, G. Dynamic DNA nanotechnology using strand displacement reactions. *Nature Chemistry* **3,** 103-114 (2011).

[13] Morrison, L.E. & Stols, L.M. Sensitive fluorescence-based thermodynamic and kinetic measurements of DNA hybridization in solution.*Biochemistry* **32,** 3195-3104 (1993).

[14] Zhang, D.Y. & Winfree, E. Control of DNA Strand Displacement Kinetics Using Toehold Exchange.*J. Am. Chem. Soc.* **131,** 17303-17314 (2009).

[15] Lakin, M. , Parker, D. , Cardelli, L. , Kwiatkoska, M. & Phillips, A. Design and Analysis of DNA Strand Displacement Devices using Probabilistic Model Checking. *Journal of the Royal Society Interface* **9,** 1470-1485 (2012).

[16] Wei, B. , Dai, M. & Yin, P. Complex shapes self-assembled from single-stranded DNA tiles *Nature* **485** 623-626 (2012).

[17] Koltai, H. & Weingarten-Baror, C. Specificity of DNA microarray hybridization: characterization, effectors, and approaches for data correction. *Nucleic Acids Research* **36,** 2395-2405 (2008).

[18] Schena, M., Shalon, D., Davis, R. W. & Brown, P. O. Quantitative Monitoring of Gene Expression Patterns with a Complementary DNA Microarray. *Science* **270,** 467-470 (1995).

[19] Gunderson, K. L., Steemers, F. J., Lee, G., Mendoza, L. G. & Chee, M. S. A genome-wide scalable SNP genotyping assay using microarray technology. *Nature Biotechnology* **37,** 549-554 (2005).

[20] Landegren, U., Kaiser, R., Sanders, J. & Hood, L. A ligase-mediated gene detection technique.*Science***241**,: 1077-1080 (1988).

[21] Nilsson, M., Malmgren, H., Samiotaki, M., Kwiatkowski, M., Chowdhary, B. P., & Landegren, U. Padlock probes: circularizing oligonucleotides for localized DNA detection. *Science***265**, 2085-2088 (1994).

[22] Tong, A. K., Li, Z., Jones, G. S., Russo, J. J., & Ju, J. Combinatorial fluorescence energy transfer tags for multiplex biological assays. *Nature biotechnology* **19**, 756-759 (2001).

[23] Botstein, D., White, R. L., Skolnick, M., & Davis, R. W. Construction of a genetic linkage map in man using restriction fragment length polymorphisms. *American journal of human genetics* **32**, 314 (1980).

[24] Hall, J. G., Eis, P. S., Law, S. M., Reynaldo, L. P., Prudent, J. R., Marshall, D. J., Allawi H. T. *et al.* Sensitive detection of DNA polymorphisms by the serial invasive signal amplification reaction. *Proc. Nat. Acad. Sci. USA* **97**, 8272-8277 (2000).

[25] Singh, S. K., Koshkin, A. A., Wengel, J., & Nielsen, P. LNA (locked nucleic acids): synthesis and high-affinity nucleic acid recognition. *Chemical communications* **4**, 455-456 (1998).

[26] Egholm, M., Buchardt, O., Nielsen, P. E., & Berg, R. H. Peptide nucleic acids (PNA). Oligonucleotide analogs with an achiral peptide backbone. *J. Am. Chem. Soc.* **114** 1895-1897 (1992).

[27] Tyagi, S. & Kramer, F.R. Molecular beacons: probes that fluoresce upon hybridization. *Nature Biotechnology* **14,** 303-308 (1996).

[28] Bonnet, G., Tyagi, S., Libchaber, A. & Kramer, F. R. Thermodynamic basis of the enhanced specificity of structured DNA probes. *Proc. Nat. Acad. Sci.* **96,** 6171-6176 (1999).

[29] Tsourkas, A., Behlke, M. A., Rose, S. D. & Bao, G. Hybridization kinetics and thermodynamics of molecular beacons. *Nucleic Acids Research* **31,** 1319-1330 (2003).

[30] Li, Q., Luan G., Guo, Q. & Liang J. A new class of homogeneous nucleic acid probe based on specific displacement hybridization, *Nucleic Acids Research* **30,** e5 (2002).

[31] Xiao, Y., Plakos, K. J. I., Lou, X., White, R. J., Qian, J., Plaxco, K. W. & Soh, H. T. Fluorescence detection of single-nucleotide polymorphisms with a single, self-complementary, triple-stem DNA probe, *Angew. Chemie Int. Ed.* **48,** 4354-4358 (2009).

[32] Zhang, D.Z , Chen. S. X. &Yin, P. Optimizing the specificity of nucleic acid hybridization, *Nature Chemistry* **4,** 208-214 (2012).

Chapter 2: Thermodynamic optimization of nucleic acid hybridization specificity

This work was published in Nature Chemistry in 2012, and describes the design and validation of our toehold probes for highly robust and specific detection of nucleic acid sequences. The key insight in this work is the observation that temperature robustness is achieved when reaction ΔH° is approximately 0, buffer robustness is achieved when reaction ΔS° is approximately 0, and concentration robustness is achieved when Δn (change in number of molecules) is 0. The toehold exchange reaction is a probe implementation that simultaneously achieves all of these design criteria, as well as ensuring a fast reaction.

Abstract: The specific hybridization of complementary sequences is an essential property of nucleic acids, enabling diverse biological and biotechnological reactions and functions. However, the specificity of nucleic acid hybridization is compromised for long strands, except near the melting temperature. Here, we analytically derived the properties of a hybridization probe that would enable near-optimal single-base discrimination and perform robustly across diverse temperature, salt, and concentration conditions. We rationally de-

signed "toehold exchange" probes that approximate these properties, and comprehensively tested them against 5 different DNA targets and 55 spurious analogs with energetically representative single-base changes (replacements, deletions, and insertions). These probes produced discrimination factors between 3 and 100+ (median 26). Without retuning, our probes function robustly from 10 °C to 37 °C, from 1 mM Mg^{2+} to 47 mM Mg^{2+}, and from 1 nM to 5 μM nucleic acid concentrations. Experiments with RNA also showed effective single-base change discrimination.

Nucleic acids are essential biomolecules, encoding and regulating the expression of hereditary information within living organisms [1]. The biological importance of nucleic acids has prompted the use of synthetic nucleic acid probes and primers for biology and biotechnology, such as through the polymerase chain reaction (PCR) [2], microarrays [3–5], and fluorescent *in situ* hybridization [6, 7]. Simultaneously, nucleic acids have emerged as powerful materials for nanoscale engineering [8–13].

The key property of nucleic acids that renders them so useful for biology, biotechnology, and bionanotechnology is the predictable and specific Watson-Crick hybridization of complementary bases. However, the thermodynamic gain of many correctly paired bases can override the thermodynamic penalty of a few mismatches, and the hybridization of long nucleic acids may be nonspecific except near the melting temperature.

High temperature or chemical denaturation is often employed to improve hybridization specificity [2, 6, 7]. At high temperatures or under chemically denaturing conditions, the standard free energy of hybridization is weaker, and marginally different sequences may be distinguished based on their binding affinities to a complement. However, operating near the melting temperature is not always feasible, such as in the case of a multiplexed system

where many different hybridization reactions must proceed simultaneously. Additionally, the melting temperature depends on factors such as salinity and nucleic acid concentrations and can be difficult to precisely predict. Similarly, chemical denaturation weakens Watson-Crick base-pairing, and suffers the same potential limitations.

Given the thermodynamic basis for discriminating closely related nucleic acid sequences near the melting temperature, it is possible to engineer frustrated complement molecules that hybridize less favorably to their intended targets than the standard complementary strands. For example, in molecular beacons [14–16], the complement is flanked by extra bases and natively forms a hairpin structure. Hybridization to the beacon's target disrupts the hairpin structure and is less thermodynamically favorable than standard hybridization; this allows for higher hybridization specificity [17, 18]. Other probes also aimed to reduce the thermodynamic favorability of hybridization [19, 20], but these are more complex and difficult to rationally design with fine control of thermodynamics. While beacons and other probes can be systematically optimized for performance at any particular set of conditions (such as temperature or salinity) [21], a robust hybridization probe that specifically hybridizes to its intended target across diverse conditions without retuning would be vastly more useful.

In this manuscript, we first present a theoretical framework for the analysis of nucleic acid hybridization specificity and derive theoretical limits, providing a benchmark for evaluating performance of hybridization probes. Next, we analytically derive probe properties that would ensure near optimal specificity across diverse temperatures, concentrations, and salinities. Finally, we present DNA and RNA toehold exchange probes and show that they experimentally discriminate single-base changes under a wide variety of conditions.

Analytic framework and probe design

Thermodynamics of hybridization specificity. Consider the hybridization of two

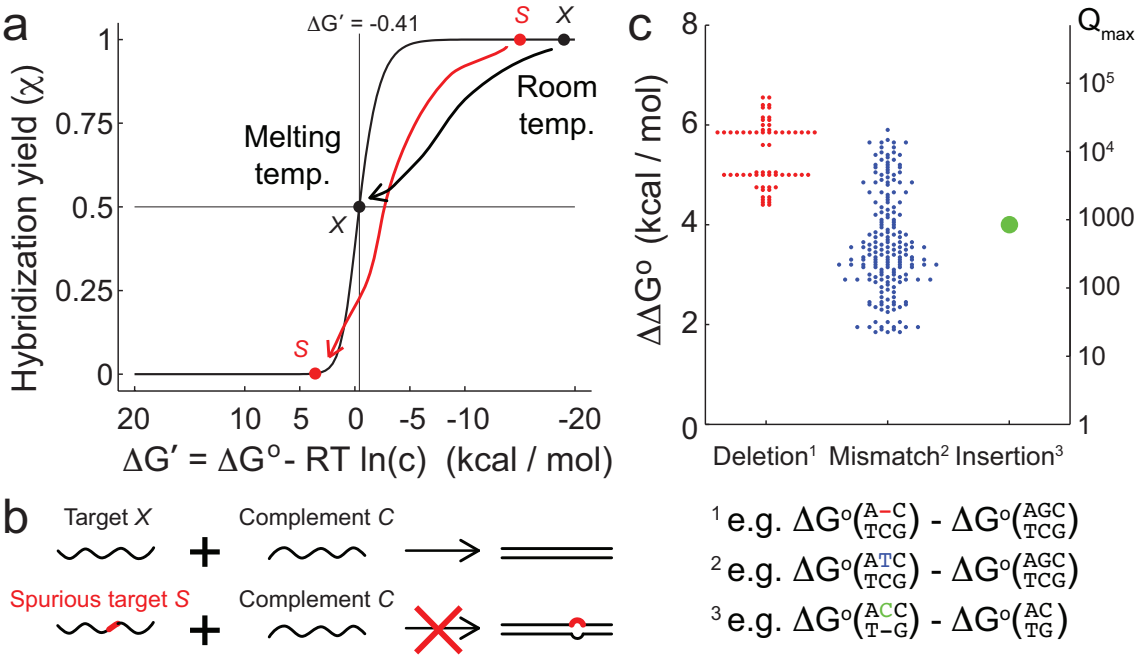

FIG. 2-1: Hybridization specificity of nucleic acids. **(a)** Hybridization yield χ is plotted against the concentration-adjusted standard free energy $\Delta G' = \Delta G^\circ + (\Delta n)RT\ln(c)$, where c is the concentration of the limiting species, and $\Delta n = -1$ for a standard bimolecular hybridization reaction. At room temperature, the binding of both the correct target (black dot) and the spurious target (red dot) are thermodynamically favorable and practically indistinguishable. In contrast, at the melting temperature, $\Delta G' = -RT\ln(\frac{(c/2)}{(c/2)^2}) - RT\ln(c) = -0.41$ kcal/mol, the hybridization yield of the correct target is 50%, and much lower for the spurious target. **(b)** In a hybridization-based assay or reaction, specificity is achieved when a spurious target that differs in sequence from the correct target by a single base (depicted as the red segment) does not hybridize significantly to the complement. **(c)** The standard free energy difference ($\Delta\Delta G^\circ$) caused by a single-base change ranges from 1.83 to 6.57 kcal/mol, and determines the maximum discrimination achievable: $Q < Q_{\max} \equiv e^{\Delta\Delta G^\circ/RT}$. Graphic constructed using thermodynamic parameters by SantaLucia and Hicks [22]; see Text S3, Tables S1-S5 for detailed numerical values. All 64 cases of single-base insertion are modeled to have identical $\Delta\Delta G^\circ$.

complementary nucleic acids, target X and complement C: $X + C \rightarrow XC$. The equilibrium constant $K_{eq} = \frac{[XC]}{[X][C]}$ can be calculated from the standard free energy ΔG°, which can in turn be predicted from the sequences of X and C [22]. The hybridization yield $\chi = \frac{[XC]}{[XC]+\min\{[X],[C]\}}$ denotes the fraction of the limiting reagent that exists in duplex form, and can be analytically calculated from K_{eq} and the initial concentrations of X and C (Text S1). More simply, χ can be written solely as a function of the *concentration-adjusted equilibrium*

constant $K'_{eq} \equiv c^{-\Delta n} K_{eq}$ (Text S1), where c denotes the initial concentration of the limiting reagent and Δn represents the change in the number of species through the course of the reaction (-1 for bimolecular hybridization). Thus, K'_{eq} is a useful dimensionless metric for evaluating equilibrium distribution: when $K'_{eq} \gg 1$, the hybridization yield χ approaches 1, and when $K'_{eq} \ll 1$, χ approaches 0. The *concentration-adjusted standard free energy* $\Delta G' \equiv -RT\ln(K'_{eq}) = \Delta G^\circ + (\Delta n)RT\ln(c)$ is similarly defined; Fig. 1a plots χ versus $\Delta G'$ for a standard hybridization reaction.

A hybridization reaction or probe is specific when there is a large difference between the hybridization yield of an intended target X and that of a spurious target S (Fig. 1a). Specificity can be quantitated as *discrimination factor* $Q = \frac{\chi_X}{\chi_S}$, where χ_X and χ_S are the hybridization yields of X and S, respectively.

A fundamental upper bound on Q is prescribed by thermodynamics:

$$Q \ < \ Q_{\max} \equiv e^{\Delta\Delta G^\circ / RT}$$

$$\begin{aligned} \text{where} \quad \Delta\Delta G^\circ \ &= \ (\Delta G^\circ(SC) - \Delta G^\circ(S) - \Delta G^\circ(C)) \\ &\quad -(\Delta G^\circ(XC) - \Delta G^\circ(X) - \Delta G^\circ(C)) \end{aligned}$$

is the difference in standard free energies of the hybridization reaction for X and S, R is the ideal gas constant, and T is the temperature (see Text S2 for analytical proof). To investigate the limits of performance, here we only consider spurious targets S that differ from X by a single base. The $\Delta\Delta G^\circ$ values for all single-base changes are plotted in Fig. 1c. For a typical $\Delta\Delta G^\circ = 4$ kcal/mol single-base change, $Q_{\max} = 853$ at 25 °C.

Properties of a specific and robust hybridization probe. A specific and robust hybridization probe should possess several functional properties: (1) high hybridization yield χ_X of the correct target, (2) high discrimination factor Q against spurious targets,

(3) robustness to target and probe concentrations, (4) robustness to temperature, and (5) robustness to the chemical composition (e.g. salinity) of the solvent.

There is a tradeoff between high χ and high Q. For standard hybridization reactions, we prove in Text S2 that as $\Delta G'$ approaches $+\infty$, Q approaches $Q_{\max}$; however, χ also approaches 0. At the melting temperature of XC, $\Delta G' \approx 0$, $\chi_X = 0.5$, and $Q > \frac{Q_{\max}}{2}$ (see Text S2 for analytical proof); this is a good tradeoff between specificity and yield. Hybridization probes that are designed to achieve $\Delta G' \approx 0$ (e.g. 1 kcal/mol $\geq \Delta G' \geq -1$ kcal/mol) will similarly exhibit near optimal specificity and reasonable hybridization yields.

Concentration robustness requires that hybridization yield χ does not have a dependence on c. Recall that χ can be expressed solely as a function of $K'_{eq} = c^{-\Delta n} K_{eq}$ (Text S1). In a reaction where $\Delta n = 0$, K'_{eq} and χ will be independent of c, and therefore robust to changes in concentration.

The dependence of χ on temperature T is due to the latter's effect on K_{eq}:

$$K_{eq} = e^{-\Delta G^\circ / RT} = e^{-\Delta H^\circ / RT} e^{\Delta S^\circ / R}$$

Under standard thermodynamic models of DNA hybridization [22], ΔH° and ΔS° are assumed to be temperature invariant ($\frac{d\Delta H^\circ}{dT}$, $\frac{d\Delta S^\circ}{dT} \approx 0$), and χ will have no dependence on T when $\Delta H^\circ = 0$. Hence, a probe that hybridizes to its target with $\Delta H^\circ = 0$ would be robust to temperature.

The effects of salts in solution on χ are also manifested through a change in K_{eq}. There are two accepted models of the effects of cation concentrations on hybridization thermodynamics: the Na^+ Equivalent model [23] and the Tightly-Bound Ion model [24]. In both models, the effects of cations are assumed to be purely entropic, and the entropic adjustment terms are functions of N, the total number of phosphates in double-stranded form.

A reaction with no change in the total number of paired bases ($\Delta N = 0$) is expected to feature hybridization yields that are unaffected by salt concentrations, as long as sufficient cations are present to allow DNA hybridization.

In summary, a hybridization probe is expected to robustly discriminate single-base changes across concentrations, temperatures, and salinities if it reacts with its reactant with (1) little change in concentration-adjusted standard free energy ($\Delta G' \approx 0$), (2) no net change in the number of nucleic acid molecules in solution ($\Delta n = 0$), (3) no net change in the standard enthalpy of reaction ($\Delta H^\circ = 0$), and (4) no net change in the number of paired bases ($\Delta N = 0$).

Toehold exchange probe design. We present *toehold exchange probes* that approximately satisfy all of the above criteria (Fig. 2). The hybridization of the probe (PC) to the correct target X is initiated at the green $5'$ single-stranded region of C (known as a *toehold* [25, 26]), proceeds through a branch migration process, and is completed via the spontaneous dissociation of the $3'$ base pairs of C (blue toehold) to release single-stranded protector P [26, 27]. The toeholds allow the forward and reverse reactions to proceed with fast kinetics. Without the toehold, the kinetics of the displacement reaction would have a half-life of months at typical experimental conditions (e.g. 100 nM DNA, pH ≈ 8, $T \approx 25$ °C, $[Mg^{2+}] \approx 12$ mM); with the presence of the 7 nt toeholds depicted, the rate constant of the forward and reverse reactions are up to 10^6 M^{-1} s^{-1}, corresponding to a half-life of 10 s [26].

The blue toehold that spontaneously dissociates is designed to be similar in length ($\Delta N \approx 0$), base composition, and thermodynamic binding strength (ΔG°, ΔH°) as the green toehold. Furthermore, the reaction is bimolecular with two products, so $\Delta n = 0$, and $\Delta G' = \Delta G^\circ$. Consequently, this $X + PC \rightarrow XC + P$ reaction has $\Delta G' \approx 0$, $\Delta n \approx 0$, $\Delta H^\circ \approx 0$, and $\Delta N \approx 0$, and is expected to be **rapid and highly specific over a wide range of temperatures, salinities, and nucleic acid concentrations**. The standard-

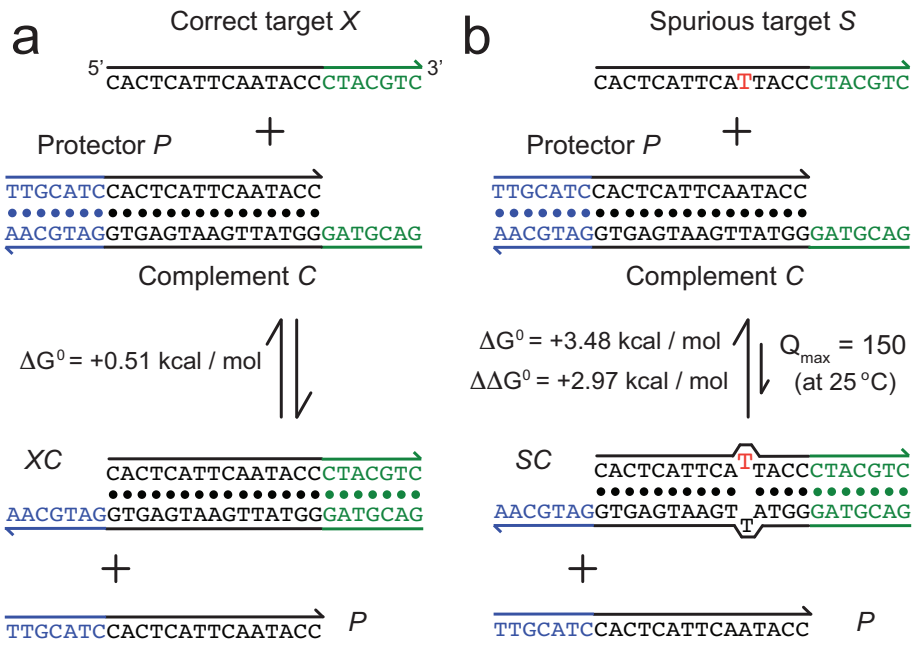

FIG. 2-2: Toehold exchange probes. **(a)** The toehold exchange probe (PC) consists of a pre-hybridized complement strand C and a protector strand P. The probe can react with an intended target X to release P and the hybridized product XC. The probe is designed based on the sequence of the target so that the standard free energy ($\Delta G^\circ = \Delta G'$) of the forward reaction is close to 0. In this example, 7 new base pairs (green 5′ toehold of C) are formed, but 7 existing base pairs are broken (blue 3′ toehold of C). For sequences shown here, mathematical analysis predicts the hybridization yield $\chi_X = 0.34$ at 25 °C, mimicking hybridization behavior at close to the melting temperature of XC (Text S4). **(b)** The hybridization of a spurious target S with one base change is less thermodynamically favorable by +2.97 kcal/mol, and is predicted to have $\chi_S = 0.0056$. Thus, the discrimination factor Q is predicted to be $\frac{0.34}{0.0056} = 61$. For comparison, $Q_{\max}$ for $\Delta\Delta G^\circ = 2.97$ kcal/mol is 150 at 25 °C.

ized conceptual design and lack of complicated secondary structures (such as pseudoknots) renders the system **quantitatively predictable** and **rationally designable**. As the toehold exchange probe is a design approach that depends only on the Watson-Crick pairing property of nucleic acids, it is **generalizable** to RNA and other nucleic acids, such as PNA [28] and LNA [29].

Experimental results

The experimentally implemented toehold exchange probes (Fig. 3a) differed slightly from

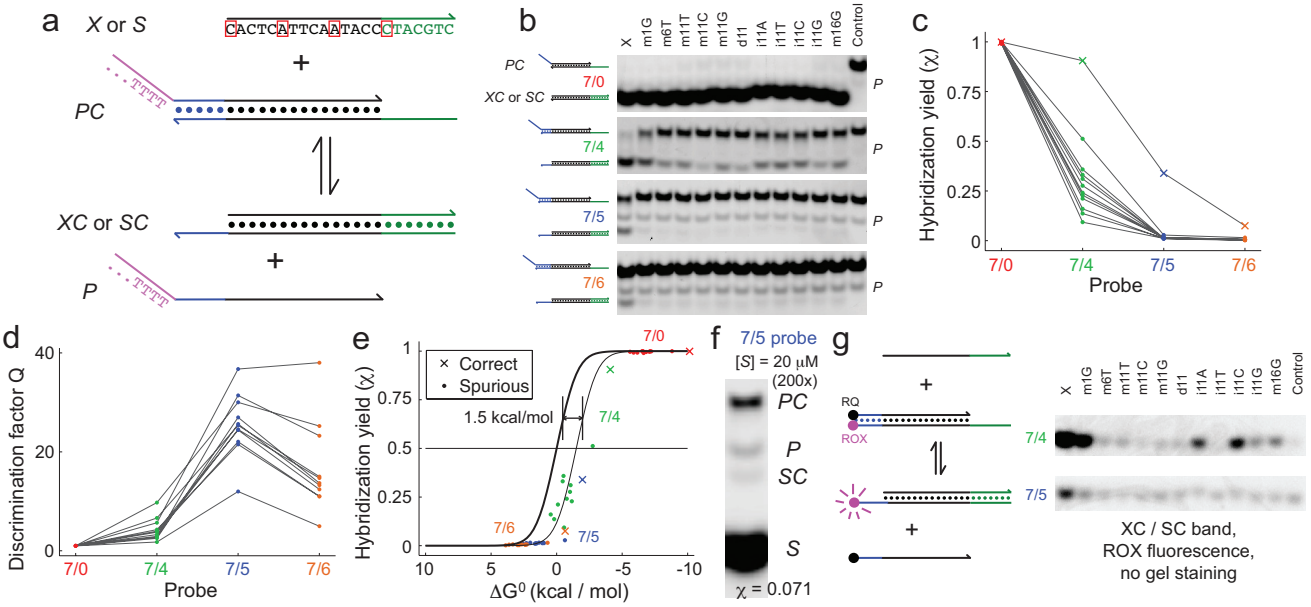

FIG. 2-3: Experimental demonstration of toehold exchange probes. **(a)** The intended DNA target sequence and the experimental probe system. Outlined in red are the positions of the one-base changes in various spurious targets. P in the experimental system has a 30 nt poly-T tail at the 5′ end (purple) to help distinguish it from other species in gel experiments. **(b)** Native PAGE results. PC was prepared at a 2:1 ratio of P to C, and annealed at 1 μM concentration of PC. X or S were added to achieve final concentrations of 200 nM target (X or S), 100 nM PC, and 100 nM P. Reactions proceeded at 25 °C for 1 hour. Four different probes were tested (e.g. 7/5 probe has a 7 nt green toehold and a 5 nt blue toehold). Middle lanes show the reaction with different spurious targets S; 'm', 'd', and 'i' respectively denote mismatch, deletion, and insertion (e.g. in m11C, the Adenine at position 11 from the 5′ end was replaced by a Cytosine, see Table S7 for sequences). The right-most lane shows the negative control (PC only). The P band is single-stranded and stains inconsistently with SybrGold. **(c)** Hybridization yields χ inferred from panel (b). χ_X are plotted as ×'s, χ_S as dots. Lines connect χ values for the same target. **(d)** Discrimination factors Q. **(e)** Plot of hybridization yield χ vs. reaction standard free energy ΔG°. χ values are plotted as ×'s and dots against the reaction ΔG° calculated by NUPACK (Text S6) [32]. The dark black trace shows the expected results from thermodynamic analysis (Text S4). Adjusting all ΔG° by +1.5 kcal/mol (thin black trace) improves the agreement between model and data. **(f)** 7/5 probe with large excess of S (equal mixture of all 11 spurious targets). **(g)** Fluorophore/quencher-labeled probe.

the theoretical construction (Fig. 2). To distinguish the hybridized products XC and SC from probe PC based on mobility in a gel, we appended 30 nt poly-T to the 5′ end of the protector P. Standard DNA thermodynamics models [22, 33] predict that this does not significantly change the ΔG° of formation of the probe PC or of the released protector P.

Probe performance. Our first target X was designed to possess no secondary struc-

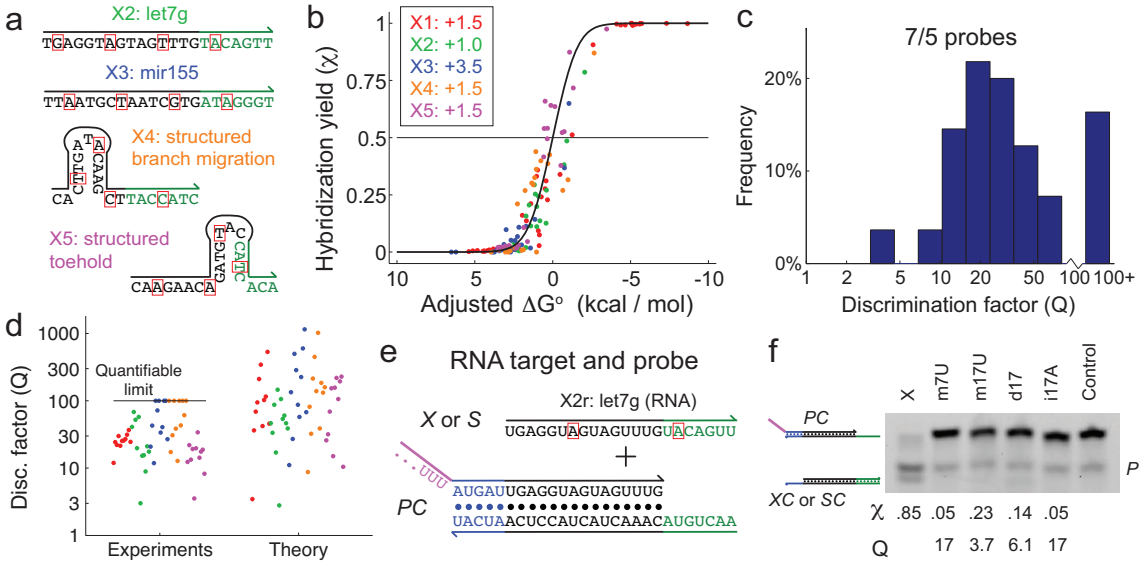

FIG. 2-4: Results for additional DNA and RNA targets. **(a)** The sequences of the 4 additional DNA targets (see Tables S6-S8 for sequences of protectors P and spurious targets S). **(b)** Hybridization yield vs. adjusted ΔG°. The same ΔG° adjustments (inset, in kcal/mol) were applied to all reactions within a set. The systems in Fig. 3 are referred to as X1. See Fig. S8-S11 for detailed results. **(c)** Distribution of observed Q for all 7/5 probes (55 total data points). Due to the limitations in quantifying gel band intensities, it was not possible to consistently measure Q values above 100 (see Methods). Median observed Q was 26. **(d)** Comparison of observed Q and Q predicted based on $\Delta\Delta G^\circ$ values (Text S6). **(e)** RNA target and probe. The target sequence is the RNA analog of the X2 DNA system shown in Fig. 4a, and is identical to the human *let7g* microRNA. **(f)** Native PAGE results. PC was prepared at a 2:1 ratio of P to C, and annealed at $[PC] = 3$ μM. X or S was added to achieve final concentrations of 2 μM X or S, 1 μM PC, and 1 μM P.

ture. Fig. 3a shows its sequence and the positions of the single-base changes of spurious targets S. The probe was allowed to react with X or S at room temperature for 1 hour before gel electrophoresis; 1 hour was verified to be sufficient to allow the reaction to proceed to equilibrium (Fig. S3). Fig. 3b shows the native polyacrylamide gel electrophoresis (PAGE) results for 4 different probes, labeled 7/0, 7/4, 7/5, and 7/6. Each probe has an initiation toehold of 7 nt, but differs in having a 0, 4, 5, or 6 nt blue toehold that spontaneously dissociates to release P.

The intensities of the PC, XC, and SC bands appear to be directly comparable: the sum of the PC and XC or SC band intensities in each lane was roughly conserved across all lanes

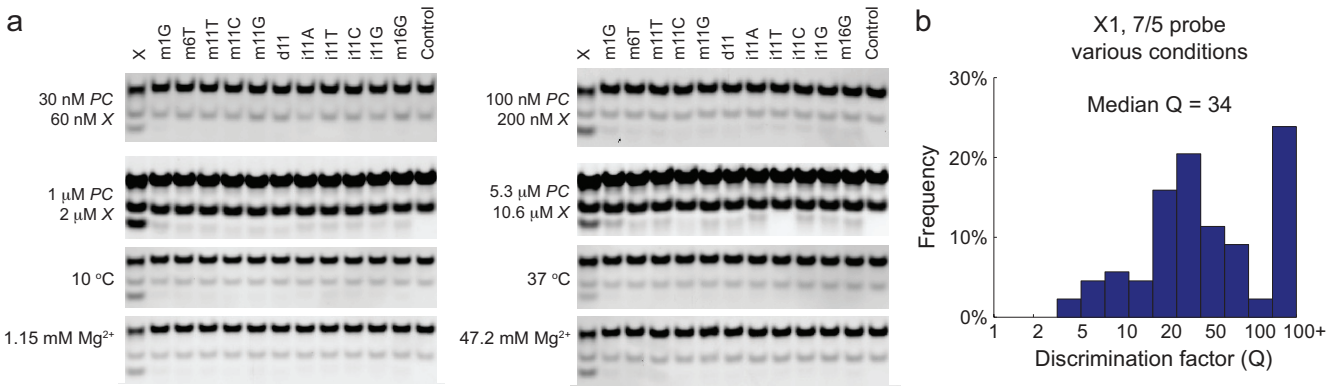

FIG. 2-5: Performance of the 7/5 probe for the $X1$ target at different conditions. **(a)** PAGE results. As in Fig. 3, the upper band is the unreacted PC complex, the middle band is excess P, and the bottom band is the product XC or SC band. **(b)** High discrimination factors were observed for all conditions tested (see Fig. S12-S14 for more details and results quantitation), with median $Q = 34$ across conditions. Histogram includes data from Fig. 3b, where the $X1$-7/5 probe was operated at standard conditions of 25 °C, 11.5 mM Mg^{2+}, and 100 nM PC.

(6.6% standard deviation, 156 samples, see Fig. S4B). We believe this is due to both species having a similar number of double-stranded base pairs, and the single-stranded nucleotides do not contribute significantly to band intensity because of their decreased efficiency of SybrGold staining. The experimentally observed hybridization yield of X is calculated as $\chi_X = \frac{\{XC\}}{\{XC\}+\{PC\}}$, where $\{XC\}$ and $\{PC\}$ denote the band intensity of XC and PC, respectively; χ_S is similarly defined. χ values are plotted in Fig. 3c.

Discrimination factors Q are calculated for each spurious target (e.g. $Q_{\mathrm{m1G}} = \frac{\chi_X}{\chi_{\mathrm{m1G}}}$) and plotted in Fig. 3d. The 7/0 probe does not achieve specificity—$Q \approx 1$ for all experiments. In contrast, the 7/4, 7/5, and 7/6 probes attain Q values between 2 and 10, 12 and 37, and 5 and 38, respectively.

The experimentally observed χ values are plotted in Fig. 3e for comparison against the χ values predicted by the reaction thermodynamics (thick black sigmoidal line), calculated using NUPACK software [32]. Adjusting the predicted ΔG° of all reactions by +1.5 kcal/mol significantly improves the agreement between theory and experiments. This +1.5 kcal/mol discrepancy may represent inaccuracy of existing DNA thermodynamic prediction tools,

specifically regarding the poly-T tail of P [33].

Theoretically, the 7/6 probes are expected to yield Q similar to or higher than the 7/5 probes. In practice, however, the observed Q was lower because χ_S for the 7/6 probes were significantly higher than predicted (values not shown). Oligonucleotide synthesis errors that remain despite purification [30, 34] likely contribute to spurious hybridization (Text S5). For example, a deletion at position 12 (from the $5'$ end) in the C strand would match the deletion of "d11", so the corresponding PC molecule would react more favorably with the "d11" spurious target than with X. Given the low values of χ_X observed for the 7/6 probes, a 7/7 toehold exchange probe (Fig. 3a) is expected to produce very low hybridization yield even with the correct target X, and hence not tested.

Theory predicts that the hybridization yield χ will vary with the concentration of X or S; this was experimentally verified (Fig. S5). However, even in a large excess ($200\times$) of spurious targets, we observed little hybridization to the probe ($\chi_S = 0.071$, Fig. 3f), and spurious targets do not significantly interfere with the hybridization of correct targets (Fig. S6).

Fig. 3g shows PAGE results for a fluorescent probe, in which C is $3'$-functionalized with the ROX fluorophore, and P is $5'$-functionalized with the Iowa Black Red Quencher (RQ). Upon hybridization to X or S, P is displaced, and the XC or SC complex fluoresces. This probe does not possess a 30 nt poly-T tail on P, but its fluorophore-quencher interaction thermodynamics also make the reaction ΔG° difficult to predict [36]. Incomplete quenching of ROX by RQ caused significant background signal (as evidenced by the visible band in the right-most Control lane), which decreased quantitation sensitivity of gel experiments. However, spectrofluorimeter experiments using these fluorophore/quencher-labeled constructs verified high discrimination factors at concentrations of 1 and 10 nM (Fig. S7). Additionally, the kinetics of equilibration were observed to be fast (rate constant $2 \cdot 10^6$ M^{-1} s^{-1}, under 20 minutes to completion at 1 nM).

Target sequence generality. To show that toehold exchange probes yield high hybridization specificity for many if not most sequences, we tested four additional sets of targets and probes (Fig. 4a). The $X2$ and $X3$ targets were the DNA analogs of the *let7g* and *mir155* microRNAs, which possess important roles in cancer [35]. The $X4$ and $X5$ targets were designed with significant secondary structure in the branch migration region and the green toehold, respectively. All five systems tested produced hybridization yields in agreement with theory (Fig. 4b, Fig. S8-S11). Each system required a slightly different ΔG° adjustment (Fig. 4b inset).

The discrimination factors Q achieved by the various 7/5 probes are plotted as a histogram in Fig. 4c. Except for two outliers that yielded $Q \approx 3$ ($X2$-m17G and $X5$-m13G), $Q \geq 8$ for all systems, with median $Q = 26$. Several spurious targets yielded no observable ($\chi_S < 0.002$) hybridization to the probe; these experiments are displayed as $Q = 100+$ on the histogram. The experimental values of Q appear to be similar in distribution to the theoretically predicted Q (Fig. 4d). Thus, the presented toehold exchange mechanism reliably separates nucleic acid sequences differing by a single nucleotide across diverse target sequences.

RNA targets. We next tested an RNA toehold exchange probe against a synthetic RNA target with sequence corresponding to the let-7g microRNA (Fig. 4ef). In this experiment, the XC band stained less efficiently than the PC band; χ and Q were thus inferred from quantitation of the PC band alone. The concentrations used are higher than for DNA experiments due to the low staining efficiency of RNA.

Robustness. Due to the $\Delta n = 0$ nature of the toehold exchange reaction (bimolecular with two products), the probes function robustly across oligonucleotide concentrations (Fig. 5, see Fig. S12 for $X1$-7/4 and $X1$-7/6 results). We were not able to accurately achieve $\Delta H^\circ = 0$ and $\Delta N = 0$ (no change in number of paired bases) due to the unexpected offset of ΔG°, but our 7/5 toehold exchange probes still managed to keep ΔH° and ΔN close to

zero and were relatively robust to temperature and salinity (Fig. 5).

Experiments based on the $X1$ target and 7/5 probe showed large discrimination factors for temperatures from 10 °C to 37 °C, salinities from 1.15 mM Mg^{2+} to 47.2 mM Mg^{2+}, and oligonucleotide concentrations from 30 nM to 5.3 μM (Fig. 5, Fig. S12-S14), with median $Q = 34$ for the $X1$ 7/5 probe across conditions. Fluorescence measurements further verified that the toehold exchange probes effectively discriminate single-base changes at concentrations down to 1 nM (Fig. S7).

Discussion

We have demonstrated that rationally designed toehold exchange probes achieve high hybridization specificity across a wide range of temperatures, salinities, and oligonucleotide concentrations. The 7/5 probes achieve a median discrimination factor of $Q = 26$ against single-base-changed spurious targets, and perform robustly across all conditions tested. For comparison, analysis of our toehold exchange probes predicts a median Q of 87, and the theoretical limit of the median is $Q_{\max} = 343$. The decreased performance may be attributed to (1) oligonucleotide synthesis impurities that lead to increased hybridization yield for spurious targets, (2) inaccurate literature values of mismatch, bulge, and dangle thermodynamics, and/or (3) limitations in quantitating hybridization yields less than 0.2%. Still, the discrimination factors experimentally achieved here are superior to previous hybridization probes (reported median $Q \leq 13$ [19]).

Previously, double-stranded probes have been used for single-nucleotide polymorphism (SNP) detection in an *in vitro* setting [37, 38]. However, these probes do not include the construction of the blue toehold that needs to spontaneously dissociate to release the protector, and hence spurious targets bind to the probes with strong thermodynamic favorability. Thus, these probes discriminate nucleic acids on a single-base level using initial **kinetics**, rather than **thermodynamics**. An equilibrium-based probe functions robustly regardless

of secondary structure (frequent in natural nucleic acids), whereas kinetics of hybridization and strand displacement reactions depend sensitively on secondary structure [30, 31]. To improve the specificity of the toehold-mediated strand displacement systems, previous works used competing sequences with perfect complementarity to the spurious targets to remove the spurious targets from solution [37, 38]. In contrast, our method does not require *a priori* knowledge of the position or identity of the single-base change.

Immediate applications of the toehold exchange probes arise in biotechnological methods that rely on the specificity of nucleic acid hybridization, such as microarray analysis [3, 4], fluorescence in situ hybridization [6, 7], SNP detection [39], etc. Enzyme-based amplification methods, such as rolling circle amplification [40] or PCR, can also benefit from methods to improve specificity; for example, double-stranded toehold exchange primers may improve the PCR yield in "high background" systems or in highly multiplexed systems where primer mishybridization may be a significant concern. Finally, branch migration and strand displacement-based synthetic nucleic acid nanodevices have been demonstrated to function within living cells [41, 42]; toehold exchange probes may potentially find use there as well.

Acknowledgements. The authors thank Mingjie Dai and Po-Shen Loh for assistance with mathematical analysis, Jaclyn Aliperti, Elizabeth Haney, Ralf Jungmann, and Tom Schaus for helpful manuscript preparation suggestions. This work was funded by the Wyss Institute for Biologically Inspired Engineering, NIH Director's New Innovator Award 1DP2OD007292, NSF CAREER Award CCF1054898, and Office of Naval Research Grant N000141010827 to P.Y. D.Y.Z. is a Howard Hughes Medical Institute postdoctoral fellow, as part of the Life Sciences Research Foundation program. There is a patent pending on the methods described in this work.

[1] Bartel, D. P. MicroRNAs: target recognition and regulatory functions. *Cell* **136,** 215-233 (2009).

[2] Saiki, R. K., Gelfand, D. H., Stoffel, S., Scharf, S. J., Higuchi, R., Horn, G. T., Mullis, K. B. & Erlich, H. A. Primer-directed enzymatic amplification of DNA with a thermostable DNA polymerase. *Science* **239,** 487-491 (1988).

[3] Schena, M., Shalon, D., Davis, R. W. & Brown, P. O. Quantitative Monitoring of Gene Expression Patterns with a Complementary DNA Microarray. *Science* **270,** 467-470 (1995).

[4] Gunderson, K. L., Steemers, F. J., Lee, G., Mendoza, L. G. & Chee, M. S. A genome-wide scalable SNP genotyping assay using microarray technology. *Nature Biotechnology* **37,** 549-554 (2005).

[5] Koltai, H. & Weingarten-Baror, C. Specificity of DNA microarray hybridization: characterization, effectors, and approaches for data correction. *Nucleic Acids Research* **36,** 2395-2405 (2008).

[6] DeLong, E. F., Wickham, G. S. & Pace, N. R. Phylogenetic Stains: Ribosomal RNA-Based Probes for the Identification of Single Cells. *Science* **243,** 1360-1363 (1989).

[7] Amann, R. I., Krumholz, L. & Stahl, D. A. Fluorescent-oligonucleotide probing of whole cells for determinative, phylogenetic, and environmental studies in microbiology. *J. Bacteriol.* **172,** 762-770 (1990).

[8] Seeman, N.C., Nanomaterials Based on DNA. *Annu. Rev. Biochem.* **79,** 65-87 (2010).

[9] Rothemund, P. Folding DNA to create nanoscale shapes and patterns. *Nature* **440,** 297-302 (2006).

[10] Douglas, S. M., Dietz, H., Liedl, T., Hogberg, B., Graf, F. & Shih, W. M. Self-assembly of DNA into nanoscale three-dimensional shapes. *Nature* **459,** 414-418 (2009).

[11] Aldaye, F.A., Palmer, A.L. & Sleiman, H.F. Assembling materials with DNA as the guide. *Science* **321,** 1795-1799 (2008).

[12] Yin, P., Choi, H.M.T., Calvert, C.R. & Pierce, N.A. Programming biomolecular self-assembly pathways. *Nature* **451,** 318-322 (2008).

[13] Zhang, D. Y. & Seelig, G. Dynamic DNA nanotechnology using strand displacement reactions. *Nature Chemistry* **3,** 103-114 (2011).

[14] Tyagi, S. & Kramer, F.R. Molecular beacons: probes that fluoresce upon hybridization. *Nature Biotechnology* **14,** 303-308 (1996).

[15] Tyagi, S., Bratu, D. P., & Kramer, F. R. Multicolor molecular beacons for allele discrimination. *Nature Biotechnology* **16,** 49-53 (1998).

[16] Tyagi, S. Imaging intracellular RNA distribution and dynamics in living cells. *Nature Methods* **6,** 331-338 (2009).

[17] Bonnet, G., Tyagi, S., Libchaber, A. & Kramer, F. R. Thermodynamic basis of the enhanced specificity of structured DNA probes. *Proc. Nat. Acad. Sci.* **96,** 6171-6176 (1999).

[18] Tsourkas, A., Behlke, M. A., Rose, S. D. & Bao, G. Hybridization kinetics and thermodynamics of molecular beacons. *Nucleic Acids Research* **31,** 1319-1330 (2003).

[19] Xiao, Y., Plakos, K. J. I., Lou, X., White, R. J., Qian, J., Plaxco, K. W. & Soh, H. T. Fluorescence detection of single-nucleotide polymorphisms with a single, self-complementary, triple-stem DNA probe, *Angew. Chemie*

Int. Ed. **48,** 4354-4358 (2009).

[20] Kolpashchikov, D. M. A Binary DNA Probe for Highly Specific Nucleic Acid Recognition, *J. Am. Chem. Soc.* **128,** 10625-10628 (2006).

[21] Dave N. & Liu, J. Fast Molecular Beacon Hybridization in Organic Solvents with Improved Target Specificity, *J. Phys. Chem. B* **114,** 15694-15699 (2010).

[22] SantaLucia, J. & Hicks, D. The Thermodynamics of DNA Structural Motifs. *Ann. Rev. Biochem.* **33,** 415-440 (2004).

[23] Peyret, N. *Prediction of Nucleic Acid Hybridization: Parameters and Algorithms.* Doctoral thesis, Wayne State University. (2000)

[24] Tan, Z. J. & Chen, S. J. Nucleic Acid Helix Stability: Effects of Salt Concentration, Cation Valence and Size, and Chain Length. *Biophys. J.* **90**, 1175-1190 (2006).

[25] Yurke, B., Turberfield, A. J., Mills, A. P., Simmel, F. C. & Neumann, J. L. A DNA-fuelled molecular machine made of DNA. *Nature* **406,** 605-608 (2000).

[26] Zhang, D.Y. & Winfree, E. Control of DNA Strand Displacement Kinetics Using Toehold Exchange. *J. Am. Chem. Soc.* **131,** 17303-17314 (2009).

[27] Zhang, D.Y., Turberfield, A.J., Yurke, B. & Winfree, E. Engineering entropy-driven reactions and networks catalyzed by DNA. *Science* **318,** 1121-1125 (2007).

[28] He, G., Rapireddy, S., Bahal, R., Sahu, B. & Ly, D.H. Strand invasion of extended, mixed-sequence B-DNA by gamma PNAs. *J. Am. Chem. Soc.* **131,** 12088-12090 (2009).

[29] Petersen, M. & Wengel, J. LNA: a versatile tool for therapeutics and genomics. *Trends Biotechnol.* **21,** 74-81, (2003).

[30] Zhang, D.Y. & Winfree, E. Robustness and modularity properties of a non-covalent DNA catalytic reaction. *Nucleic Acids Research* **38,** 4182-4197 (2010).

[31] Gao, Y., Wolf, L.K. & Georgiadis, R.M. Secondary structure effects on DNA hybridization kinetics: a solution versus surface comparison. *Nucleic Acids Research* **34,** 3370-3377 (2006).

[32] Dirks, R.M., Bois, J.S., Schaeffer, J. M., Winfree, E. & Pierce, N.A. Thermodynamic Analysis of Interacting Nucleic Acid Strands. *SIAM Review* **49,** 65-88 (2007).

[33] Bommarito, S.; Peyret, N. & SantaLucia, J. Thermodynamic parameters for DNA sequences with dangling ends. *Nucleic Acids Resesarch* **28**, 1929-1934 (2000).

[34] Temsamani, J., Kubert, M. & Agrawal, S. Sequence identity of the n-1 product of a synthetic oligonucleotide. *Nucleic Acids Research* **23,** 1841-1844 (1995).

[35] J. Lu *et al.* MicroRNA expression profiles classify human cancers. *Nature* **435,** 834-838 (2005).

[36] S. A. Marras, F. R. Kramer & S. Tyagi. Efficiencies of fluorescence resonance energy transfer and contact-mediated quenching in oligonucleotide probes. *Nucleic Acids Research* **30,** e122 (2002).

[37] Li, Q., Luan G., Guo, Q. & Liang J. A new class of homogeneous nucleic acid probe based on specific displacement hybridization, *Nucleic Acids Research* **30,** e5 (2002).

[38] Subramanian, H. K. K., Chakraborty, B., Sha, R. & Seeman, N. C. The label-free unambiguous detection and

symbolic display of single nucleotide polymorphisms on DNA origami. *Nano Letters* **11,** 910-913 (2010).

[39] Kim, S. & Misra A. SNP genotyping: technologies and biomedical applications. *Annu. Rev. Biomed. Eng.* **9,** 289-320 (2007).

[40] Lizardi, P.M. *et al.* Mutation detection and single-molecule counting using isothermal rolling-circle amplification. *Nature Genetics* **19,** 225-232 (1998).

[41] Isaacs, F.J. *et al.*, Engineered riboregulators enable post-transcriptional control of gene expression. *Nature Biotechnology* **22,** 841-847 (2004).

[42] Venkataraman, S., Dirks, R.M., Ueda, C.T. & Pierce, N. Selective cell death mediated by small conditional RNAs. *Proc. Nat. Acad. Sci.* **107,** 16777-16783 (2010).

Methods

DNA oligonucleotides. DNA and RNA oligonucleotides used in this study were purchased from Integrated DNA Technologies (IDT). DNA oligonucleotides shorter than 50 nt in length were HPLC purified by IDT, while DNA oligonucleotides 50 nt or longer were PAGE purified by IDT. RNA oligonucleotides underwent RNAse-free HPLC by IDT.

Standard buffer conditions. Individual DNA oligonucleotides were resuspended and stored in TE buffer (10 mM Tris · HCl pH balanced to 8.0, with 1 mM EDTA·Na_2, purchased as 20× stock from Invitrogen) at 4 °C. Directly preceding experiments, TE buffer with 62.5 mM $MgCl_2$ was added at 1:4 ratio to the sample, achieving a final $MgCl_2$ concentration of 12.5 mM. Because roughly 1 mM of the Mg^{2+} is chelated by the EDTA present in solution, the free concentration of Mg^{2+} is estimated to be 11.5 mM.

Probe preparation. The probes always consisted of two strands, the protector and the complement. In all experiment, the probe was prepared by adding a 2× excess of protector to the complement in 1× TE/Mg^{2+} buffer, and the solution was then annealed from 92 °C to room temperature over the course of 70 minutes. Other experiments not displayed have shown that annealing was not necessary for probe formation.

Polyacrylamide gel electrophoresis (PAGE). Native polyacrylamide gel electrophoresis (PAGE) was used to evaluate hybridization yield. All experiments shown used data from 10% native polyacrylamide gel electrophoresis. The gel solutions were prepared from 40% 19:1 acrylamide:bisacrylamide stock (J.T. Baker Analytical) in 1× TAE/Mg^{2+} solution, and casted in 1.5 mm thick plastic gel cassettes (Invitrogen).

Native loading dye containing xylene cyanol-FF (Sigma Aldrich) in 50% glycerol was added to all samples, achieving final glycerol concentration of 10% by volume. Most gels were run at 25 °C using Novex Mini-cell chambers (Invitrogen), using 100 V for 90 minutes. For temperature studies shown in Fig. S12, the 10 °C sample was run at 100 V for 120

minutes in a 10 °C water bath and the 37 °C sample was run at 100 V for 70 minutes in a 37 °C water bath.

After running, gels containing DNA were stained with SybrGold stain (Invitrogen) for 25 to 45 minutes. The gel containing RNA was stained with SybrGreen II stain (Invitrogen) for 30 minutes.

Gel quantitation. Gel band quantition used for infering reaction completion used a Typhoon FLA 9000 gel imager. The ImageQuant TL software (GE Healthcare) was subsequently used to perform band detection, background subtraction, and band quantitation. Due to the limitations of the gel imager, bands showing hybridization yields below 0.2% could not be consistently quantified (due to SybrGold background). The hybridization yield of the correct product (for 7/5 experiments) varied between 20% and 70%; consequently, the limit for discrimination factor Q varied between 100 and 350. To prevent reader confusion regarding different Q limits for different systems, we opted to go with the lowest of these numbers (100), rounding down all observed Q greater than 100 to be "100+". See Fig. S4 for further details on gel band quantitation.

Standard free energy calculations. NUPACK [32] was used to calculate the standard free energies of DNA strands and complexes. NUPACK uses a number of different parameters in its calculations; the values used are detailed and justified below.

Temperature was set to 25 °C, as that was the temperature at which experiments were performed. Salt concentration was set to 0.05 M Na^+ and 0.0115 M Mg^{2+}. In actuality, the experimental concentration of Na^+ is 0.002 M, but 0.05 M Na^+ was the lowest NUPACK allowed. However, since Mg^{2+} acts as the main counterion, it is likely that this difference does not significantly change the standard free energies. The "Dangles" parameter was set to "some," although setting it to all would yield identical results because there are no instances of coaxial stacks in any structures.

Time-based fluorescence studies. Kinetic fluorescence measurements were per-

formed using a PTI QuantaMaster40 spectrofluorimeter and Hellma Semi-Micro 114F spectrofluorimeter cuvettes. Excitation wavelength was set to be 584 nm, and emission wavelength was set to be 602 nm, consistent with the properties of the ROX fluorophore. Slit sizes were set at 5 nm for all monochromators. An external temperature bath maintained a reaction temperature of 25±1 °C.

Chapter 3: Conditionally fluorescent molecular probes for detecting single base changes in double-stranded DNA

This work was published in Nature Chemistry in 2013, and describes the design and validation of modified toehold probes for specific detection of double-stranded nucleic acid sequences. The key insight in this work is the observation that double-stranded DNA variants will possess sequence variation on both strands, and hybridization to a mismatched probes could result in two mismatch bubbles that lead to quadratically better discrimination. We applied these probes to DNA purified from wildtype and rifampicin-resistant E. Coli, and validated mutations in a 180 nt region of the rpoB gene in all resistant colonies.

Abstract: Small variations in nucleic acid sequences can have far-reaching phenotypic consequences. Reliably distinguishing closely related sequences is therefore important for research and clinical applications. Here, we demonstrate that conditionally fluorescent DNA probes are capable of distinguishing variations of a single base in a stretch of target DNA. These probes use a novel programmable mechanism in which each single nucleotide poly-

morphism generates two thermodynamically destabilizing mismatch bubbles rather than the single mismatch formed during typical hybridization-based assays. Up to 12,000-fold excess of a target containing a single nucleotide polymorphism is required to generate the same fluorescence as one equivalent of the intended target, and detection works reliably over a wide range of conditions. Using these probes we detected point mutations in a 198 base pair subsequence of the *E. Coli rpoB* gene. Our probes are constructed from multiple oligonucleotide fragments, circumventing synthesis limitations and enabling long continuous DNA sequences to be probed.

Nucleic acids are the genetic signature molecules for all life; sequences and expression levels of biological nucleic acids provide information about the state of an individual cell or a whole organism. Often, small differences — even single base changes — between otherwise identical nucleic acid sequences can have important biological and biomedical implications: single base mutations such as insertions, deletions, and single nucleotide polymorphisms (SNPs) form the genetic basis for a variety of human diseases [1, 2] or can confer drug resistance to pathogenic bacteria or viruses [3, 4]. Consequently, the fast, simple, and accurate detection, analysis, and quantitation of nucleic acid sequences with single base resolution are important research goals with vast potential for biomedical applications.

Virtually all nucleic acid detection technologies utilize the specificity of Watson-Crick base pairing; single-stranded probe [5] or primer [6] molecules capture intended DNA or RNA target molecules of complementary sequence. However, cross-hybridization between closely related probe-target pairs can occur; such imperfect probe-target binding may be kinetically trapped (i.e. dissociate slowly) and practically prevent intended hybridization reactions. In order to achieve single-base specificity, many diagnostic assays exploit the

sensitivity of enzymes [8–11] to the presence of mismatch bubbles within their DNA substrates. DNA-templated, non-enzymatic ligation reactions can also be highly sensitive to point mutations in the template [12, 13].

Alternatively, the complementary probe molecules themselves can be engineered to possess greater specificity to the intended target molecule. For example, incorporation of chemically modified bases [14, 15] can increase the affinity of a probe to a correct target. Consequently, disruption of correct base pairing results in a higher energetic penalty and better discrimination [16, 17]. Hairpins and other structural elements can be introduced into the probe molecule to make binding to both the correct and SNP target less energetically favorable such that small energetic differences can result in strong differences in the hybridization yield [18–20]. However, reaction conditions often need to be finely tuned for optimal performance, and it is difficult to assay long nucleic acid molecules for single base changes. A comprehensive review of SNP detection methods can be found in [2].

Here we present a class of conditionally fluorescent molecular probes that effectively discriminate single-base changes in primarily double-stranded DNA (dsDNA), work robustly for a wide range of conditions, and identify single base changes within long stretches of DNA. Our approach relies on a novel mechanism that we termed "double-stranded toehold exchange," and uses a rationally designed double-stranded probe with forked single-stranded overhangs (Fig. 1a). We first demonstrated our probes on a set of synthetic dsDNA targets. The reaction of the probe with any SNP target – a molecule that differs from the intended target by a single base pair – exhibited negligibly low yield. Experimentally, up to a 12,000-fold excess of a target was needed to achieve the same fluorescence signal as a stoichiometric amount of the intended target, comparable to the best enzyme-based methods. Subsequently, we extended our approach to the detection of point mutations in the *E. coli rpoB* gene. Our probes correctly identified point mutations responsible for resistance to the antibiotic rifampicin [21, 22].

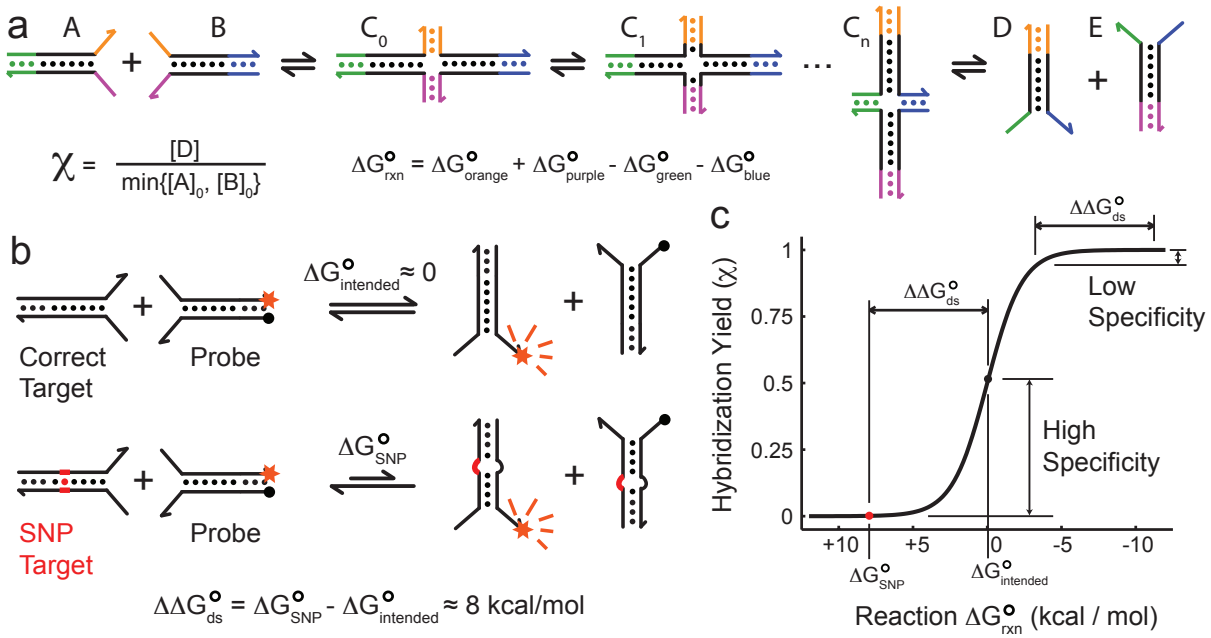

FIG. 3-1: Schematic representation of the double-stranded toehold exchange mechanism **(a)** The reaction starts with the hybridization of the initiation toeholds (orange and purple), forming a four-stranded complex C_0. Next, the four-stranded complex undergoes a series of single-base reconfiguration events known as branch migration [23]. The various states of branch migration (C_i) are roughly isoenergetic, and thus each branch migration step is reversible and unbiased. When the branch migration reaches state C_n where the four-stranded complex is held together only by the dissociation toeholds (blue and green), these dissociation toeholds can spontaneously dissociate to release the two product molecules. **(b)** A highly specific, conditionally fluorescent molecular probe based on four-stranded toehold exchange. The probe is functionalized at the balancing toeholds with a fluorophore and a quencher on separate strands; at the end of the reaction, the fluorophore is delocalized from the quencher and fluorescence increases. The lengths and sequences of the toeholds are designed so that the $\Delta G^\circ_{\text{intended}}$ of reaction between the probe and the intended target is roughly 0. The reaction between the probe and the SNP target will result in two mismatch bubbles, and the reaction $\Delta G^\circ_{\text{SNP}}$ will be about 8 kcal/mol. **(c)** Plot of the analytic hybridization yield (χ) at equilibrium of the $A + B \rightleftharpoons D + E$ reaction against the reaction ΔG° (assuming that identical initial concentrations of A and B). Designing $\Delta G^\circ_{\text{intended}} \approx 0$ ensures a balance of high specificity and high yield.

Double-stranded toehold exchange. The double-stranded toehold exchange mechanism is shown in Fig. 1a. The reactants (A and B) are two primarily double-stranded nucleic acid molecules; each possesses single-stranded overhangs at the 5' end of one strand and at the 3' end of the other. These overhangs, shown in orange and purple, are termed *initiation toeholds*. Toeholds of matching color are complementary to each other, and hybridize to initiate

the reaction. The initial four-stranded complex (C_0) then undergoes a "branch migration" process through a series of isoenergetic four-stranded states (C_1 through C_n) [23]. Finally, when the branch migration reaches the other terminus (C_n), the blue and green *dissociation toeholds* spontaneously fall apart to release two primarily double-stranded products (D and E).

The equilibrium concentrations of the various states depend on the length and base compositions of the toeholds, as well as the length of the homologous branch migration region (shown in black, see Text S1). In solutions with low divalent metal cation concentrations, the transition rates between different intermediate C states are high [26], and the reaction is rate limited by toehold association and dissociation processes. With proper selection of toehold strengths, both the forward and reverse kinetics are fast, and the reaction rapidly equilibrates from any initial state.

We here focus on the problem of constructing high specificity probes for SNP detection, we envision that the double-stranded toehold exchange can also be used for a variety of other applications, such as the modular construction of complex biomolecular circuits for the logical and temporal control of DNA [27–32] and other molecules [33–35].

Conditionally fluorescent dsDNA probe. To adapt the double-stranded toehold exchange mechanism into highly specific molecular probes for dsDNA (Fig. 1b), we designed the initiation and dissociation toeholds to be similar in length and sequence so that the reaction with the intended target has $\Delta G^\circ_{\text{intended}} \approx 0$. The reaction with SNP targets will have $\Delta G^\circ_{\text{SNP}}$ that is about +8 kcal/mol [36], due to the formation of the two mismatch bubbles (Fig. 1b). The probes discriminate intended targets from SNP targets by taking advantage of the fact that small ΔG° changes near $\Delta G^\circ = 0$ have disproportionately large effects on the hybridization yield χ (Fig. 1c). Because $\Delta G^\circ_{\text{intended}}$ is designed to be approximately 0, a favorable balance is achieved between the binding yield of the intended

target (roughly 50%) and the specificity (within a constant factor of optimal, see Fig. 1c and Text S2). Thus, the probe is designed to bind specifically to one particular sequence; a spurious molecule that differs by even a single base pair from the intended target, regardless of position within the duplex, exhibits significantly lower binding at equilibrium.

We use fluorescence to directly measure hybridization yield. At the opposite end of the initiation toeholds, the probe is functionalized with a fluorophore on one strand and a quencher on the other strand; the close proximity of the fluorophore and quencher ensures that the probe is natively in a dark state. Upon completion of the double-stranded toehold exchange, the fluorophore and quencher are no longer colocalized on the same molecule, and fluorescence increases.

To implement the desired $\Delta G^{\circ}_{\text{intended}} \approx 0$ criterion, we designed the initiation toeholds (orange and purple) to form 5 base pairs (bp) each, and the dissociation toeholds (blue and green) to form 4 bp each (see Text S1 for discussion on toehold lengths). The dissociation toeholds are shorter than the initiation toeholds because the interaction between the fluorophore and quencher stabilizes the reactants [37].

Results

To test whether the fluorescent probe based on double-stranded toehold exchange functions as intended, we first designed an arbitrary 14 base pair dsDNA sequence. The initiation and dissociation toeholds (see Methods for sequence design) were then appended to the ends, resulting in an intended target molecule with 18 base pairs. To facilitate experimentation on the effects of reaction ΔG°, we designed the probe to each possess 6 nt of initiation toehold, but the effective toehold is determined by the shorter of the toeholds for the probe and the target, and the latter was designed to be 5 nt for the experiments shown here in the main text. Fourteen SNP target molecules were designed that each differed from the intended target by one base pair (Fig. 2a). These base changes were distributed

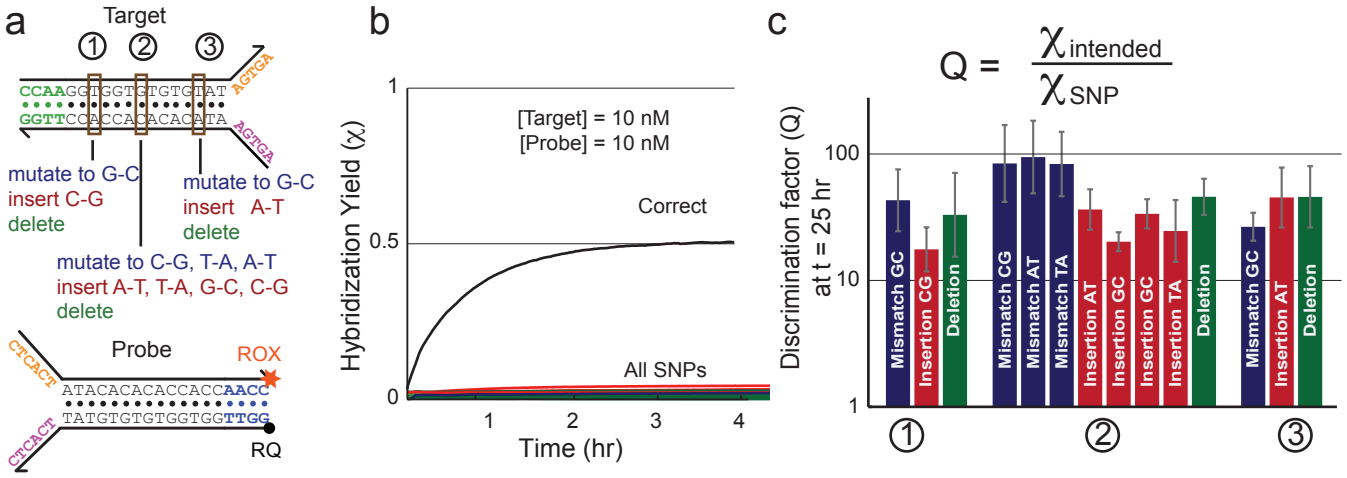

FIG. 3-2: Discrimination of SNPs by the dsDNA probe. **(a)** Sequence of the intended target and the positions/identities of base pair changes that lead to the 14 SNP targets. Circled 1, 2, and 3 denote the positions of the mismatch. Mismatches, insertions, and deletions are respectively shown in blue, red, and green. **(b)** Hybridization yield, as inferred from fluorescence kinetics (see Fig. S1 and Methods). The probe is present in solution initially, and the intended or SNP target is introduced at $t \approx 0$. Experiments were run at 25 °C in 1 M Na^+. The trace for intended target is shown in black, and traces for SNP targets are shown in the colors described above (see Fig. S2 for zoom-in of SNP reactions). **(c)** Reactions equilibration appears to be complete after 4 hours; to ensure equilibration, however, the reactions were allowed to proceed until $t = 25$ hr. The hybridization yields at $t = 25$ hr are taken to be the equilibrium values, and discrimination factors $Q = \frac{\chi_{\text{intended}}}{\chi_{\text{SNP}}}$ are calculated for each SNP target. Observed Q values range between 17 and 99 (median = 43). Error bars show standard deviations calculated from three repetitions of each experiment.

at three different positions along the testing region, and included insertions, deletions, and replacements.

Fig. 2b shows the inferred hybridization yield $\chi = \frac{[D]}{[B]_0}$, where D is the fluorescent product and $[B]_0$ is the initial concentration of probe (for all experiments, $[A] \geq [B]$). See Methods and Fig. S1 for details on derivation of χ from raw fluorescence values. The discrimination factor $Q = \frac{\chi_{\text{intended}}}{\chi_{\text{SNP}}}$ quantifies the single-base specificity of the probe as the ratio of the hybridization yields (fluorescence) generated by equal concentrations of the intended and SNP targets; Q at $t = 25$ hr is plotted in Fig. 2c, and ranged between 17 and 99, with a median of 43. Operation of the probe is robust to the concentration of the probe; at lower probe concentrations, kinetics are slower, but discrimination at equilibrium is preserved (Fig. S3).

For spurious targets that differ from the intended target by more than one base pair, analysis predicts that the discrimination factor will be roughly exponential in the number of base pair changes (e.g. a spurious target with 2 base pair changes would yield a discrimination factor of roughly $Q \approx 43^2 \approx 1800$). However, the sensitivity of our equipment precludes the accurate measurement of hybridization yields lower than about 0.002; consequently, spurious targets that differ by two or more base pairs were not tested.

It is important to note that, like molecular beacons and other nucleic acid hybridization probes, our double-stranded probe does not in itself employ molecular or fluorescence amplification. For our *E. Coli* experiments, the colony PCR step provided the amplification to generate enough target for fluorescence analysis. Without amplification, the sensitivity of our probes is limited by the sensitivity of the fluorescence readout. For a typical fluorimeter, the sensitivity limit is around 100 pM of unquenched fluorophores (Fig. S4).

Concentration equivalence. The concentration equivalence R denotes the excess of SNP target needed to yield the same level of fluorescence (50% of maximum) as that of the intended target at equal concentration to the probe. An R-fold excess of the SNP target yields a false positive, so R determines the specificity of a diagnostic assay based on this technology. For typical hybridization probes, $R \approx Q$; however, for our double-stranded probes, the value of R is approximately Q^2 (see Text S3 for mathematical details). The quadratic relation between R and Q is due to the fact that there are two products whose concentrations will increase to compensate for an increase in target concentration to maintain equilibrium: for the same value of $K_{eq} = \frac{[D][E]}{[A][B]}$, both $[D]$ and $[E]$ increase to balance out an increase in $[A]$. An increase in the amount of SNP targets will thus only have a square root effect on the observed fluorescence (rather than a linear effect); consequently, high stoichiometric ratios of SNP targets have a much smaller effect on the double-stranded probes than on standard hybridization probes.

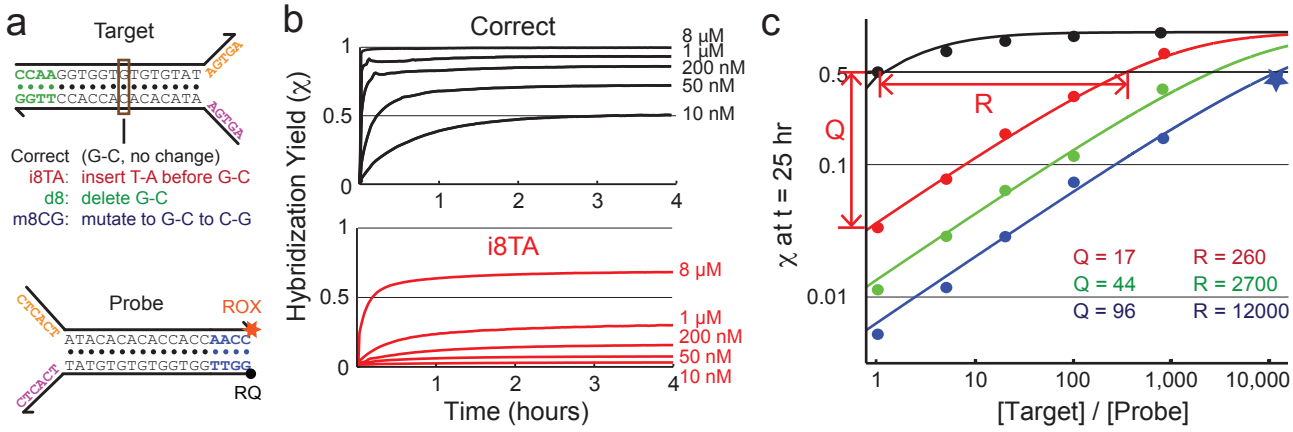

FIG. 3-3: Analysis and measurement of the concentration of SNP target needed to generate the same hybridization yield as a stoichiometric (relative to probe) amount of intended target (concentration equivalence R). **(a)** Sequences of intended and SNP targets used for experiments in this figure. **(b)** Hybridization yields (χ) of various concentrations of intended and "i8TA" SNP target. In all traces, initial probe concentration $[B]_0 = 10$ nM. **(c)** Hybridization yields plotted against the stoichiometric ratio of the target. As with previous experiments, the hybridization yield was inferred from fluorescence value at $t = 25$ hr. Experimentally determined values are shown as dots and star, and solid lines show the analytic model prediction based on best-fit ΔG° values (Text S1). All experiments other than the star data point were performed with 10 nM probe; the star data point reaction was performed with 2 nM probe to conserve reagents. Concentration equivalence R values are calculated based on best-fit models at 50% hybridization yield, and ranges between 260 and 12,000. Analysis shows and experiments verify that $R \approx Q^2$, with $Q = \frac{\chi_{\text{indented}}}{\chi_{\text{SNP}}}$ being the discrimination factor.

Fig. 3b shows the response of the probe to various concentrations of the intended target and one particular SNP target "i8TA." Whereas 10 nM of the intended target results in approximately 50% hybridization yield at equilibrium ($\chi_\infty = 0.5$), between 1 and 8 μM of the SNP target is needed to generate the same yield (fluorescence), indicating that the R for "i8TA" is between 100 and 800. Similar experiments were performed for two additional SNP targets, "d8" and "m8CG," and the hybridization yields χ of these reactions at $t = 25$ hr are plotted against the concentrations of the SNP targets in Fig. 3c. The solid lines in Fig. 3c show the analytic dependence of equilibrium χ on the concentrations of the intended and SNP targets using best-fit reaction ΔG° (Text S2). Listed R values show the horizontal distance between black curve for the intended target and the colored curves for the SNP targets. The listed Q values are determined from the hybridization yields at 1:1

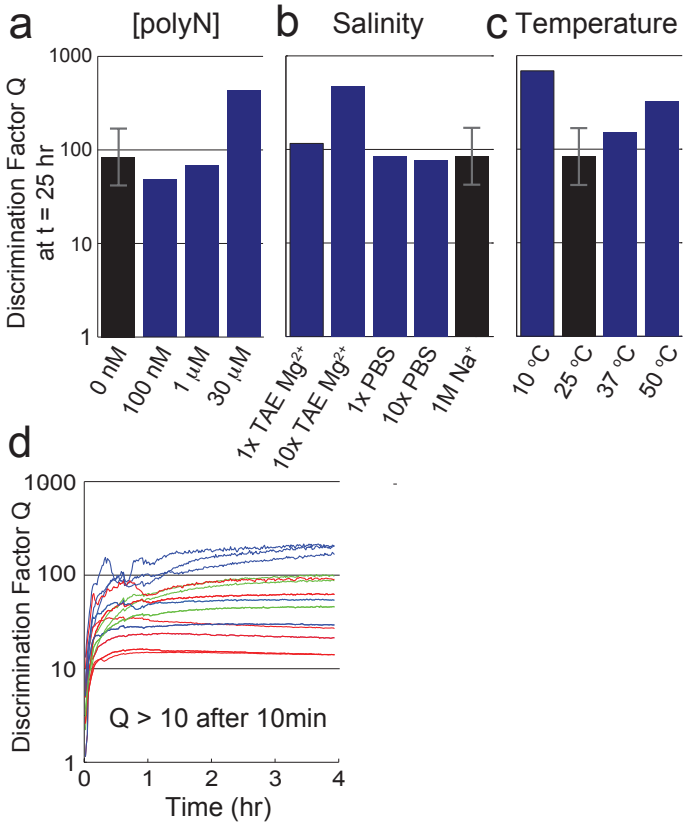

FIG. 3-4: Characterization of the background, temperature, salinity, and time robustness of the probe. The probe operates robustly to discriminate SNPs **(a)** in the presence of high concentrations of 50 nt polyN strands, **(b)** in different salinity buffers, and **(c)** at different temperatures (see also Fig. S5 and S6). **(d)** The discrimination factor Q approaches its final value after about 10 minutes of reaction, and maintains high discrimination indefinitely. The initial rise and bumpiness in Q can be attributed to fluorescence signal instability directly following addition of target to solution (see Fig. S2).

stoichiometry of target to probe after 25 hours of reaction. Thus, experiments verify that R varies roughly as the square of Q.

Robustness. Diagnostic assays of DNA samples benefit from solution robustness because biological samples or PCR products can be directly analyzed without separate purification and/or buffer exchange procedures. The primarily double-stranded nature of the targets and probes confers a high degree of robustness to non-cognate single-stranded nucleic acids in solution. Fig. 4a shows that discrimination is robust in up to 30 μM of a 50 nucleotide polyN sequence mixture (in which every position has roughly equal probability of being G,

C, A, or T). In contrast, probes and reactions based on single-stranded oligonucleotides are significantly affected by 1 μM of polyN sequence mixture [31].

Likewise, temperature robust diagnostic assays would be desirable in point-of-care and/or resource-limited settings, where precise temperature control equipment may not be available. At different salinities or temperatures, the $\Delta G^\circ \approx 0$ property required for high specificity is preserved because changes to the thermodynamic favorability of base pairing affects both the reactants and products equally; consequently, probes should be highly specific at equilibrium across a wide range of temperatures and salinities. Experimentally, the probes showed high discrimination at equilibrium between the intended target and the SNP target in 1× PBS, 10× PBS, 12.5 mM Mg^{2+}, and 125 mM Mg^{2+} (at 25 °C, Fig. 4b) and at 10 °C, 25 °C, 37 °C, and 50 °C (in 1 M Na^+, Fig. 4c).

We next asked how quickly our probes could distinguish an SNP target from an intended target. For this, we calculated the hybridization yields for the data in Fig. 2b as a function of time; that is, we divided the fluorescence values for an SNP target by the fluorescence value for the intended target at each time point (Fig. 4d). We found that $Q > 10$ for all SNP targets less than 20 minutes after the initiation of the reaction; thus a reliable result is obtained long before the detection reaction reaches equilibrium, and this high Q is maintained indefinitely (Fig. 4d). In contrast, previous double-stranded DNA probes that utilize four-way branch migration [26, 38–41] do not use the dissociation toeholds and discriminate SNPs using kinetics; consequently, at equilibrium, both intended and SNP targets will be nearly 100% bound to probe and discrimination is only possible at early time points in the reaction, increasing the likelihood of false positive results (Fig. S7 and S8).

Finally, we performed a number of experiments comparing the SNP discrimination performance of our dsDNA probes to molecular beacons (Fig. S9 and S10). In all cases, dsDNA probes showed significantly higher discrimination factors; this was particularly true for ex-

periments targeting a subsequence of the *E. Coli rpoB* gene, as the target had significant secondary structure. Our dsDNA probes were not affected by secondary structure, and furthermore could reliably distinguish 1 nucleotide change within 198 nt, whereas molecular beacons were limited to detection of 1 nucleotide change within 15 nt.

Biologically-derived samples. Single base mutations in bacterial genomes can confer resistances to antibiotics. For example, the *rpoB* gene encodes the β subunit of bacterial RNA polymerase; many mutations in *rpoB* preserve polymerase function but confer rifampicin-resistance in *E. coli, M. tuberculosis,* and other bacteria [21, 22]. To prevent widespread antibiotic resistance, it is desirable to treat non-rifampicin resistant infectious bacteria with rifampicin, and resort to less widespread drugs only when necessary. To facilitate such tactical use of antibiotics, fast, accurate, and low-cost drug resistance assays are needed.

As a proof-of-concept demonstration that double-stranded toehold exchange probes can be used for drug resistance assays, we designed and tested three probes targeting subsequences of the *rpoB* gene (Fig. 5a). The two shorter probes tested nucleotides 1531-1599 and 1684-1728 (corresponding to codons 511-533 and 562-576). The probes were functionalized with spectrally distinct fluorophores (ROX and Tye563), and operated simultaneously in solution. The longer probe tested the entire 198 base pair subsequence from 1531-1728 (codons 511-576). The target DNA was generated from *E. coli* colonies via a two-step process: colony PCR was first used to pre-amplify the *rpoB* subsequence, and unbalanced PCR was used to generate each of the two strands that comprise the target (Fig. 5b).

Probes used here were discontinuous and were assembled from 4 complementary overlapping sequences, rather than just 2 (Fig. 5b). This design changes was necessary because fluorophore- or quencher-functionalized oligonucleotides of more than 50 nt cannot be efficiently synthesized. Our experiments revealed that the probe effectively discriminates SNPs despite nicks in the branch migration region.

Experimentally, DNA from all ten rifampicin-resistant colonies exhibited mismatch behavior in either the 1531-1599 region or the 1684-1728 region; in contrast, the wild-type DNA induced increase in fluorescence for probes targeting both regions (Fig. 5c, Fig. S11-S15). Sequencing confirmed the presence of one or more mutations in these two regions for all ten colonies.

The probes for the 1531-1599 region and for the 1684-1738 region utilized different toehold sequences; the difference in toehold strengths may have contributed to the different kinetics observed for the blue and green traces in Fig. 5c. Kinetics are highly sensitive to toehold thermodynamics (e.g. 0.4 kcal/mol change results in 2-fold difference in kinetics). However, equilibrium-based probes, such as the double-stranded toehold exchange probes present here, are robust to these kinetic differences.

We also demonstrated that similar probes and targets with only one initiation toehold and one dissociation toehold function to reliably discriminate single-base changes, albeit with slower kinetics than probes using forked toeholds (Fig. S16). Target and probe molecules with only a single overhang are more easily prepared from biological samples, e.g. using a restriction enzyme or PCR with a modified primer.

Discussion

Using the mechanism of double-stranded toehold exchange, we developed a novel technology for the reliable detection of individual base pair changes in double-stranded DNA. Our discrimination method worked reliably for a wide range of mutations at different positions within a duplex, with a median discrimination factor $Q = 43$. Detection was robust to changes in temperature and salinity, and even to up to 30 μM of a mixture of non-cognate single-stranded DNA (representing a 3000-fold excess over probe and target concentrations). Depending on the type of base change, a 260- to 12,000-fold excess of the SNP target was tolerated before the signal due to the mutated target became comparable to that of a correct

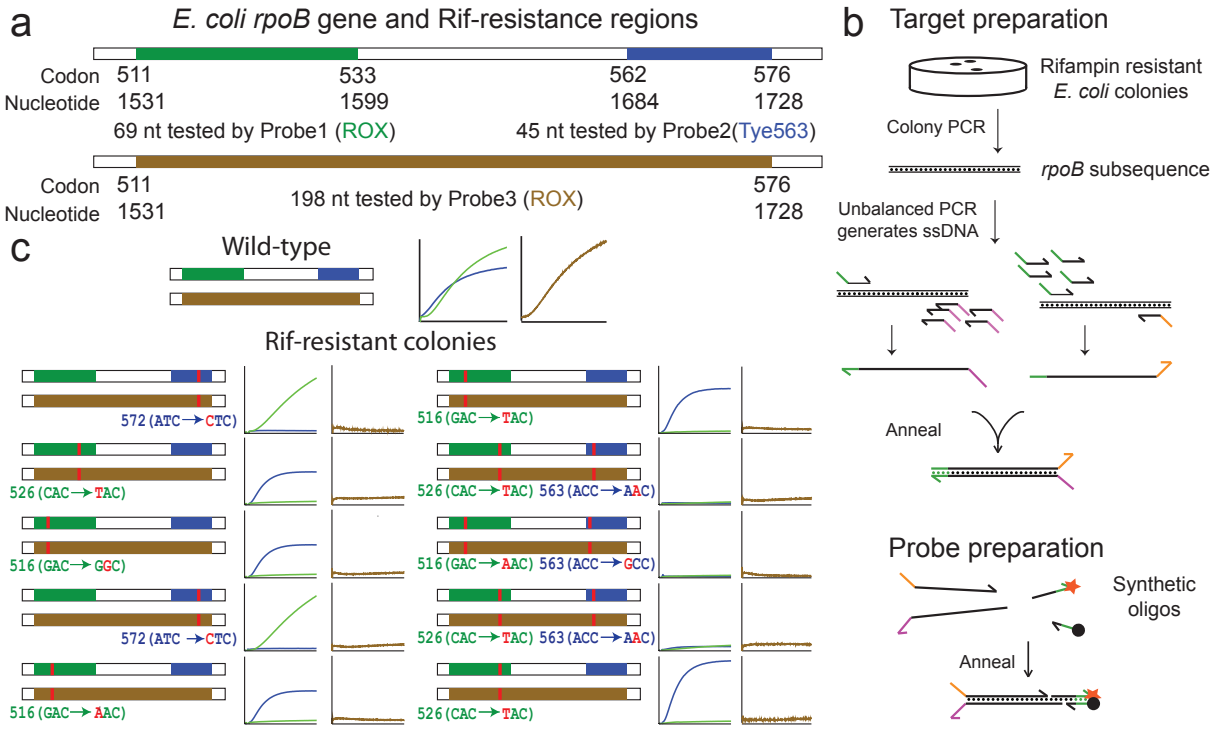

FIG. 3-5: Detection of SNPs in *E. coli*-derived samples. **(a)** Rifampicin resistance is typically confered by mutations in one of two regions in the *rpoB* gene, nucleotides 1531-1599 and 1684-1728, corresponding to amino acid residues 511-533 and 562-576. Here, we generated three distinct probes, one to test each region, and one to test both simultaneously. See Fig. S17 for sequences of probes and targets. **(b)** DNA from ten rifampicin-resistant colonies were extracted and individually amplified by colony PCR. Subsequently, unbalanced PCR using an excess of one primer with an overhang is used to generate the initiation toeholds. These DNA samples were allowed to react with our fluorescent probes. The probes were constructed by annealing four separate oligonucleotides, and possessed non-overlapping nicks that do not interfere with probe function. **(c)** The left side of each column shows the approximate position of the mutations, as determined by sequencing. The right side of each column shows the fluorescence response of the *rpoB* subsequences to the two fluorescent probes. A mutation in the green (blue) region would result in no increase in the fluorescence for Probe 1 (Probe 2), as shown in the green (blue) trace. The experimental results agree with the sequencing results in all experiments. The fluorescence data shown for the left experimental panels represents the behavior over 3 hours of reaction; the right panels show 10 hours of reaction. See Fig. S11-S15 for zoomed-in view of data.

target.

The high specificity of our probes derives from a combination of two factors: First, we rationally designed the probes to react with the intended target with $\Delta G^\circ = 0$, where slight thermodynamic changes due to a single-base mismatch have a disproportionately large

effect on the hybridization yield. Specificity is reduced when $\Delta G^\circ < 0$, for example when initiation toeholds are significantly longer than dissociation toeholds (Fig. S18). Second, our assay has the advantage that a base pair change in the target leads to the formation of two mismatch bubbles in the reaction products. Assays that probe single-stranded targets yield only one mismatch bubble per base change, and the smaller ΔG° change between correct and SNP target cannot be distinguished as easily based on thermodynamics.

We further showed that correct and mutated targets can already be clearly distinguished during the approach to equilibrium. Under conditions where reaction equilibration occurs on the time scale of hours, we were able to identify all mutated targets within the first 20 minutes of the reaction, and fluorescence discrimination was maintained for the remainder of the 25 hours in which we observed the reactions.

The ability to identify single point mutations is critical for diagnosing antibiotic resistance in TB and other diseases [43, 44], because most drug resistances can be traced to individual point mutations in narrowly defined regions within a few genes (see e.g. Ref. [4]). Our probes can be used to screen extended genetic regions (potentially containing multiple SNPs in different positions) and can be multiplexed to screen mutations occurring in different genes, making this a promising technology for developing rapid and reliable infectious disease diagnostics. As a first step in this direction, we used our method for the detection of mutations that confer rifampicin resistance to *E. coli*. Probes were constructed to test two highly variable regions of the rpoB gene and also a 198 base pair domain encompassing both regions. DNA from wild-type *E. coli* and 10 different resistant colonies were reacted with probes, and sequencing confirmed that probes correctly detected the presence of single base pair changes in all cases. Furthermore, we demonstrated multiplexing — two probes labeled with different fluorophores functioned simultaneously in the same detection reaction. This could allow the use of an internal control probing a conserved sequence to compensate for sample-to-sample variability.

Importantly, these experiments on biologically-derived target DNA utilized discontinuous probes that contain non-overlapping nicks. With this approach, we were able to significantly increase the read length of molecular probes, which traditionally has been 50 nt or fewer due to synthesis limitations and also due to reduced specificity of long oligonucleotide hybridization. We demonstrated the ability to detect a single base change in a continuous region of DNA 198 base pairs long, and we envision that this technology can be extended to enable SNP detection in significantly longer DNA, potentially even probing lengths necessary to solve the haplotype phasing problem [42]. Furthermore, by using our discontinuous dsDNA probes, we enable a highly accurate "sequence comparison" mechanism that could function as a complement to next generation sequencing technologies (current sequencing reads are limited to less than 500 nt).

Finally, our probes can even be useful for the detection of single-stranded targets that are first converted to dsDNA with forked toeholds using PCR-based methods. Single-stranded nucleic acids often have considerable secondary structure at or near room temperature. Such self-interactions within a target or a single-stranded probe can interfere with the detection reaction, both at a kinetic level [50, 51] or at a equilibrium thermodynamics level [31, 52]. The double-stranded nature of our probe and target discourages undesirable pathways that lead to either kinetic traps or spurious interactions. Such a procedure would not necessarily increase the complexity of the detection process, since most existing nucleic acid detection technologies require a PCR-based pre-amplification step.

Acknowledgements. The authors thank Eric Klavins for insightful discussion and helpful manuscript preparation suggestions. This work was funded by NIH Award 1K99EB015331 to D. Y. Z., by NSF CAREER Award 0954566 to G. S, and by a DARPA Young Faculty Award to G. S.

Author contributions. S. X. C., D. Y. Z., and G. S. conceived the project and designed

the experiments. S. X. C. conducted the experiments. S. X. C., D. Y. Z., and G. S. analyzed the data and co-wrote the paper.

Additional information. Correspondence may be addressed to G. S. (gseelig@uw.edu) or D. Y. Z. (dyz1@rice.edu). There is a patent pending on the methods described in this work.

[1] Gunderson, K. L., Steemers, F. J., Lee, G., Mendoza, L. G. & Chee, M. S. A genome-wide scalable SNP genotyping assay using microarray technology. *Nature Biotechnology* **37,** 549-554 (2005).

[2] Kim, S. & Misra A. SNP genotyping: technologies and biomedical applications. *Annu. Rev. Biomed. Eng.* **9,** 289-320 (2007).

[3] Arnold, C. *et al.* Single-nucleotide polymorphism-based differentiation and drug resistance detection in Mycobacterium tuberculosis from isolates or directly from sputum. *Clin. Microbiol. Infect.* **11,** 122-130 (2005).

[4] Bang, H. *et al.* Improved rapid molecular diagnosis of multidrug-resistant tuberculosis using a new reverse hybridization assay, REBA MTB-MDR. *Journal of Medical Microbiology* **60,** 1447-1454 (2011).

[5] Schena, M., Shalon, D., Davis, R. W. & Brown, P. O. Quantitative Monitoring of Gene Expression Patterns with a Complementary DNA Microarray. *Science* **270,** 467-470 (1995).

[6] Saiki, R. K., Gelfand, D. H., Stoffel, S., Scharf, S. J., Higuchi, R., Horn, G. T., Mullis, K. B. & Erlich, H. A. Primer-directed enzymatic amplification of DNA with a thermostable DNA polymerase. *Science* **239,** 487-491 (1988).

[7] Shendure, J., *et al.* Accurate Multiplex Polony Sequencing of an Evolved Bacterial Genome. *Science* **309,** 1728-1732 (2005).

[8] Landegren, U., Kaiser, R., Sanders, J. & Hood, L. A ligase-mediated gene detection technique.*Science***241**,: 1077-1080 (1988).

[9] Tong, A. K., Li, Z., Jones, G. S., Russo, J. J., & Ju, J. Combinatorial fluorescence energy transfer tags for multiplex biological assays. *Nature biotechnology* **19**, 756-759 (2001).

[10] Botstein, D., White, R. L., Skolnick, M., & Davis, R. W. Construction of a genetic linkage map in man using restriction fragment length polymorphisms. *American journal of human genetics* **32**, 314 (1980).

[11] Hall, J. G., Eis, P. S., Law, S. M., Reynaldo, L. P., Prudent, J. R., Marshall, D. J., Allawi H. T. *et al.* Sensitive detection of DNA polymorphisms by the serial invasive signal amplification reaction. *Proc. Nat. Acad. Sci. USA* **97**, 8272-8277 (2000).

[12] Xu, Y., Karalkar, N. B., & Kool, E. T. Nonenzymatic autoligation in direct three-color detection of RNA and DNA point mutations. *Nature biotechnology* **19**, 148-152 (2001).

[13] Grossmann, T. N., & Seitz, O. Nucleic acid templated reactions: consequences of probe reactivity and readout strategy for amplified signaling and sequence selectivity. *Chemistry-A European Journal* **15** 6723-6730 (2009).

[14] Singh, S. K., Koshkin, A. A., Wengel, J., & Nielsen, P. LNA (locked nucleic acids): synthesis and high-affinity nucleic acid recognition. *Chemical communications* **4**, 455-456 (1998).

[15] Egholm, M., Buchardt, O., Nielsen, P. E., & Berg, R. H. Peptide nucleic acids (PNA). Oligonucleotide analogs with an achiral peptide backbone. *J. Am. Chem. Soc.* **114** 1895-1897 (1992).

[16] Simeonov, A., & Nikiforov, T. T. Single nucleotide polymorphism genotyping using short, fluorescently labeled locked nucleic acid (LNA) probes and fluorescence polarization detection. *Nucleic acids research* **30** , e91-e91 (2002).

[17] Komiyama, M., Ye, S., Liang, X., Yamamoto, Y., Tomita, T., Zhou, J.-M., & Aburatani, H. PNA for one-base differentiating protection of DNA from nuclease and its use for SNPs detection. *J. Am. Chem. Soc.* **125** 3758-3762 (2003).

[18] Tyagi, S. & Kramer, F.R. Molecular beacons: probes that fluoresce upon hybridization. *Nature Biotechnology* **14,** 303-308 (1996).

[19] Zhang, D. Y., Chen, S. X. & Yin, P. Optimizing the specificity of nucleic acid hybridization, *Nature Chemistry* **4**, 208-214 (2012).

[20] Guo, Z., Liu, Q., Smith, L. M. Enhanced discrimination of single nucleotide polymorphisms by artificial mismatch hybridization. *Nature biotechnology* **15**, 331-335 (1997).

[21] Severinov, K., Soushko, M., Goldfarb, A. & Nikiforov, V. rifampicin Region Revisited. *J. Biol. Chem.* **268,** 14820-14825 (1993).

[22] Telenti, A. *et al.* Detection of rifampicin-resistance mutations in Mycobacterium tuberculosis. *Lancet* **341,** 648-650 (1993).

[23] Thompson, B. J., Camien, M. N. & Warner, R. C. Kinetics of branch migration in double-stranded DNA. *Proc. Nat. Acad. Sci.* **73,** 2299-2303 (1976).

[24] Panyutin, I. G. & Hsieh, P. The kinetics of spontaneous DNA branch migration. *Proc. Nat. Acad. Sci.* **91,** 2021-2025 (1994).

[25] Zhang, D.Y. & Winfree, E. Control of DNA Strand Displacement Kinetics Using Toehold Exchange. *J. Am. Chem. Soc.* **131,** 17303-17314 (2009).

[26] Panyutin, I. G. & Hsieh, P. Formation of a single base mismatch impedes spontaenous DNA branch migration. *J. Mol. Biol.* **230,** 413-424 (1993).

[27] Zhang, D. Y. & Seelig, G. Dynamic DNA nanotechnology using strand displacement reactions. *Nature Chemistry* **3,** 103-114 (2011).

[28] Seelig, G., Soloveichik, D., Zhang, D.Y. & Winfree, E. Enzyme-free nucleic acid logic circuits. *Science* **314,** 1585-1588 (2006).

[29] Zhang, D.Y., Turberfield, A.J., Yurke, B. & Winfree, E. Engineering entropy-driven reactions and networks catalyzed by DNA. *Science* **318,** 1121-1125 (2007).

[30] Soloveichik, D., Seelig, G. & Winfree, E. DNA as a universal substrate for chemical kinetics. *Proc. Nat. Acad. Sci.* **107,** 5393-5398 (2010).

[31] Zhang, D.Y. & Winfree, E. Robustness and modularity properties of a non-covalent DNA catalytic reaction.

Nucleic Acids Res. **38,** 4182-4197 (2010).

[32] Qian, L., Winfree, E. Scaling up digital circuit computation with DNA strand displacement cascades. *Science* **332,** 1196-1201 (2011).

[33] Nandagopal, N. & Elowitz M. B. Synthetic biology: integrated gene circuits. *Science* **333,** 1244-1248 (2011).

[34] Purnick, P. E. M. & Weiss, R. The second wave of synthetic biology: from modules to systems. *Nat. Rev. Mol. Cell Biol.* **10,** 410-422 (2009).

[35] Bunka, D. H. J., Platonova, O. & Stockley, P. G. Development of aptamer therapeutics. *Current Opinion in Pharmacology* **10,** 557-562 (2010).

[36] SantaLucia, J. & Hicks, D. The Thermodynamics of DNA Structural Motifs. *Ann. Rev. Biochem.* **33,** 415-440 (2004).

[37] S. A. Marras, F. R. Kramer & S. Tyagi. Efficiencies of fluorescence resonance energy transfer and contact-mediated quenching in oligonucleotide probes. *Nucleic Acids Research* **30,** e122 (2002).

[38] Biswas, I., Yamamoto, A. & Hsieh, P. Branch migration through DNA sequence heterology. *J. Mol. Biol.* **279,** 795-806 (1998).

[39] Lishanski, A. Screening for single-nucleotide polymorphisms using branch migration inhibition in PCR-amplified DNA. *Clinical Chemistry* **46,** 1464-1470 (2000).

[40] Yang, Q. *et al.* Allele-specific Holliday junction formation: a new mechanism of allelic discrimination for SNP scoring. *Genome Research* **13,** 1754-1764 (2003).

[41] Liu, Y. P., Behr, M. A., Small, P. M., Kurn, N. Genotypic determination of Mycobacterium tuberculosis antibiotic resistance using a novel mutation detection method, the branch migration inhibition M. tuberculosis antibiotic resistance test. *J. Clin. Microbiol.* **38,** 3656-3662 (2000).

[42] Browning, S. R. & Browning, B. L. Haplotype phasing: existing methods and new developments. *Nat. Rev. Genetics* **12,** 703-714 (2011).

[43] McNerney, R. & Daley, P. Towards a point-of-care test for active tuberculosis: obstacles and opportunities. *Nat. Rev. Microbiol.*, **9,** 204-213 (2011).

[44] Niemz, A., Ferguson, T. M. & Boyle, D. S. Point-of-care nucleic acid testing for infectious diseases. *Trends in biotechnology*, **29,** 240-250 (2011).

[45] Piatek, A.S. *et al.* Molecular beacon sequence analysis for detecting drug resistance in Mycobacterium tuberculosis. *Nat. Biotechnol.* **16,** 359-363 (1998).

[46] Boehme, C.C. *et al.* Rapid Molecular Detection of Tuberculosis and rifampin Resistance. *N. Engl. J. Med.* **363,** 1005-1015 (2010).

[47] Xiao, Y., Plakos, K. J. I., Lou, X., White, R. J., Qian, J., Plaxco, K. W. & Soh, H. T. Fluorescence detection of single-nucleotide polymorphisms with a single, self-complementary, triple-stem DNA probe, *Angew. Chemie Int. Ed.* **48,** 4354-4358 (2009).

[48] Tyagi, S. Imaging intracellular RNA distribution and dynamics in living cells. *Nature Methods* **6,** 331-338 (2009).

[49] Manganelli, R., Tyagi, S. & Smith, I. Real-time PCR using molecular beacons. *Methods Mol. Med.* **54,** 295-310 (2001).

[50] Seelig, G., Yurke, B. & Winfree, E. Catalyzed relaxation of a metastable DNA fuel. *J. Am. Chem. Soc.* **128,** 12211-12220 (2006).

[51] Gao, Y., Wolf, L.K. & Georgiadis, R.M. Secondary structure effects on DNA hybridization kinetics: a solution versus surface comparison. *Nucleic Acids Research* **34,** 3370-3377 (2006).

[52] Zhang, J., Finney, R.P., Clifford, R.J., Derr, L.K. & Buetow, K.H. *Genomics* **85,** 297308 (2005).

Methods

Probe design.

We designed pairs of forked toeholds with self-similar sequences to avoid secondary structure (e.g. for target in Fig. 2, orange toehold is 5'-AGTGA-3' and purple toehold is 3'-AGTGA-5'); this is true for both initiation toeholds and dissociation toeholds. This allows accurate prediction of probe binding thermodynamics and kinetics.

DNA oligonucleotides. All DNA oligonucleotides were purchased from Integrated DNA Technology (IDT). Fluorophore- and quencher-labeled oligonucleotides were HPLC purified; non-labeled oligonucleotides used in Fig. 5 were purchased as Ultramers; primers for PCR were unpurified; all remaining oligonucleotides were PAGE purified. Individual DNA oligonucleotides were resuspended to 100 μM and stored in EB buffer (10 mM Tris · HCl, pH 8.5; Qiagen).

IDT provided Electrospray Ionization mass spectrometry data sheets as quality control; Fig. S19 shows one representative ESI spectrum and Table S3 shows a summary of all ESI results (all 47 oligonucleotides showed over 75% purity, and 45 oligonucleotides were over 90% pure).

Probe preparation. Probe molecules consist of either two distinct strands (Fig. 2 through 4) or four distinct strands (Fig. 5). The strands are mixed stoichiometrically and then thermally annealed (Biorad T100), cooling uniformly from 98 °C to 25 °C over the course of 73 minutes. Two-stranded probe molecules were then gel purified to ensure stoichiometry using a 10% polyacrylamide gel; four-stranded probe molecules were not purified.

Gel solutions were prepared from 40% 19:1 acrylamide:bisacrylamide stock (J.T. Baker Analytical) in 1x tris-acetate-EDTA buffer (TAE)/Mg^{2+} solution, and cast between 20 cm by 20 cm glass plates with 1.5 mm spacers. Samples were loaded with 80% glycerol to

achieve 10% glycerol concentration by volume. The gel was run at room temperature using Hoefer SE600 chamber at 140 Volts for 4 hours. Gel bands were visualized using Entela UL3101 UV light, using a fluorescent backplate (Whatman UV254 Polyester 4410222), and then cut out and eluted into 1 mL buffer.

Target preparation. Target molecules used in Fig. 2 through 4 were prepared similarly to two-stranded probes, via annealing and purification as described above. *E. coli*-derived targets used for Fig. 5 were constructed in a multi-step process. 10 μL of competent cells were cultured in 5 mL LB at 37 °C for 48 hours, and then split into 1 mL aliquots. Each aliquot was centrifuged for 10 minutes, after which supernatant was decanted. Precipitate was resuspended in 200 μL LB and plated on a LB plate with either 0 μg/mL (wild-type) or 300 μg/mL rifampicin (Sigma R3501). Colonies were allowed to form overnight at 37 °C.

Ten rifampicin-resistant colonies were picked from the plates, and each was amplified with colony PCR (13 minutes at 98 °C, followed by 40 cycles of 98 °C (15 s), 50 °C (20 s), and 72 °C (40 s), followed by 5 minutes at 72 °C; Biorad T100) with 500 nM of each primer. Subsequently, colony PCR amplification products were used as templates for unbalanced PCR (with 500 nM of one primer and 5 nM of the other, 40 cycles). Both primers had a designed toehold at the 5' end that would serve as initiation or dissociation toehold experiments. The two strands of the target were constructed using unbalanced PCR separately, and annealed afterwards.

Time course fluorescence studies. Kinetic fluorescence measurements were performed using a Horiba Fluoromax 3 spectrofluorimeter and Hellma Semi-Micro 114F spectrofluorimeter cuvettes. Probes targeting the 562-576 codon region of the *rpoB* gene in Fig. 5 used the TYE563 fluorophore (excitation 549 nm; emission 563 nm). For all other experiments, probes used the ROX fluorophore (excitation 584 nm, emission 603 nm). Slit sizes were set at 5 nm for all monochromators. An external temperature bath maintained a designated reaction temperature (25±1 °C unless explicitly stated in Fig. 4).

A four-sample changer was used, so that time-based fluorescence experiments were performed in groups of 4. For simultaneous detection experiments in Fig. 5, each data point represents the integrated fluorescence over 10 seconds per two minutes of reaction. For all other experiments, each data point represents the integrated fluorescence over 10 seconds per minute of reaction.

Fluorescence normalization and hybridization yield inference. All fluorescence values were normalized and converted into hybridization yields χ via the following formula:

$$\chi = \frac{F - F_b}{F_s - F_b}$$

where F is observed fluorescence, F_b is background fluorescence observed due to the addition of only buffer, and F_s is the saturated fluorescence observed after addition of a 40-fold excess of correctly-matched target. See Fig. S1 for details.

Text S1. Design principles for double-stranded toehold exchange

Recall that the double-stranded toehold exchange process can be modeled as a series of states connected by transition rates (Fig. S1A). We omit intermediate states in which the four strands are co-localized, but in which the toeholds are incompletely hybridized (Fig. S1B), because these states suffer both entropic and enthalpic penalties, and consequently will not be prevalent in solution. Intermediate states in which internal base pairs are "breathing" (Fig. S1C) are likewise omited. The reduced states of the reaction are thus:

$$A + B \rightleftharpoons C_0 \rightleftharpoons ... \rightleftharpoons C_i \rightleftharpoons ... \rightleftharpoons C_n \rightleftharpoons D + E \tag{1}$$

In the consideration of the energies of each of these states with respect to determination of occupancy (concentration) at equilibrium, we assume a standard DNA thermodynamic model in which only Watson-Crick base stacking energies are considered. Furthermore, for simplicity, we assume that the energies of all 4-helix multiloops in the various branch migration states C_i are identical in strength. Under these assumptions, the $(n+1)$ different branch migration states C_i are identical in energy, and can thus be grouped into a conglomerate state C with energy:

$$\Delta G^\circ_C = \Delta G^\circ_{C_i} - RT\ln(n+1) \tag{2}$$

Doing so preserves the partition function of the original system in eq. 1:

$$\begin{aligned} Z &= e^{-\Delta G^\circ_{A+B}/RT} + (\sum_{i=0}^{n} e^{-\Delta G^\circ_{C_i}/RT}) + e^{-\Delta G^\circ_{D+E}/RT} \\ &= e^{-\Delta G^\circ_{A+B}/RT} + e^{\ln(n+1)} e^{-\Delta G^\circ_{C_i}/RT} + e^{-\Delta G^\circ_{D+E}/RT} \\ &= e^{-\Delta G^\circ_{A+B}/RT} + e^{-(\Delta G^\circ_{C_i} - RT\ln(n+1))/RT} + e^{-\Delta G^\circ_{D+E}/RT} \end{aligned}$$

In this reduced reaction system $A + B \rightleftharpoons C \rightleftharpoons D + E$, the equilibrium concentration of C is low ($e^{-\Delta G^\circ_C/RT} \ll Z$) when either $\Delta G^\circ_C > \Delta G^\circ_{A+B}$ or $\Delta G^\circ_C > \Delta G^\circ_{D+E}$. The difference between the values of ΔG°_{A+B} and $\Delta G^\circ_{C_0}$ is due to the combined ΔG° values of the orange and purple initiating toeholds. Furthermore, to correctly account for the bimolecular $A+B$ state in the Markov model, we need to adjust its ΔG° by the a concentration term $RT\ln(c)$, where c is the current concentration of the excess species of A and B (scaled to 30 M for hybridization initiation entropy). Although c will change with time and progression of the reaction, it is bounded; assuming that $[A]_0 < [B]_0$, $[B]_0 \geq c \geq [B]_0 - [A]_0$.

$$\begin{aligned} \Delta G^\circ_{A+B} &= \Delta G^\circ_{C_0} - \Delta G^\circ_{\text{toeholds}} + RT\ln(c) \\ &= \Delta G^\circ_C + RT\ln(n+1) - \Delta G^\circ_{\text{toeholds}} + RT\ln(c) \end{aligned}$$

To satisfy $\Delta G^\circ_C > \Delta G^\circ_{A+B}$,

$$\Delta G^\circ_{\text{toeholds}} > RT\ln(c(n+1))$$

The conditions for $\Delta G^\circ_C > \Delta G^\circ_{D+E}$ is similar, except using the blue and green toehold energies instead.

The equilibrium concentrations of C must be low for the dsDNA probe to function properly. When the equilibrium concentration of the C states are **not** low, much of the probe could be trapped in intermediates, which not only results in low fluorescence for correct target binding (due to failure to dissociate), but also slow the kinetics of the overall reaction when the probe is trapped in intermediates with the SNP targets.

For our experiments, n varied between 14 and 233, c was typically 10 nM, so $RT\ln(c(n+1))$ varied between -9.8 kcal/mol and -11.4 kcal/mol. Our blue and green toeholds were typically weaker (4 base pairs each), with total $\Delta G^\circ_{\text{toeholds}} = -8.86$ kcal/mol, according to

established thermodynamic parameters [36]. The interaction between the ROX fluorophore and the Iowa Black RQ quencher likely also contributes to the thermodynamic stability of the toeholds. Consequently, our experiments in Fig. 5 and Fig. S15 that use a 200 nt branch migration region may suffer from intermediate state trapping.

Because higher temperatures and lower salinity concentrations tends to weaken the thermodynamic contributions of base paring (making $\Delta G^\circ_{\text{toeholds}}$ less negative), it is expected that the probes for very long regions will show superior performance at elevated temperatures and reduced salinities.

Text S2. Conditionally fluorescent probes for dsDNA

The high specificity conditionally fluorescent dsDNA probe involves a special case of double-stranded toehold exchange, in which the standard free energy ΔG° of the probe binding to the intended target is approximately 0. This is achieved by designing the initiation and dissociation toeholds to be approximately the same length and strength. We aim for $\Delta G^\circ \approx 0$ because this gives a good tradeoff between hybridization yield of the intended target and the discrimination factor between intended and SNP targets:

1. Equilibrium hybridization yield χ_∞ at $\Delta G^\circ_{\text{intended}} = 0$.

The equilibrium constant for the $A + B \rightleftharpoons D + E$ reaction is $K_{eq} = \frac{[D][E]}{[A][B]} = \frac{[D]^2}{[A][B]}$, where A is the target, B is the probe, D is the fluorescent product, and E is the dark product. In a detection reaction, there are no product $[D]$ and $[E]$ initially; therefore any production of D must necessarily be accompanied by production of E, and the concentrations of the two products are always equal.

We define n to be the stoichiometric ratio between the initial concentrations of A and B ($n = \frac{[A]_0}{[B]_0}$). The hybridization yield χ is calculated based off the limiting species of target and probe ($\chi = \frac{[D]}{\min\{[A]_0,[B]_0\}}$), and varies with time. Here we show derivation for the case

where $n \geq 1$, but similar results follow for $n < 1$. With some simplification, the equilibrium hybridization yield χ_∞ can be expressed as a function of stoichiometry n and equilibrium constant K_{eq}:

$$K_{eq} = \frac{\chi_\infty^2}{(1-\chi_\infty)(n-\chi_\infty)} \tag{3}$$

$$\chi_\infty = \frac{K_{eq} + K_{eq} \cdot n - \sqrt{K_{eq}}\sqrt{K_{eq}(n-1)^2 + 4n}}{2(K_{eq}-1)} \tag{4}$$

except in the case of $K_{eq} = 1$, in which case $\chi_\infty = \frac{n}{n+1}$.

2. Discrimination factor Q at $\Delta G^\circ_{\text{intended}} = 0$.

The discrimination factor Q is defined as:

$$Q = \frac{\chi_\infty(\text{intended})}{\chi_\infty(\text{SNP})}$$

With $\Delta G^\circ_{\text{intended}} = 0$, the numerator becomes $\frac{n}{n+1}$. The denominator can be calculated based on substituting $\Delta G^\circ_{\text{SNP}} = \Delta\Delta G^\circ_{\text{ds}}$ into equation (4). The value of $\Delta\Delta G^\circ_{\text{ds}}$ depends on the identity and local neighborhood of the SNP, and generally varies between +6 and +10 kcal/mol at room temperature. Here, the exact value of χ_∞(SNP) does not matter; we merely wish to establish a lower bound on Q.

At very high values of n, the system may lose specificity because the overwhelming amount of SNP target can produce equilibrium yield $\chi_\infty > 0.5$. We will discuss this scenario later in text S3; here we limit ourselves to in which $\chi_\infty < 0.5$ (e.g. $n < 1000$),. In

this case, we can bound the value of Q:

$$\begin{aligned} K_{eq} = \frac{\chi_\infty^2}{(1-\chi_\infty)(n-\chi_\infty)} &< \frac{\chi_\infty^2}{0.5(n-0.5)} \\ \frac{2n-1}{4} e^{-\Delta\Delta G^\circ_{\text{ds}}/RT} &< \chi_\infty^2 \\ \sqrt{\frac{2n-1}{4}} e^{-\Delta\Delta G^\circ_{\text{ds}}/2RT} &< \chi_\infty(\text{SNP}) \end{aligned}$$

$$\begin{aligned} Q &= \frac{\chi_\infty(\text{intended})}{\chi_\infty(\text{SNP})} \\ &> \frac{\frac{n}{n+1}}{\sqrt{\frac{2n-1}{4}} e^{-\Delta\Delta G^\circ_{\text{ds}}/2RT}} \\ &= \frac{2n}{(n+1)\sqrt{2n-1}} e^{\Delta\Delta G^\circ_{\text{ds}}/2RT} \\ &\geq \frac{1}{\sqrt{2n-1}} e^{\Delta\Delta G^\circ_{\text{ds}}/2RT} \end{aligned}$$

The value of Q increases monotonically as $\Delta G^\circ_{\text{intended}}$ increases [19]. At the limit of $\Delta G^\circ_{\text{intended}} \to +\infty$,

$$\begin{aligned} K_{eq} &= \frac{\chi_\infty^2}{(1-\chi_\infty)(n-\chi_\infty)} \\ e^{-\Delta G^\circ/RT} &= \chi_\infty^2 \\ \chi_\infty(\text{intended}) &= e^{-\Delta G^\circ_{\text{intended}}/2RT} \\ \chi_\infty(\text{SNP}) &= e^{-\Delta G^\circ_{\text{SNP / 2RT}}} = e^{-\Delta\Delta G^\circ_{\text{ds}}/2RT} \cdot e^{-\Delta G^\circ_{\text{intended}}/2RT} \\ Q_{\max} &= \frac{\chi_\infty(\text{intended})}{\chi_\infty(\text{SNP})} = e^{\Delta\Delta G^\circ_{\text{ds}}/2RT} \end{aligned}$$

Thus, at $\Delta G^\circ_{\text{intended}} = 0$ and reasonably small $n < 1000$, the discrimination factor is within a small constant factor $\frac{1}{\sqrt{2n-1}}$ of optimal.

3. Representative equilibrium hybridization yields and discrimination factors

Stoichiometry n	χ_∞ (intended, $\Delta G^\circ = 0.00$ kcal/mol)	χ_∞ (SNP, $\Delta G^o = +6.00$ kcal/mol)	$Q = \frac{\chi_\infty(\text{Intended})}{\chi_\infty \text{SNP}}$
1	0.500	0.0063	79.4
10	0.909	0.0199	45.7
100	0.990	0.0615	16.1
1000	0.999	0.182	5.50

TABLE 3-1: Effects of stoichiometry n on hybridization yield of intended and SNP targets, and corresponding discrimination factor Q.

The solid lines shown in Fig. 3 of the main text plots the analytic dependence of χ_∞ on stoichiometry n shown in Equation (4), assuming the following best-fit ΔG° values:

Target	ΔG° (kcal/mol)
Intended (black)	-0.2
i8TA (red)	+3.9
d8 (green)	+5.1
m8CG (blue)	+6.0

Table S1 shows analytic equilibrium hybridization yields for representative values of n and ΔG°. Dividing the equilibrium hybridization yield for $\Delta G^\circ = 0.00$ by that for $\Delta G^\circ = +6.00$ kcal/mol, we obtain the analytic discrimination factor Q. Although discrimination factor is highest at $n = 1$, the SNP can still be effectively distinguished at 1000x excess of target over probe. Because analysis is symmetrical with respect to A and B, stoichiometries $n < 1$ will yield the same discrimination factor as stoichiometry $n' = \frac{1}{n}$.

Text S3. Mathematical relation between R and Q.

The concentration equivalence R is an alternative measure of specificity, and denotes the ratio of the quantity of SNP versus intended target needed to yield the same level of fluorescence (50% of maximum here): Conceptually, an R-fold excess of the SNP target yields a false positive, so R determines the specificity of a diagnostic assay based on this technology.

Hybridization probes.

For typical ($A + B \rightarrow D$) hybridization probes, $R \approx Q$. First, we show the derivation for Q in the case of known n:

$$\begin{aligned} K_{eq} &= \frac{[D]}{[A][B]} = \frac{\chi_\infty}{(n - \chi_\infty)(1 - \chi_\infty)[B]_0} \\ \chi_\infty &= \frac{n+1}{2} + \frac{1}{2K_{eq}[B]_0} - \frac{\sqrt{K_{eq}^2[B]_0^2 n^2 + K_{eq}^2[B]_0^2 + 1 + 2K_{eq}^2[B]_0^2 n + 2K_{eq}[B]_0 - 2K_{eq}[B]_0 n}}{2K_{eq}[B]_0} \end{aligned}$$

The last expression of χ_∞ is rather complicated, but if we assume that $\chi \ll 0.5$ (and thus in the specific regime of the reaction), the solution for simplifies to:

$$\chi_\infty \approx K_{eq}[B]_0 n = e^{-\Delta G^\circ / RT}[B]_0 n$$

The discrimination factor Q is calculated as:

$$\begin{aligned} Q &= \frac{\chi_\infty(\text{intended})}{\chi_\infty(\text{SNP})} \\ &\approx \frac{e^{-\Delta G^\circ_{\text{intended}}/RT}[B]_0 n}{e^{-\Delta G^\circ_{\text{SNP}}/RT}[B]_0 n} \\ &= e^{-\Delta G^\circ_{\text{intended}}/RT + \Delta G^\circ_{\text{SNP}}/RT} \end{aligned}$$

We define $\Delta\Delta G^\circ_{\text{ss}} = \Delta G^\circ_{\text{SNP}} - \Delta G^\circ_{\text{intended}}$, and the above simplifies to:

$$Q = e^{\Delta G^\circ_{\text{ss}}/RT}$$

Next, we derive R based on $\chi_\infty = 0.5$:

$$
\begin{aligned}
e^{-\Delta G^\circ/RT} = K_{eq} &= \frac{[D]}{[A][B]} = \frac{\chi_\infty}{(n-\chi_\infty)(1-\chi_\infty)[B]_0} \\
[B]_0(n-0.5) &= e^{\Delta G^\circ/RT} \\
n &= \frac{[B]_0 + 2e^{\Delta G^\circ/RT}}{2[B]_0}
\end{aligned}
$$

From this expression, we can solve for R:

$$
\begin{aligned}
R &= \frac{n_{\text{SNP}}}{n_{\text{intended}}} \\
&= \frac{[B]_0 + 2e^{\Delta G^\circ_{\text{SNP}}/RT}}{[B]_0 + 2e^{\Delta G^\circ_{\text{intended}}/RT}}
\end{aligned}
$$

We define $\Delta\Delta G^\circ_{\text{ss}} = \Delta G^\circ_{\text{SNP}} - \Delta G^\circ_{\text{intended}}$, and the above simplifies to:

$$
R = \frac{[B]_0 + 2e^{\Delta G^\circ_{\text{ss}}/RT} e^{\Delta G^\circ_{\text{intended}}/RT}}{[B]_0 + 2e^{\Delta G^\circ_{\text{intended}}/RT}}
$$

When the intended hybridization is too favorable ($e^{\Delta G^\circ_{\text{intended}}/RT} \ll [B]_0$), the reaction is not specific, and the concentration equivalence approaches 1. In contrast, when ($e^{\Delta G^\circ_{\text{intended}}/RT} > [B]_0$), the concentration equivalence can be approximated as: $R \approx e^{\Delta G^\circ_{\text{ss}}/RT}$. Thus, $R \approx Q$ for the $A + B \rightarrow D$ hybridization probe reaction in the specific regime of the probe.

Double stranded toehold exchange probes.

For the $A + B \rightleftharpoons D + E$ reaction with $\Delta\Delta G^\circ_{\text{ds}} = \Delta G^\circ_{\text{SNP}} - \Delta G^\circ_{\text{intended}}$, similar logic as

the above leads to:

$$\begin{aligned} \chi_\infty &\approx \sqrt{ne^{-\Delta G^\circ/RT}} \\ Q &= e^{\Delta G^\circ_{\mathrm{ds}}/2RT} \end{aligned}$$

Similarly for R:

$$\begin{aligned} n &= \frac{1+e^{\Delta G^\circ/RT}}{2} \\ R &\approx e^{\Delta G^\circ_{\mathrm{ds}}/RT} \end{aligned}$$

Thus, for the double-stranded probe, $R \approx Q^2$ in the specific regime where hybridization yields are below 0.5. Experimentally, the median discrimination factor Q that we observe is 43; consequently, we expect that up to an up to $R = Q^2 \approx 1800$-fold excess of an SNP target will be tolerated before yielded the same fluorescence signal as 1x of the intended target.

Note that $\Delta G^\circ_{ds} \approx 2\Delta G^\circ_{ss}$, since the double-stranded probe results in 2 mismatch bubbles per base pair change in the target, whereas the conventional hybridization probes results in 1 mismatch bubble per base change. Thus, the observed discrimination factor Q will be roughly the same for the double-stranded probe as under the conventional hybridization probe under optimal conditions, but the concentration equivalence R will be roughly quadratically larger.

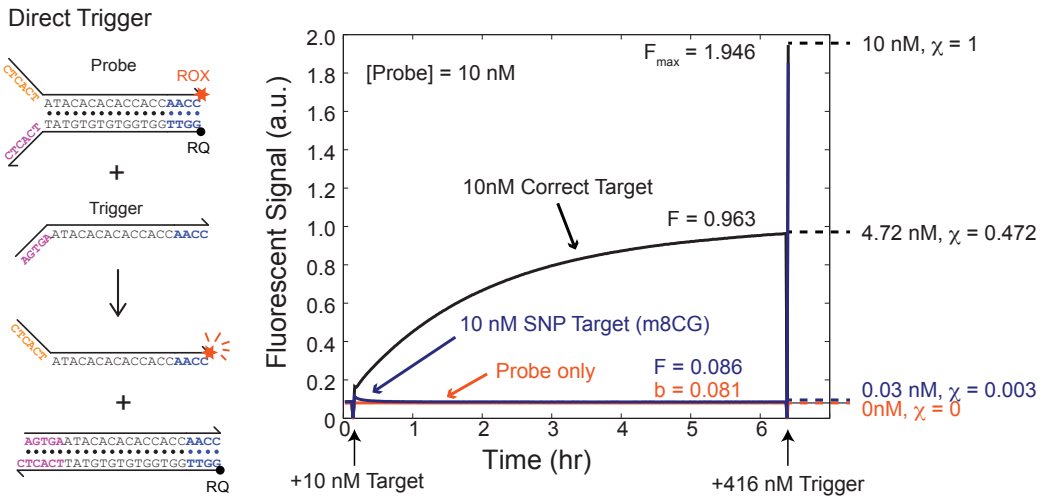

FIG. 3-6: Fluorescence normalization and discrimination factor Q determination. Shown to the right are sample fluorescence traces for the probe alone (orange), the probe with correct target (black), and the probe with the "m8CG" SNP target (blue). At time $t = 0$, the reaction is started by addition of target, if any. At time $t = 6.4$ hr, the reaction is terminated by addition of a large excess of a direct trigger that reacts with the probe (left panel); this fluorescence value after equilibration of this latter reaction corresponds to 100% reaction yield. The hybridization yields of the correct and SNP targets are calculated as: $\chi = \frac{F - F_b}{F_{\max} - F_b}$, where F denotes the fluorescence value of the reaction after 6.4 hours of reaction, F_b denotes the time-varying background fluorescence observed from addition of pure buffer, and $F_{\max}$ denotes the equilibrium after post-trigger.

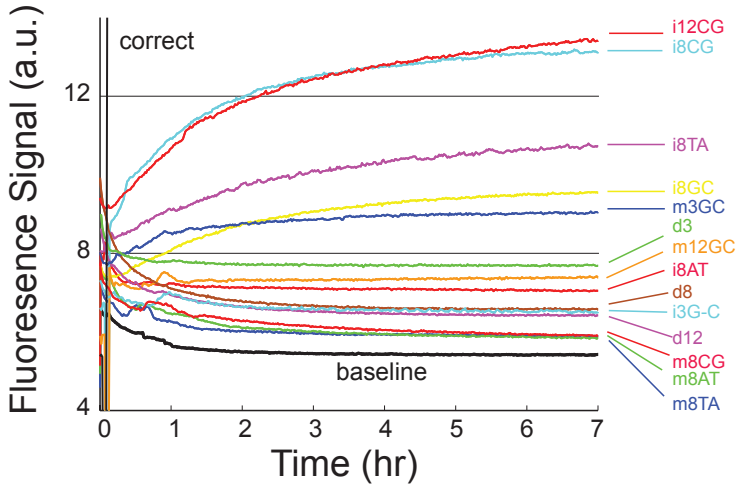

FIG. 3-7: Expanded view of reaction between probe and SNP targets from Fig. 2, plotted as non-normalized fluorescence. The reaction of the probe with the correct target is shown in black and rises very quickly with respect to SNP traces. Note that the arbitrary fluorescence units of different figures differ from each other. The baseline trace shows the average of 4 separate reactions of probe with no target; buffer was added at $t = 0$ to preserve similarity of reaction conditions and correct for dilution effects. Fluorescence value for the baseline and SNP traces showed an initial decline of fluorescence at $t < 1$ hr; this decline is repeatable and likely due to the settling of air bubbles introduced from mixing by repeated pipetting.

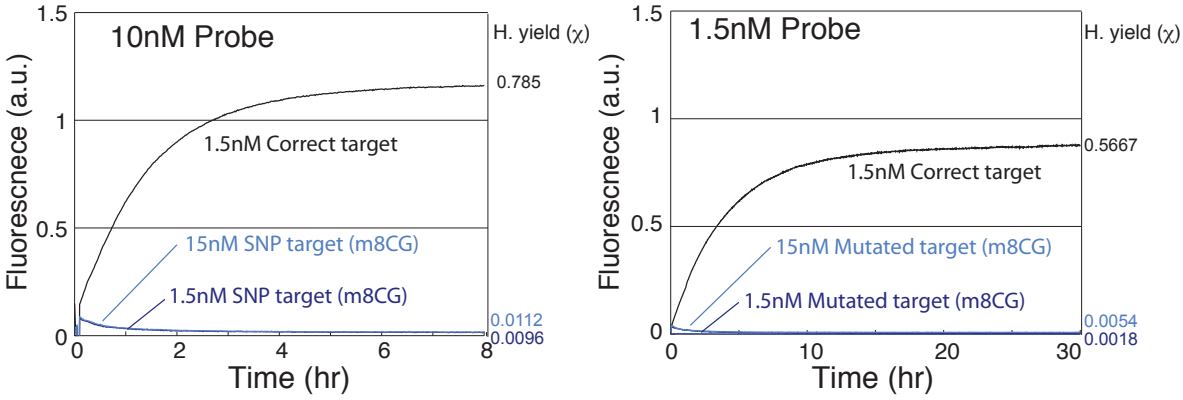

FIG. 3-8: Probe effectively discriminates correct target from SNP targets regardless of probe concentration, as predicted by theory. Consistent with analysis and Fig. 3 from the main text, increased concentrations of SNP targets have a sub-linear effect on the hybridization yield.

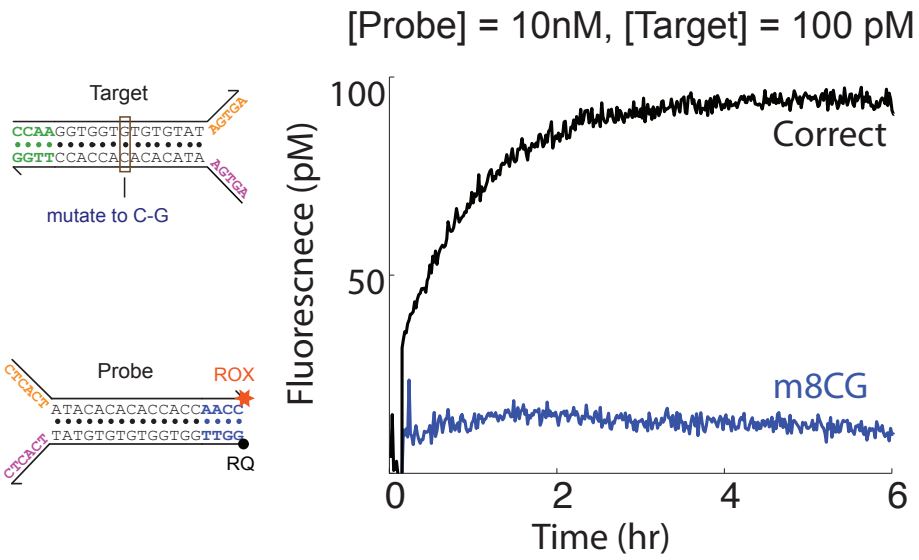

FIG. 3-9: Discrimination of 100 pM intended target from m8CG SNP variant.

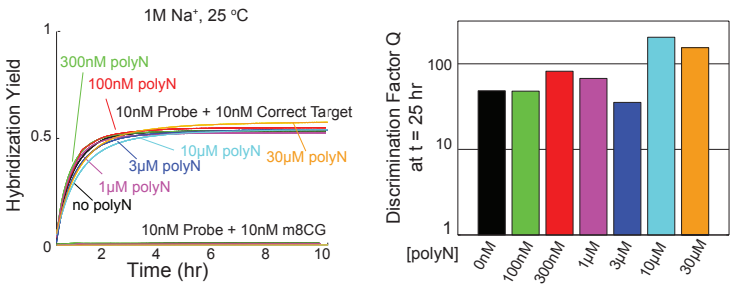

FIG. 3-10: Poly-N single-stranded DNA has no significant effect on the thermodynamic or kinetic behavior of the probe reaction, even at high concentration excesses. This result contrasts that of probe based on three-stranded toehold exchange for discriminating single-stranded DNA and RNA [31].

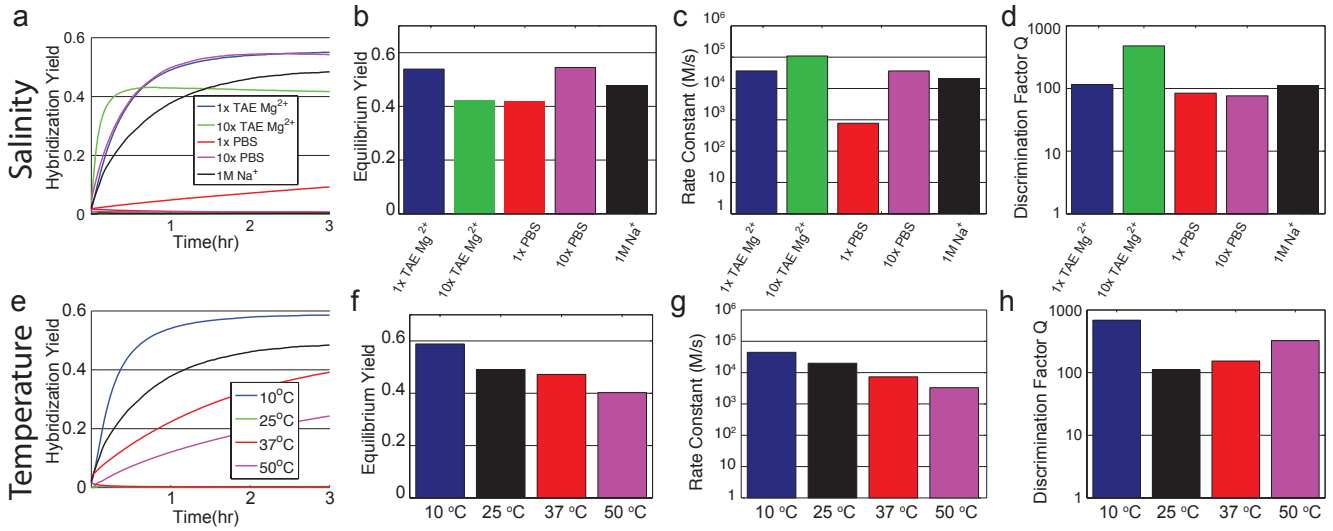

FIG. 3-11: Temperature and salinity effects on probe performance. **(a)** and **(e)** show the hybridization yield over the first three hours of reaction for varying salinities and temperatures, respectively. **(b)** and **(f)** summarizes the fluorescence after 20 hours of reaction. **(c)** and **(g)** summarizes the best-fit rate constants of the forward reaction ($A + B \rightleftharpoons D + E$) to the kinetic traces shown in panels (a) and (e). **(d)** and **(h)** summarizes the discrimination factors Q observed at $t = 20$ hr.

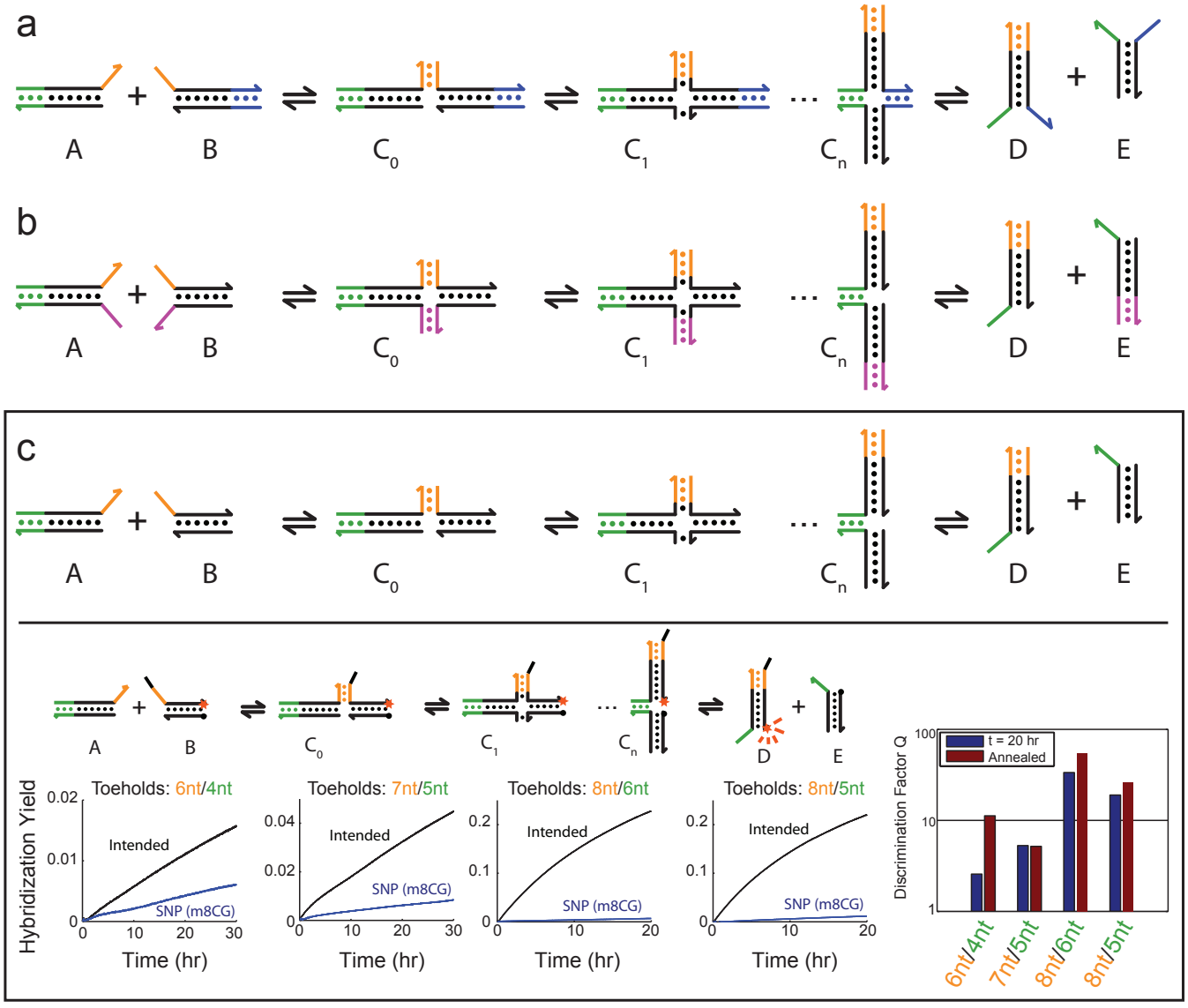

FIG. 3-12: Alternate designs for four-way toehold exchange, in which only a subset of the 4 toeholds are used. Here, we only experimentally tested the design shown in panel (C), which uses exactly 1 initiation toehold and 1 dissociation toehold, and may be easier to prepare than probes with 2 initiation and 2 dissociation toeholds. This probe effectively discriminates intended target from SNP target, although with significantly slower kinetics than the design presented in the main paper.

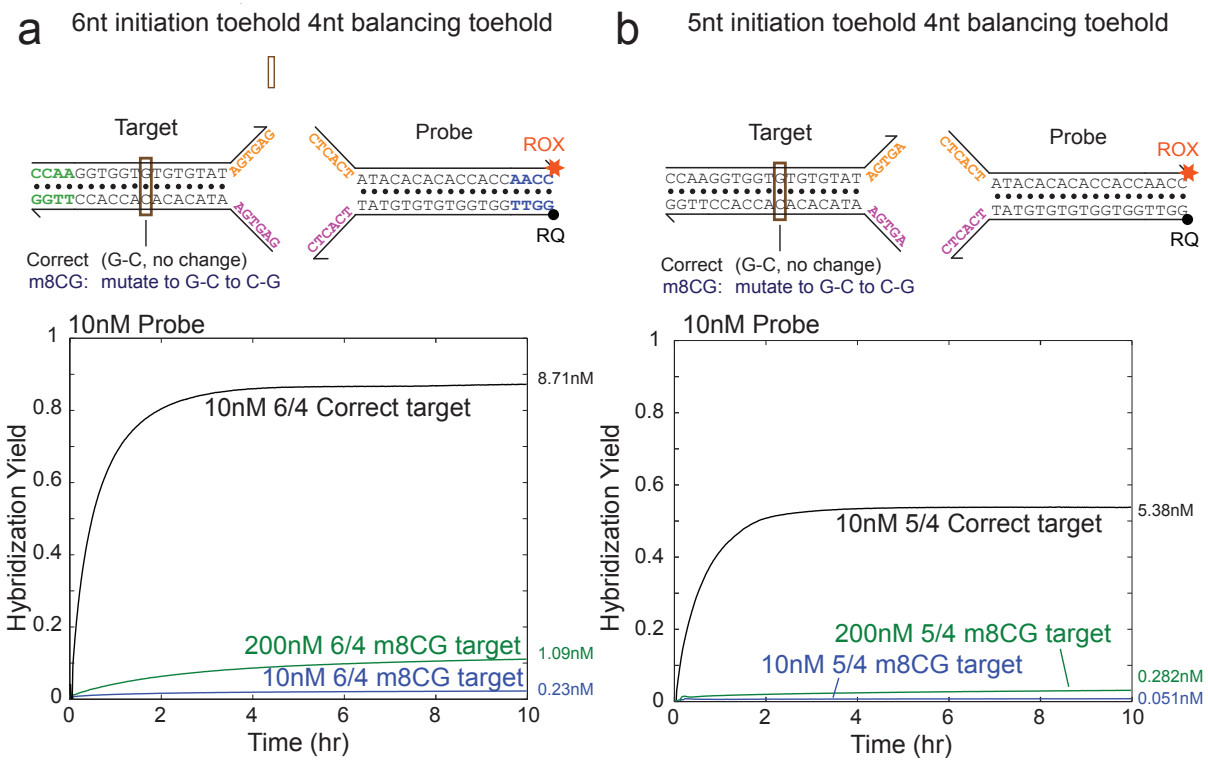

FIG. 3-13: Probes exhibit reduced specificity with toehold sequences cause ΔG° to be significantly negative. Here, the probes with 6 nt initiation toeholds and 4 nt dissociation toeholds show more reaction with 200 nM "m8CG" SNP target than the default probes with 5 nt initiation toeholds.

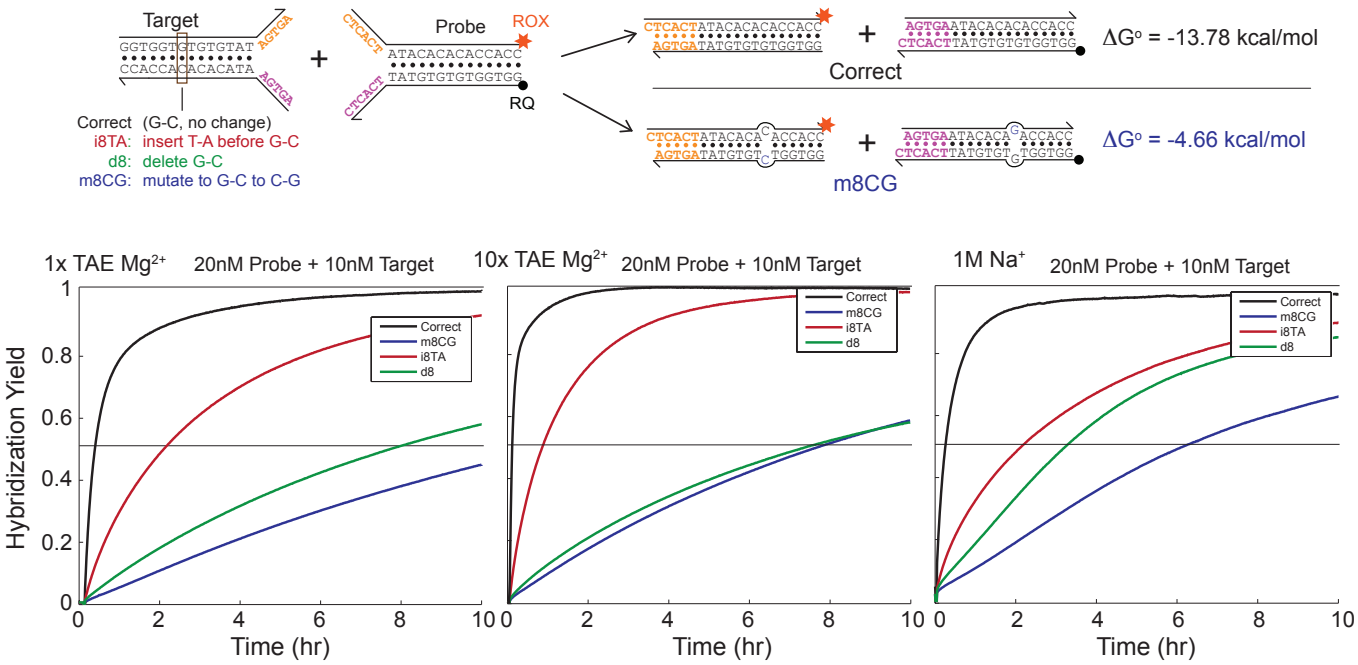

FIG. 3-14: Double-stranded probes without dissociation toeholds react with both correct and SNP targets with thermodynamic favorability ($\Delta G^\circ < 0$). Experimental results across a variety of salinities demonstrate that that SNP target react signficantly with the probe, leading to a false positive signal.

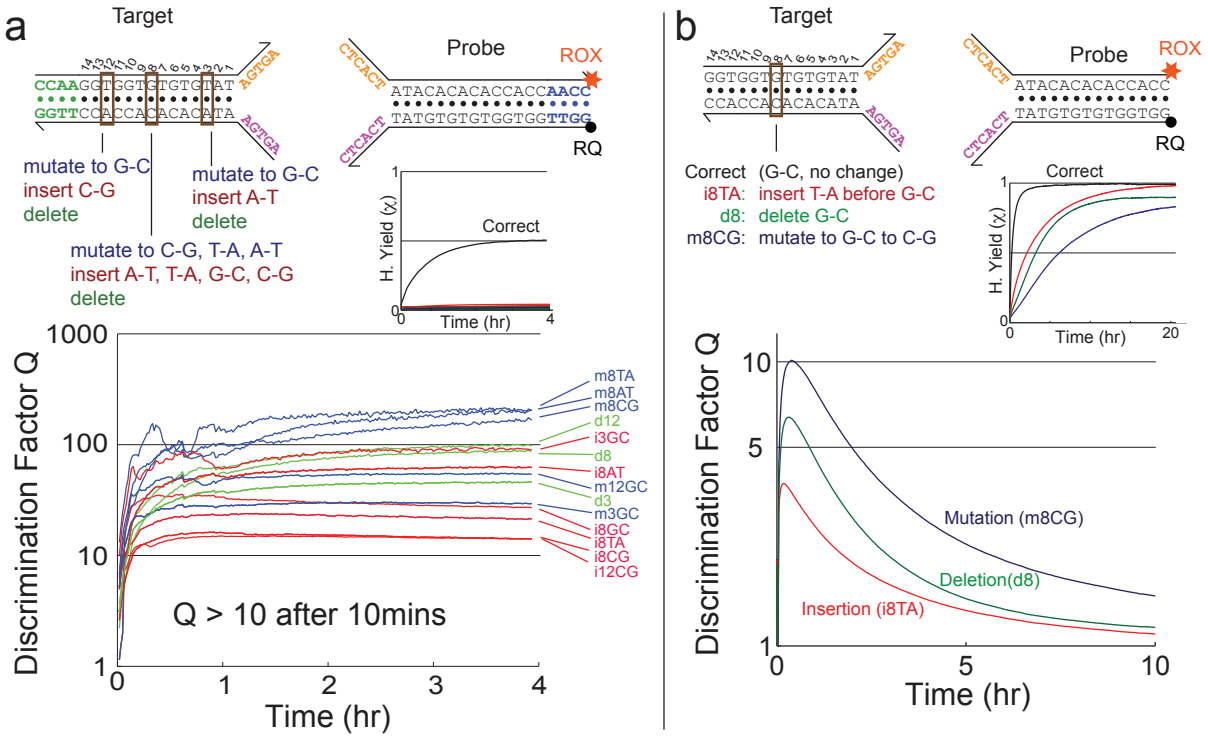

FIG. 3-15: Comparison of the **(a)** toehold exchange probe with the **(b)** probe lacking balancing toeholds. The observed discrimination factor Q are plotted versus time. The values of Q quickly approached their equilibrium values, and in all cases were higher than 10 after 20 minutes. In contrast, the probe lacking balancing toeholds can be used to kinetically discriminate SNPs in the early timepoints of the reaction, but observed discrimination factors Q decrease as the reactions approach equilibrium. Note that even the highest Q observed for the probes lacking balancing toeholds is lower than corresponding Q values for the toehold exchange probes.

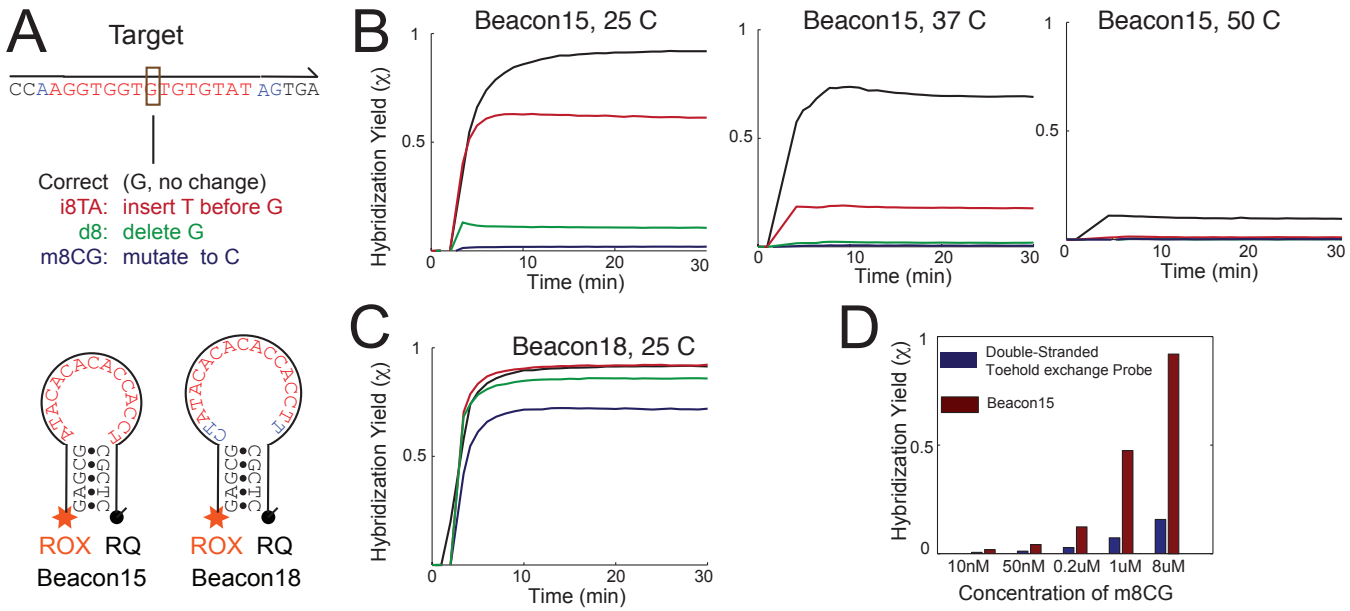

FIG. 3-16: Performance of two different molecular beacons on discriminating SNPs. Compare with Fig. 2b for performance of double-stranded probe. At elevated temperatures (50 °C), molecular beacons show improved specificity, but at the cost of hybridization yield. We also tested molecular beacons targeting a 21 nt sequence, but these did not show significant difference between correct and SNP targets (data not shown).

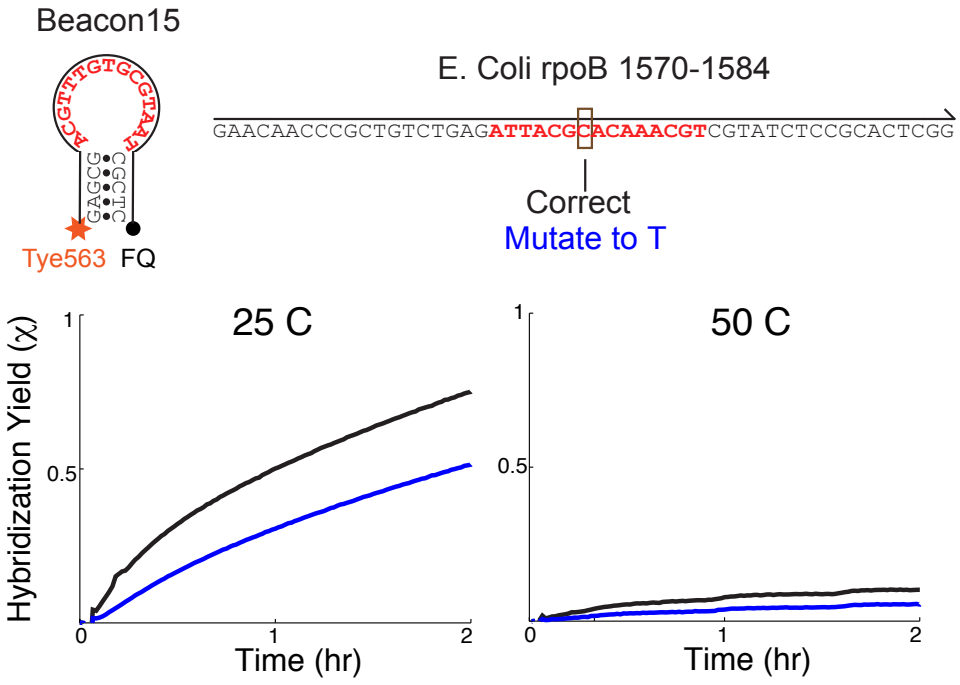

FIG. 3-17: Performance of molecular beacon targeting 15 nt subsequence of the *E. Coli rpoB* gene, nucleotides 1570-1584. Compare with Fig. 5 for performance of double-stranded probe on subsequences ranging from 45 nt to 198 nt. Molecular beacon SNP discrimination performance is significantly worse than in the case of the synthetic targets (Fig. S18), because of secondary structure inherent in the target sequence. In contrast, double-stranded probes are not affected by secondary structure.

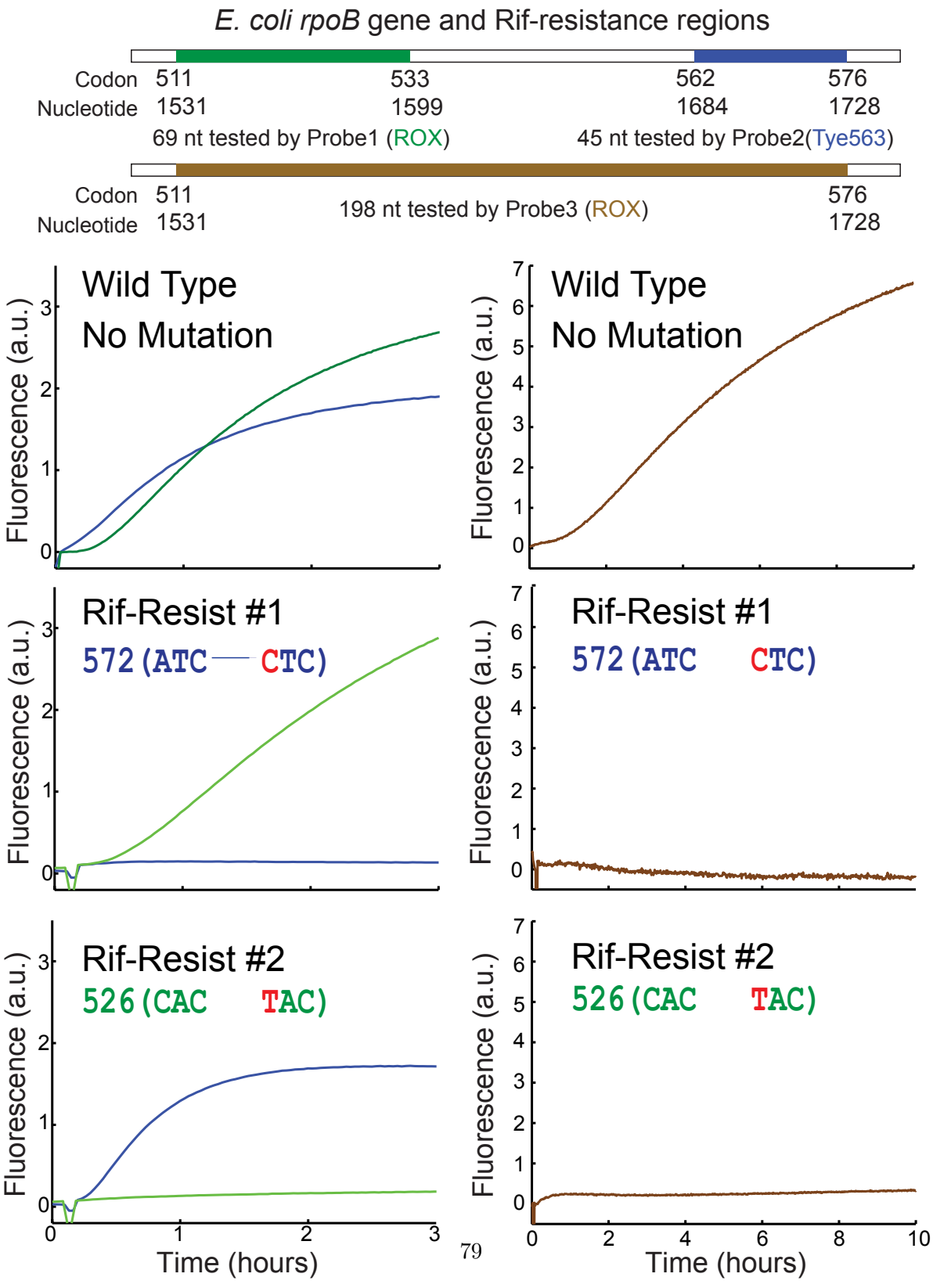

FIG. 3-18: Detection of Rif-resistance in *E. coli* using double-stranded probes; wild type and resistant colonies #1 and #2. (Summarized in Fig. 5 of main paper).

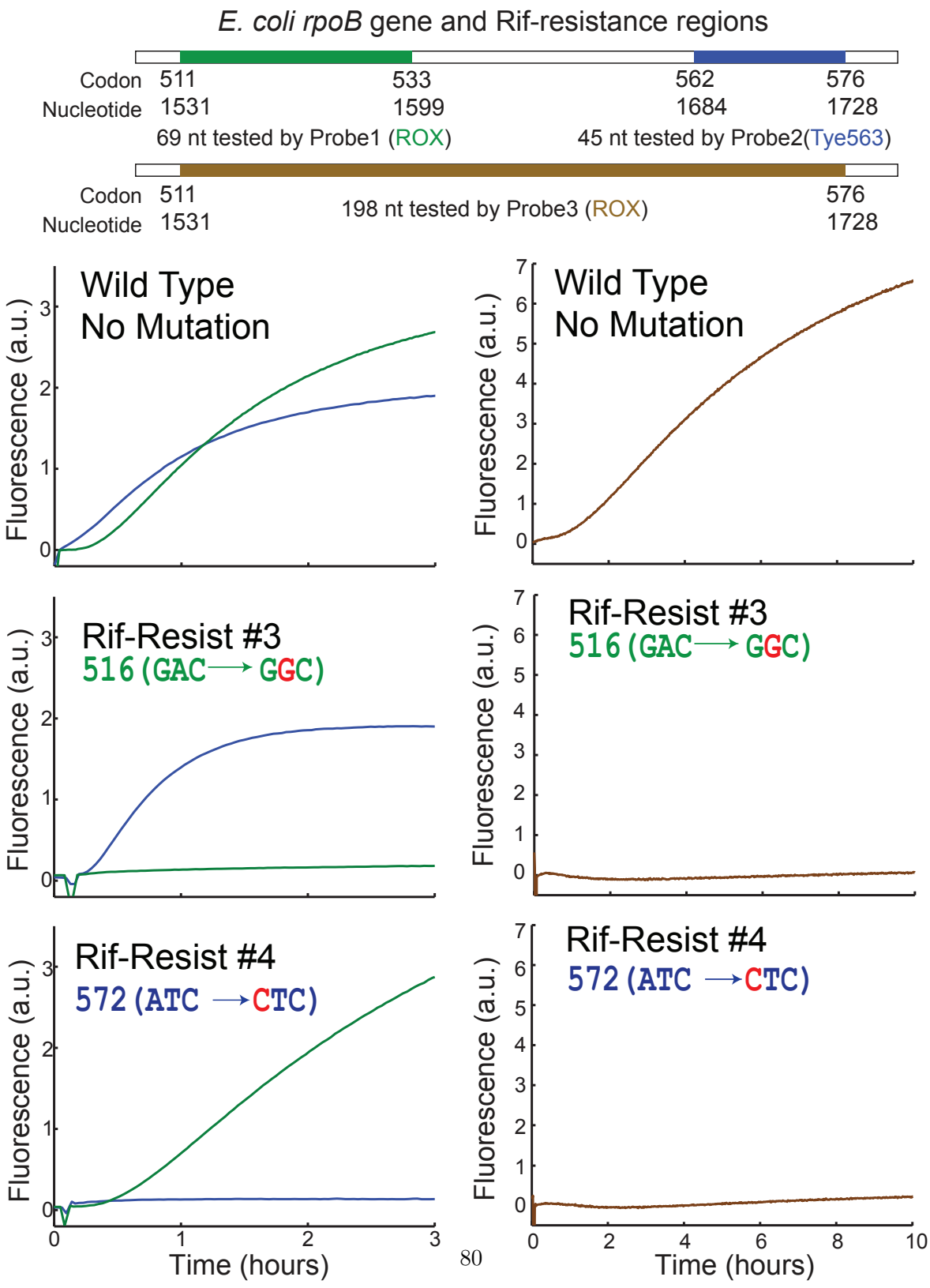

FIG. 3-19: Detection of Rif-resistance in *E. coli* using double-stranded probes; wild type and resistant colonies #3 and #4.

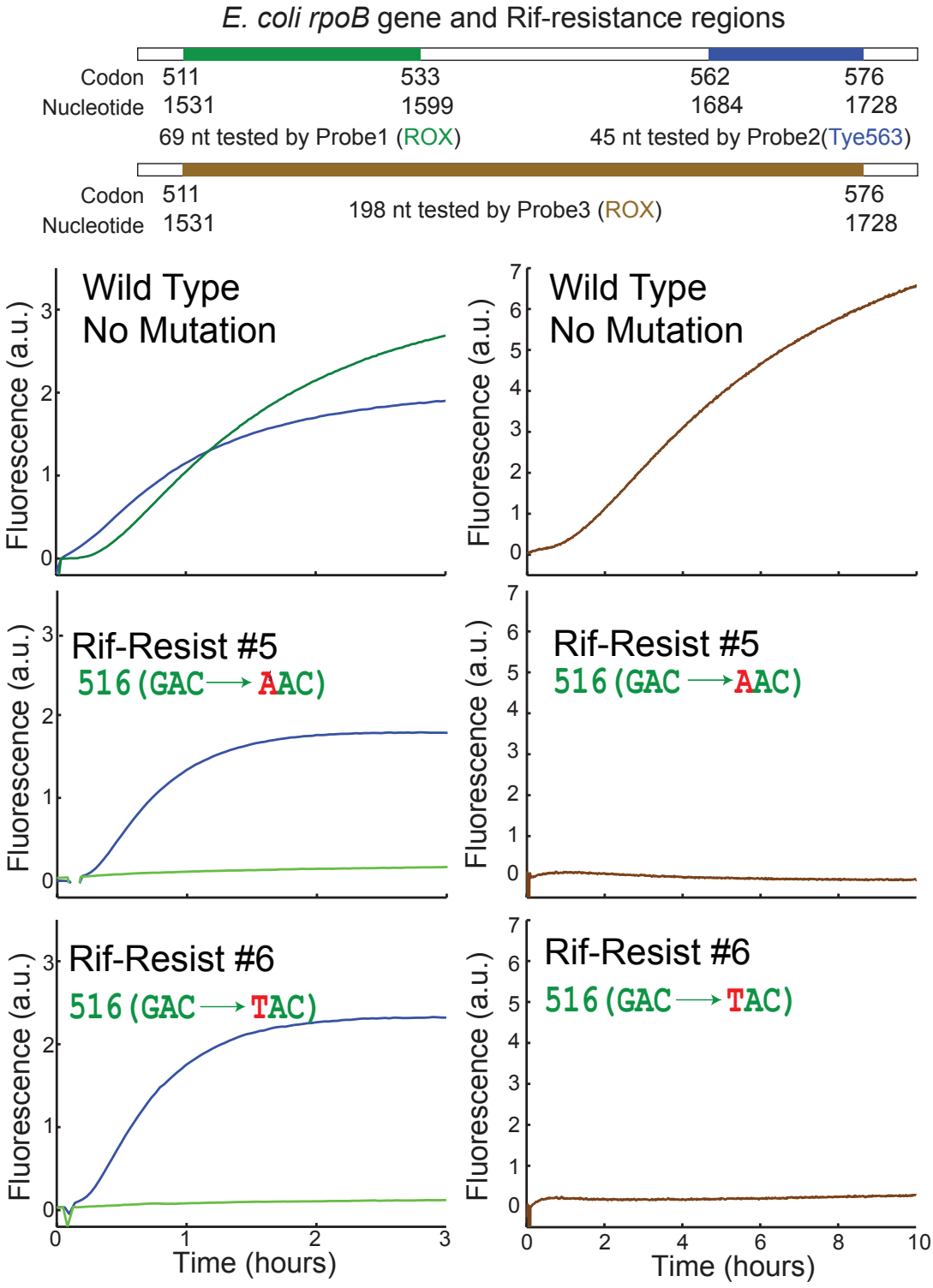

FIG. 3-20: Detection of Rif-resistance in *E. coli* using double-stranded probes; wild type and resistant colonies #5 and #6.

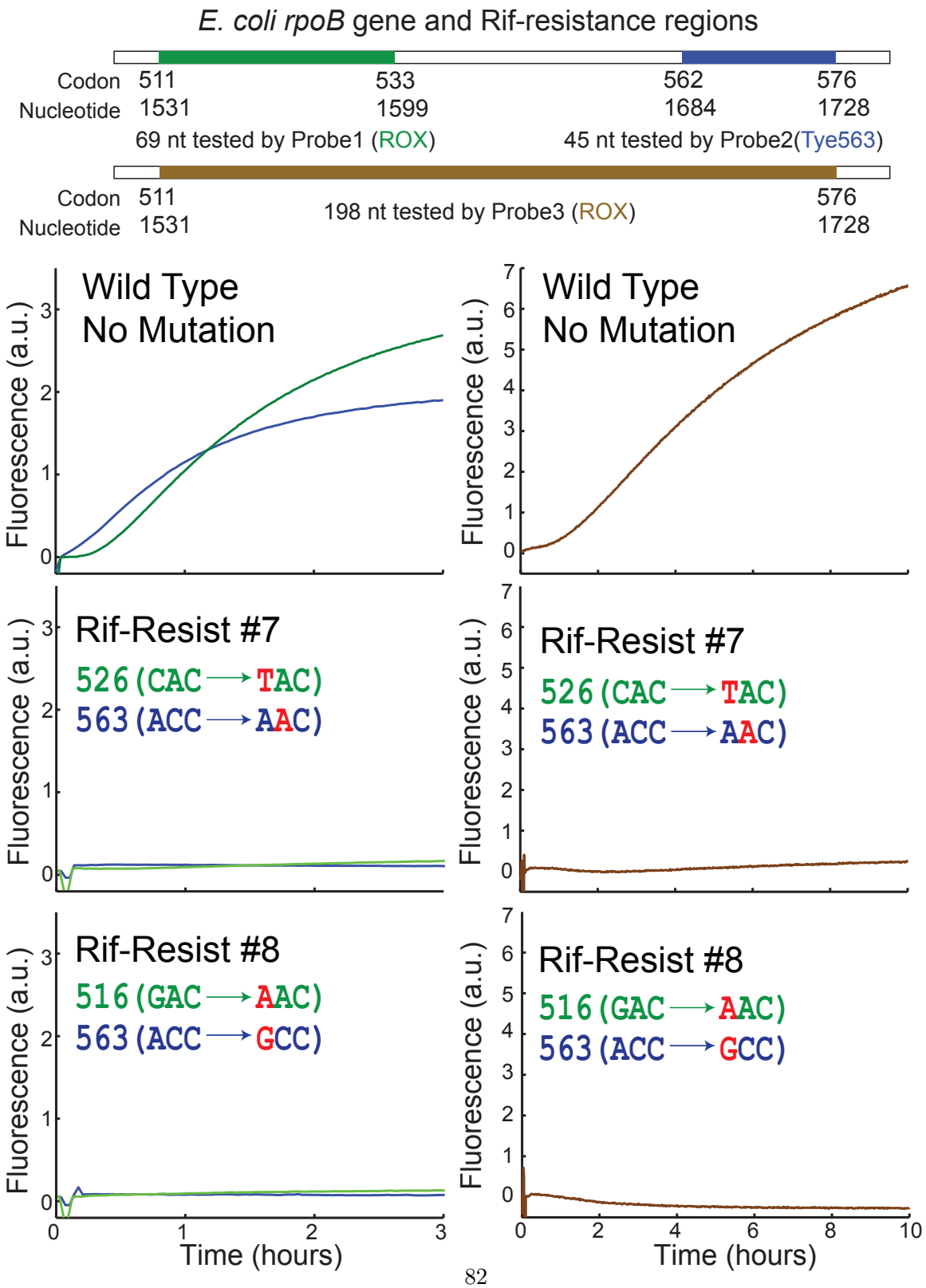

FIG. 3-21: Detection of Rif-resistance in *E. coli* using double-stranded probes; wild type and resistant colonies #7 and #8.

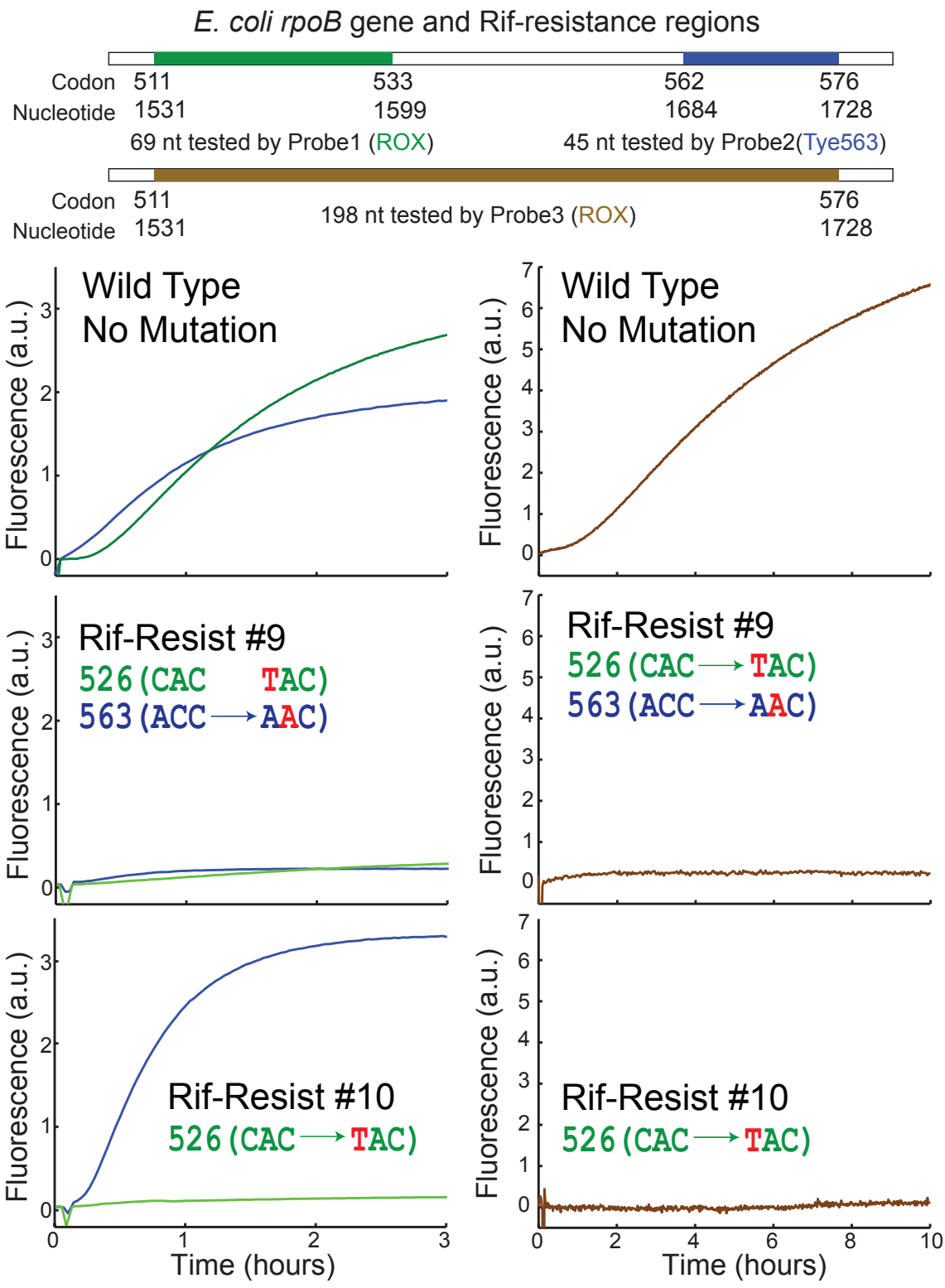

FIG. 3-22: Detection of Rif-resistance in *E. coli* using double-stranded probes; wild type and resistant colonies #9 and #10.

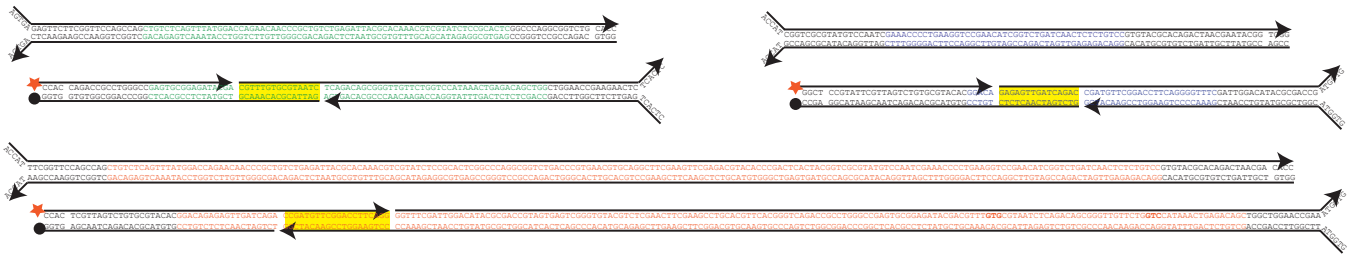

FIG. 3-23: Schematic of the targets and probes used in Fig. 5 of the main paper. Probes are composed of four strands, rather than 2. The non-overlapping nicks in the probe are not expected to affect performance of the probes, except when the SNP is directly adjacent to the nick. Colored bases show subsequences of the *rpoB* that are probed; black letters show primers binding sites for PCR amplification. Yellow background highlights complementary non-overlapping nick region.

Name	Primer Sequence
Ecoli-rpoB-Colony-F	ATGATATCGACCACCTCGGCA
Ecoli-rpoB-Colony-R	ACGTAGTTGCCTTCTTCGATAGCAGACA
Ecoli-rpoB-Region1-F1	**AGTGA** GAGTTCTTCGGTTCCAGCCAG
Ecoli-rpoB-Region1-F2	**TCACT** GAGTTCTTCGGTTCCAGCCAG
Ecoli-rpoB-Region1-R	**GGTG** CAGACCGCCTGGGCC
Ecoli-rpoB-Region2-F1	**ACCAT** CGGTCGCGTATGTCCAATC
Ecoli-rpoB-Region2-F2	**TGGTA** CGGTCGCGTATGTCCAATC
Ecoli-rpoB-Region2-R	**CCGA** CCGTATTCGTTAGTCTGTGCGTACAC
Ecoli-rpoB-full-F1	**CACCAT** TTCGGTTCCAGCCAG
Ecoli-rpoB-full-F2	**GTGGTA** TTCGGTTCCAGCCAG
Ecoli-rpoB-full-R	**GTG** TCGTTAGTCTGTGCGTACAC

TABLE 3-2: PCR primers for *E. coli*-derived target. Shown in bold are initiation and dissociation toehold domains.

Sales Order Number: 7035281
Reference ID: 59975168
Manufacturing ID: 99118333

IDT Oligo ESI Analysis

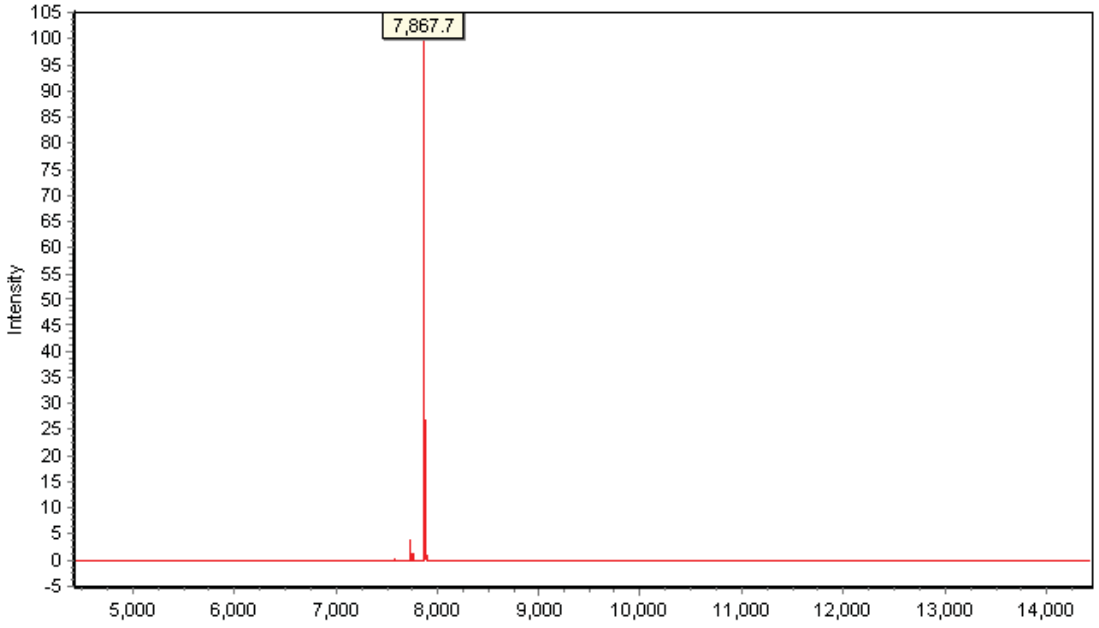

Calculated Molecular Weight: 7,867.5
Measured Molecular Weight: 7,867.7

Sequence Name: Readout-R1-Rox
Oligo Sequence: 5'- CTC ACT ATA CAC ACA CCA CCA ACC /3Rox_N/ -3'

Results provided by Integrated DNA Technologies, Inc. July 01, 2011

FIG. 3-24: Representative Electrospray Ionization (ESI) mass spectrometry spectrum. The oligonucleotide analyzed here is the fluorophore-labeled strand of the probe.

Sequence Name	Oligo Sequence	Calculated Molecular Weight	Measured Molecular Weight	Purification
Readout-R1-Rox	CTC ACT ATA CAC ACA CCA CCA ACC /3Rox_N/	7,867.50	7,867.70	HPLC
4WS-PrB6/4	/5IAbRQ/GGT TGG TGG TGT GTG TAT TCA CTC	7,857.20	7,857.50	HPLC
4WS-TT5/4	CCA AGG TGG TGT GTG TAT AGT GA	7,174.70	7,174.90	PAGE
4WS-TB5/4	AGT GAA TAC ACA CAC CAC CTT GG	7,001.60	7,002.20	PAGE
4WS-ST5/4-m11c	CCA AGG TGG TCT GTG TAT AGT GA	7,134.70	7,135.40	PAGE
4WS-SB5/4-m13g	AGT GAA TAC ACA GAC CAC CTT GG	7,041.60	7,042.00	PAGE
4WS-ST5/4-m11a	CCA AGG TGG TAT GTG TAT AGT GA	7,158.70	7,159.30	PAGE
4WS-SB5/4-m13t	AGT GAA TAC ACA TAC CAC CTT GG	7,016.60	7,017.20	PAGE
4WS-ST5/4-m11t	CCA AGG TGG TTT GTG TAT AGT GA	7,149.70	7,150.30	PAGE
4WS-SB5/4-m13a	AGT GAA TAC ACA AAC CAC CTT GG	7,025.60	7,025.60	PAGE
4WS-TT5/4-i11a	CCA AGG TGG TAG TGT GTA TAG TGA	7,487.90	7,488.40	PAGE
4WS-TB5/4-i13t	AGT GAA TAC ACA CTA CCA CCT TGG	7,305.80	7,306.20	PAGE
4WS-TT5/4-i11g	CCA AGG TGG TGG TGT GTA TAG TGA	7,503.90	7,504.10	PAGE
4WS-TB5/4-i13c	AGT GAA TAC ACA CCA CCA CCT TGG	7,290.80	7,291.20	PAGE
4WS-TT5/4-i11c	CCA AGG TGG TCG TGT GTA TAG TGA	7,463.90	7,464.20	PAGE
4WS-TB5/4-i13g	AGT GAA TAC ACA CGA CCA CCT TGG	7,330.80	7,331.00	PAGE
4WS-TT5/4-i11t	CCA AGG TGG TTG TGT GTA TAG TGA	7,478.90	7,479.10	PAGE
4WS-TB5/4-i13a	AGT GAA TAC ACA CAA CCA CCT TGG	7,314.80	7,315.50	PAGE
4WS-TT5/4-d11	CCA AGG TGG TTG TGT ATA GTG A	6,845.50	6,846.60	PAGE
4WS-TB5/4-d13	AGT GAA TAC ACA ACC ACC TTG G	6,712.40	6,712.60	PAGE
4WS-TT5/4-m7g	CCA AGG GGG TGT GTG TAT AGT GA	7,199.70	7,200.50	PAGE
4WS-TB5/4-m17c	AGT GAA TAC ACA CAC CCC CTT GG	6,977.60	6,978.40	PAGE
4WS-TT5/4-i7c	CCA AGG CTG GTG TGT GTA TAG TGA	7,463.90	7,464.40	PAGE
4WS-TB5/4-i18g	AGT GAA TAC ACA CAC CAG CCT TGG	7,330.80	7,330.90	PAGE
4WS-TT5/4-d7	CCA AGG GGT GTG TGT ATA GTG A	6,870.50	6,871.30	PAGE
4WS-TB5/4-d17	AGT GAA TAC ACA CAC CCC TTG G	6,688.40	6,688.80	PAGE
4WS-TT5/4m17g	CCA AGG TGG TGT GTG TGT AGT GA	7,190.70	7,191.50	PAGE
4WS-TB5/4m7c	AGT GAA CAC ACA CAC CAC CTT GG	6,986.60	6,987.10	PAGE
4WS-TT5/4-i17a	CCA AGG TGG TGT GTG TAA TAG TGA	7,487.90	7,487.90	PAGE
4WS-TB5/4-i8t	AGT GAA TTA CAC ACA CCA CCT TGG	7,305.80	7,306.00	PAGE
4WS-TT5/4-d17	CCA AGG TGG TGT GTG TTA GTG A	6,861.50	6,862.50	PAGE
4WS-TB5/4-d7	AGT GAA ACA CAC ACC ACC TTG G	6,697.40	6,698.10	PAGE

TABLE 3-3: ESI summary for oligonucleotides used in Figure 2, Figure 3 and Figure 4

Sequence Name	Oligo Sequence	Calculated Molecular Weight	Measured Molecular Weight	Purification
4wsr-Probe-FL-Ecoli-rpoB	/56-ROXN/CCA CCA GAC CGC CTG GGC CGA GTG CGG AGA TAC GA	11,472.80	11,471.90	HPLC
4wsr-Probe-FL2-Ecoli-rpoB	CGT TTG TGC GTA ATC TCA GAC AGC GGG TTG TTC TGG TCC ATA AAC TGA GAC AGC TGG CTG GAA CCG AAG AAC TCT CAC TC	24,670.00	24,667.00	Ultramer
4wsr-Probe-Q-Ecoli-rpoB	GAT TAC GCA CAA ACG TCG TAT CTC CGC ACT CGG CCC AGG CGG TCT GGT GG/3IAbRQSp/	16,042.50	16,041.20	HPLC
4wsr-Probe-Q2-Ecoli-rpoB	CTC ACT GAG TTC TTC GGT TCC AGC CTG TCT CAG TTT ATG GAC CAG AAC CAG AAC CCG CTG TCT GA	19,877.90	19,875.80	Ultramer
Ecoli-rpoB-probe-region2-fl	/5TYE563/GGC TCC GTA TTC GTT AGT CTG TGC GTA CAC GGA CA	11,244.60	11,245.40	HPLC
Ecoli-rpoB-probe-region2-fl2	GAG AGT TGA TCA GAC CGA TGT TCG GAC CTT CAG GGG TTT CGA TTG GAC ATA CGC GAC CGA TGG TG	20,192.10	20,191.70	Ultramer
Ecoli-rpoB-probe-region2-q	TGA TCA ACT CTC TGT CCG TGT ACG CAC AGA CTA ACG AAT ACG GAG CC/3IABkFQ/	14,834.70	14,833.70	HPLC
Ecoli-rpoB-probe-region2-q2	GTG GTA CGG TCG CGT ATG TCC AAT CGA AAC CCC TGA AGG TCC GAA CAT CGG TC	16,318.60	16,318.20	Ultramer
Ecoli-rpoB-Probe-full-FL	/56-ROXN/CCA CTC GTT AGT CTG TGC GTA CAC GGA CAG AGA GTT GAT CAG ACC GAT GTT CGG ACC TTC AGG	20,134.30	20,132.10	HPLC
Ecoli-rpoB-Probe-full-FL2	GGT TTC GAT TGG ACA TAC GCG ACC GTA GTG AGT CGG GTG TAC GTC TCG AAC TTC GAA GCC TGC ACG TTC ACG GGT CAG ACC GCC TGG GCC GAG TGC GGA GAT ACG ACG TTT GTG CGT AAT CTC AGA CAG CGG GTT GTT CTG GTC CAT AAA CTG AGA CAG CTG GCT GGA ACC GAA ATG GTG	55,881.00	55,886.40	Ultramer
Ecoli-rpoB-Probe-full-Q	TCT GAT CAA CTC TCT GTC CGT GTA CGC ACA GAC TAA CGA GTG G/3IAbRQSp/	13,857.10	13,856.80	HPLC
Ecoli-rpoB-Probe-full-Q2	GTG GTA TTC GGT TCC AGC CAG CTG TCT CAG TTT ATG GAC CAG AAC AAC CCG CTG TCT GAG ATT ACG CAC AAA CGT CGT ATC TCC GCA CTC GGC CCA GGC GGT CTG ACC CGT GAA CGT GCA GGC TTC GAA GTT CGA GAC GTA CAC CCG ACT CAC TAC GGT CGC GTA TGT CCA ATC GAA ACC CCT GAA GGT CCG AAC ATC GG	61,527.70	61,535.00	Ultramer

TABLE 3-4: ESI summary for oligonucleotides used in Figure 5

Chapter 4: Reaction Network Approaches to Improving DNA Hybridization Probe Specificity

This work has been experimentally completed and is currently undergoing final proofreading, and describes the construction of reaction circuits cascading two strand displacement reactions. The key insight in this work is the idea that clever biomolecular circuit design can circumvent thermodynamic limitations on specificity described in my earlier work (Nature Chemistry, 2012). We performed experimental validation to show significantly better discrimination of sequence variants in single-stranded DNA and RNA. Using this approach, we were able to reliably discriminate members of the let-7 family of microRNAs (known to be challenging) with over 10-fold affinity difference. In principle, more complex circuits may be used to further improve specificity.

Abstract: Electric circuit design principles are applied to biochemical reaction networks to improve the quantitative performance of selective hybridization probes in recognizing single nucleotide variations. Rational hybridization probe design and biochemical circuit design

is integrated to solve the SNP detection problem with significantly better performance. We show that the single nucleotide selectivity of such a circuit in binding to single-stranded DNA and RNA is roughly quadratically better than either component alone. As an additional benefit, the integrated circuit inherits the property of amplification, and provides 10-fold better sensitivity than standard hybridization probes.

The specificity of Watson-Crick base pairing has been used for over 30 years as the basis of nucleic acid biotechnology, in applications ranging from DNA amplification by the polymerase chain reaction [1] to single nucleotide polymorphism (SNP) genotyping [2] to modern sequencing-by-synthesis [3]. Although typically bioinformatics is employed to optimize nucleic acid probe specificity, typically by means of temperature optimization, there have also been attempts to engineer synthetic nucleotide analogs with improved molecular specificity [4–6], as well as hybridization probes with greater molecular specificity due to supramolecular architecture [7–11].

Simultaneously, general principles from the electrical engineering discipline of circuit design has been applied to biochemistry to enable a wide range of biochemical circuits using DNA as the primary construction medium [12].

Here, we show that rational hybridization probe design and biochemical circuit design can be integrated to solve the SNP detection problem with significantly better performance than either approach alone. We show that the single nucleotide selectivity, quantitated as the discrimination factor (DF), of such a circuit in binding to single-stranded DNA and RNA is roughly quadratically better than either component alone. As an additional benefit, the integrated circuit inherits the property of amplification, and provides 10-fold better sensitivity than standard hybridization probes. Our results conceptually demonstrate

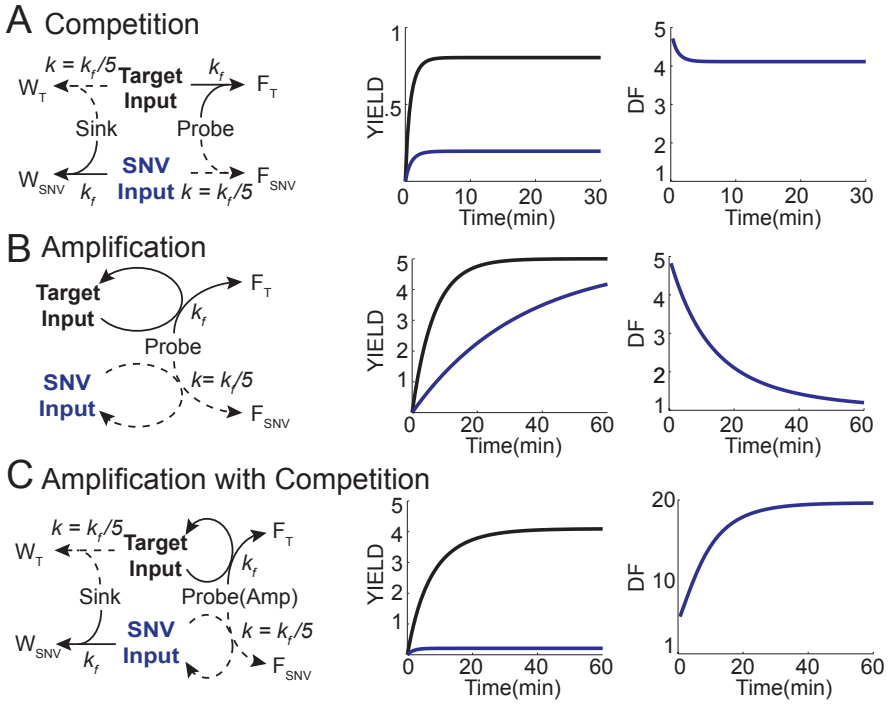

FIG. 4-1: Different approaches to single nucleotide discrimination. **(A)** A competitive hybridization circuit involving Target-specific probes and SNV specific sinks. This approach [8, 9] uses the differential hybridization kinetics of the Target and SNV to the Probe and Sink. **(B)** An amplification circuit in which Targets and SNVs catalytically generate a fluorescent product. This approach [13] uses the differential catalytic kinetics of the Target and SNV to the Probe. **(C)** Our approach to integrate a competitive hybridization circuit with an amplification circuit to achieve higher discrimination than either component approach.

the power of circuit design to quantitatively improve biotechnology.

We first consider abstract reaction models of a competition probe circuit, an amplification circuit, and the integrated competitive amplification circuit. Mathematically we find that a combination of competition and amplification can result in a higher degree of discrimination between two similar analytes, the Input Target (I_T) and the SNV Target (I_{SNV}), than is possible with either mechanism alone. Subsequently, we perform experimental studies to validate our theoretical findings.

Reaction Model Analysis

We consider three different discrimination systems, one based on competition between two hybridization probes, a second system consisting of a single probe capable of signal amplification through a catalytic reaction pathway, and a third system that combines competition with amplification. For our analysis we assume that either a target input I_T or an input with an single nucleotide variant I_{SNV} is added to the discrimination system but not both. Furthermore, we assume that the reaction of target input I_T with the discrimination system results in a fluorescence signal F_T while reaction of the mutated input I_{SNV} results in a signal F_{SNV}.

As a quantitative metric of probe selectivity we will use the discrimination factor DF= $[F_T]/[F_{SNV}]$, which denotes the ratio of the elicited signal for the perfect match target sequences versus that of the single nucleotide variant (SNV). Here, $[F_T]$ ($[F_{SNV}]$) denotes the concentration of the F_T (F_{SNV}) species responsible for the signal. (Note that in practice these signals will be produced by the same molecular species but in different experimental contexts.) A highly specific assay will result in a large discrimination factor while a failure to discriminate between the two types of inputs results in DF=1.

An ideal detection system should not only be specific but also sensitive. Biological analytes are often present at low concentrations and a sensitive probe would result in a strong signal even for small amount of a target. As a quantitative measure for the sensitivity we will use the yield $\chi_T = [F_T]/[I_T]_0$, that is the ratio of amount of signal produced to the amount of target added initially. We note that in a system without amplification the yield cannot exceed $\chi = 1$ since a single target molecule can at best result in a single copy of the F_T molecule.

Discrimination by competition. Here, we present a simple mathematical analysis to establish the maximal discrimination and sensitivity achievable in an idealized competitive system. Experimentally, a competitive hybridization probe was first realized by Li et al. [9] and we will further characterize that system below. The system consists of two main

components, the probe P and the sink S (Fig. **??**A). The probe P is specific to the target input I_T; this is reflected in the $I_T + P$ reaction having a rate constant k_f that is greater than the rate constant k_s of the $I_{SNV} + P$ reaction. Similarly, the sink S is specific to I_{SNV}, and the rate constant of its reaction with I_{SNV} is k_{f2} while that with I_T is k_{s2}, with $k_{f2} > k_{s2}$. For simplicity, we assume that $k_f = k_{f2}$ and $k_s = k_{s2}$, a good approximation for most experimentally relevant situations.

To obtain the discrimination factor DF and yield χ for this system, we first need to calculate how much signal $[F_T]$ is produced by a given initial amount of target $[I_T]_0$. From Fig. **??**A) we see that in the presence of target I_T the chemical reaction network (CRN) is given by

$$I_T + P \xrightarrow{k_f} F_T \tag{1}$$

$$I_T + S \xrightarrow{k_s} W_T \tag{2}$$

where W_T is a "waste" product not observed in an experiment. The coupled differential equations that can be derived from this CRN do not have a closed-from solution. However, we can still find $[F_T]_\infty$, *i.e.* the signal strength at equilibrium by considering that

$$\frac{[\dot{F_T}]}{[\dot{W_T}]} = \frac{k_f[I_T][P]}{k_s[I_T][S]} \approx \frac{k_f[P]_0}{k_s[S]_0}. \tag{3}$$

The approximation holds when $[P]_0, [S]_0 \gg [I_T]_0$, so that $[P]$ and $[S]$ are effectively constant through the course of the reaction. For the above expression we see that $[\dot{F_T}]/[\dot{W_T}]$ is constant and, consequently, the ratio of concentrations $[F_T]/[W_T]$ also remains constant at all times. Integration with the initial conditions $[W_T]_0 = [F_T]_0 = 0$ results in $[F_T]/[W_T] = k_f[P]_0/(k_s[S]_0)$. Moreover, at equilibrium, we have $[I_T]_0 = [F_T]_\infty + [W_T]_\infty$ since all target I_T was converted into either F_T or W_T. Combining this conservation law with the previous

result we obtain

$$[F_T]_\infty = \frac{k_f[P]_0}{k_f[P]_0 + k_s[S]_0}[I_T]_0. \tag{4}$$

An expression for $[F_{SNV}]_\infty$ can be derived using an analogous procedure and has exactly the same form as the expression for $[F_T]_\infty$ but with the roles of k_f and k_s interchanged.

Substituting our results into the definition for the discrimination factor, DF = $[F_T]/[F_{SNV}]$, we find that DF= k_f/k_s for an idealized competitive system. The yield can be similarly calculated as $\chi_T = \frac{k_f}{k_f+k_s}$. For our simulations, we arbitrarily set $k_s = k_f/5$; this leads to DF = 5 and yield $\chi = 5/6$. Numerical time course simulations for $[F_T]$, $[F_{SNV}]$ and DF are shown in Fig. **??**A. The numerical value for the discrimination factor rapidly drops to a steady state value slightly below the analytically derived value of DF=5. This is not surprising since for the simulations the concentrations of probe and sink are not constant over the course of the reaction as we assumed in our analytical derivation above.

Amplification. Next, we consider the effect of an amplification probe P_{amp}, which is catalytically converted to a fluorescent signal species by I_T or I_{SNV} (Fig. 1B). As above, we will refer to the signals produced by I_T as F_T and I_{SNV} as F_{SNV} although, in an experiment, they would result from the same molecular species. The amplification probe is specific to I_T, so the rate constant of $P_{amp} + I_T$ is k_f while the rate constant of $P_{amp} + I_{SNV}$ is k_s. In the case where I_T is added to the probe we have

$$I_T + P_{amp} \xrightarrow{k_f} I_T + F_T. \tag{5}$$

The corresponding differential equations can be integrated to yield $[F_T] = [P_{amp}]_0(1 - e^{-k_f[I_T]t})$. The equations and result for the mismatched input I_{SNV} is completely analogous with k_s instead of k_f and F_{SNV} in the place of F_T.

We note that at equilibrium, all P_{amp} is converted into F regardless of the rate constant difference; thus, there is no endpoint discrimination. However, at early time points the different kinetics provide significant discrimination, as can be seen from Taylor expansion of the full expression for the discriminations factor:

$$\mathrm{DF}_{max} \approx \frac{k_f[I_T]t}{k_s[I_{SNV}]t} = \frac{k_f}{k_s}. \tag{6}$$

We find $\chi_T = (1-e^{-k_f[I_T]t})[P_{amp}]_0/[I_T]$ for the yield of this system. When t is small, the yield is about 0, and when $t \to \infty$ we get maximum yield $\frac{[P_{amp}]_0}{[I_T]}$. In principle, maximum yield is thus limited only by the concentration of P_{amp}, but in practice oligonucleotide synthesis errors typically limit the yield achievable in an experimental system to about 50 [13].

Combining competition with amplification. Finally, we will show that combining competition with amplification can result in a system that has quadratically better end point discrimination than a purely competitive system while also being similarly sensitive to a system with amplification only (Fig. 1C). We first consider the CRN for the case where the target input I_T is present:

$$I_T + P_{amp} \overset{k_f}{\to} I_T + F_T, \tag{7}$$

$$I_T + S \overset{k_s}{\to} W_T. \tag{8}$$

The corresponding set of differential equations for the concentration trajectories can be integrated. Here, we are most interested in the equilibrium discrimination and we therefore consider only the limit for large times:

$$[F_T]_\infty = [P]_0 \left[1 - \left(1 - \frac{[I_T]_0}{[S]_0}\right)^{k_f/k_s}\right] \approx [P]_0 \frac{k_f [I_T]_0}{k_s [S]_0}. \quad (9)$$

For mathematical convenience, we further assume that the initial amounts of catalytic probe and sink are equal, $[S]_0 = [P]_0$, resulting in a slightly more compact expression of the equilibrium signal, $[F_T]_\infty = [I_T]_0 k_f/k_s$.

The chemical reactions with the input I_{SNV} are essentially of the same form as those for I_T but with k_f replacing k_s and vice versa, and therefore $[F_{SNV}]_\infty = [I_{SNV}]_0 k_f/k_s$ Combining these results we find that the discrimination factor is

$$DF_\infty = \frac{[F_T]}{[F_{SNV}]} = \left(\frac{k_f}{k_s}\right)^2. \quad (10)$$

For our simulations with $k_f/k_s = 5$, we indeed observed DF ≈ 25 (Fig. **??**). Furthermore, the yield is $\chi_T \approx \frac{k_f}{k_s} = 5$ for our simulation.

Experimental Results

Next, we experimentally tested the predictions for the three different probe systems made by our analysis. For our experiments we used the rationally designed Target and SNV sequences shown in Fig. 2A. Probe sequences were designed to be self-similar to minimize the effects of non-local structure on overall thermodynamics. The CAC>CGC mutation is the most difficult SNV to discriminate against, because CGC will form a G-T wobble with the GTG complement subsequence of the CAC target. At 25 °C in 1 M Na+, the $\Delta\Delta G^\circ$ of the CGC/GTG wobble pair compared to CAC/GTG is only +2.11 kcal/mol [14] (compared to +6.61 kcal/mol for CGC>CCC). Theoretically, it has been shown that DF is upper-bounded by $e^{\Delta\Delta G^\circ/R\tau}$, where R is the universal gas constant and τ is the temperature in Kelvin [11]. Thus, hybridization probes for the CAC>CGC is limited to DF < 35 (compared

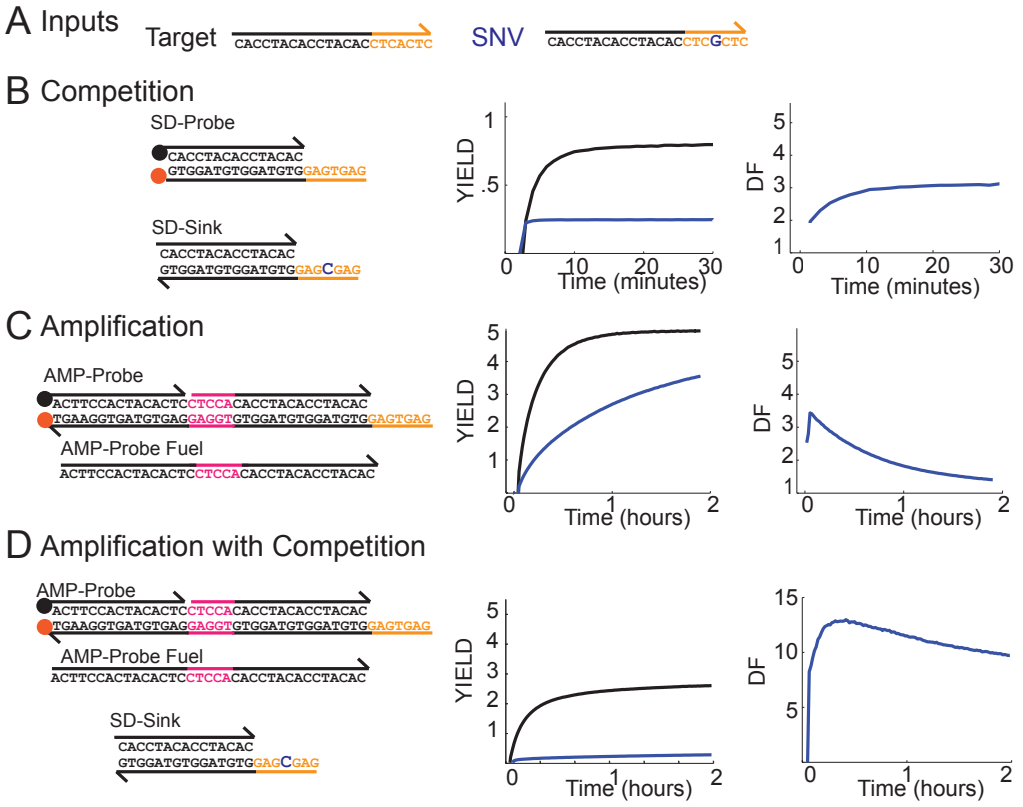

FIG. 4-2: Experimental results on CAC>CGC SNV discrimination using the three different circuits. **(A)** Sequences of the Target and SNV. **(B)** Competition circuit. Probe and Sink sequences for the competitive circuit, and experimentally observed fluorescence results. Initial concentrations were $[\text{SD-Probe}]_0 = 10$ nM, $[\text{SD-Sink}]_0 = 10$ nM. At time $t = 0$, concentrated Target or SNV (1 μM) was introduced to achieve input concentration of 5 nM. **(C)** Amplification circuit. Probe component architecture and sequences, and experimentally observed fluorescence results. Initial concentrations were $[\text{AMP-Probe}]_0 = 10$ nM, $[\text{AMP-Fuel}]_0 = 30$ nM. At time $t = 0$, concentrated Target or SNV (1 μM) was introduced to achieve input concentration of 2 nM. **(D)** Competitive amplification circuit. combined amplification and competition circuit system. Note that a slightly different Sink architecture is used here to ensure similarity of rate constants between the amplification probe and the sinks.

to DF $<$ 70,000 for CGC>CCC). In practice, experimentally observed DF are frequently significantly smaller than this theoretical upper bound; for example, in our experiments, the CAC>CGC SNV could only be discriminated with DF ≈ 3.1 and DF ≈ 3.4, for competitive probes [9] and amplification probes [15], respectively. We chose to perform on our systematic experimental studies on the CAC>CGC mutation in order to have a consistent basis for

comparison, and also to serve as a lower-bound for the selectivity our integrated biochemical circuit can achieve.

Discrimination by competition. Competitive DNA strand displacement probes were first introduced by Li et al. [9] and we here follow their design specifications. The probe is a partially double-stranded DNA molecule with a single-stranded overhang, the "toehold," which serves as a binding site for initiating the reaction between target and probe. The toehold is 7 nt long while the double-stranded domain is XX bp. The probe is labeled with a fluorophore strand on the target-complementary strand, and labeled with a quencher on the other strand, so that natively the probe is in a dark state (Fig. 2B). When the probe reacts with a target molecule, the quencher-labeled strand is displaced from the fluorophore-labeled strand, and the observable fluorescence increases. The sink has the same design as the probe, except that both strands are unlabeled and the sequence is chose to provide e perfect match to the SNV target.

For our initial experiments we designed the SNV target sequence such that a mismatch is created with the toehold domain of the probe. The time-based fluorescence and the inferred discrimination factor for this system are shown on the right hand side of Fig. 2B. We fund that at equilibrium, the DF is roughly 3.1 and the yield of the Target is roughly 0.8.

Amplification Circuit. To realize a catalytic signal amplification reaction we used the entropy driven catalyst system introduced by Zhang et al. [15]. The amplification system has two components: a single-stranded Fuel and a three-stranded Probe (Figs. 2C and S1). In the absence of either Target or SNV, the Fuel and the Probe are metastable and do not react significantly.

However, in the presence of the Target, a fast pathway for the rearrangement of the Probe and Fuel strands becomes available. The Target is transiently bound to the Fuel during this process but is eventually released and thus acts catalytically. The same reaction pathway can also be catalyzed by the SNV Target albeit with slower kinetics.

Example kinetics data for this systems are shown in Fig. 2C. Experimentally, we see that the discrimination factor at early time points is DF=3.8, but approaches DF=1 at later time points, consistent with our model. The early initial rise in of the discrimination factor is due to slight differences in the time at which the reaction began or in mixing.

Combining competition with amplification. Next, we set out to test our prediction that a combination of competition with amplification should dramatically enhance probe specificity. The kinetics traces for target input (black) and SNV input (blue) are shown in Fig. 2D. The reaction of the competitive amplification circuit with the Target results in a maximum yield of 2.5, while the reaction with the SNV input has low yield (0.2), leading to a large DF.

The final DF value for this system is ≈ 10, quadratically larger than the maximal discrimination factor measured for competition or amplification alone. Although this result demonstrates that amplification in parallel with competition results in sensitive and specific probes, the numerical agreement between the model and data may be somewhat coincidental. The amplification reaction is a multi-step process involving at least two strand displacement steps, but our model assumes that this process can be reasonably approximated as a bimolecular reaction with rate constant k_f (or k_s for the SNV input). Thus, unlike in the case of the non-amplifying probe, k_f (k_s) cannot be interpreted as the rate constant for a single strand displacement reaction. Given that k_f describes different processes depending on the context, it is difficult to directly compare discrimination factors measured with different probes.

We also note that our model assumes that rate of reaction between the SNV input and sink is equal to the rate of reaction between Target and Amplifier. Although this is not a necessary condition for the system to work, it simplifies the interpretation of the results. However, this condition is clearly not met for the current system: the reaction between target and amplifier involves multiple strand displacement steps while the reaction between

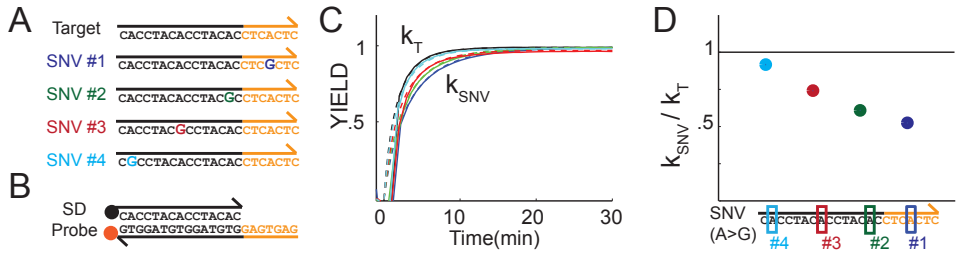

FIG. 4-3: Position dependence of a single nucleotide variation (SNV) on the reaction rate of strand displacement. **(A)** The sequences of the target and four distinct SNVs. Each SNV is the same CAC>CGC triplet replacement, and should have highly similar thermodynamics. **(B)** The sequence of the Probe matches the Target. Reaction with SNV inputs involves making a mis-binding of CGC and GTG with energy penalty 2.11 kCal/Mol. **(C)** Kinetics traces for different inputs. Reaction with the target input is the fastest; reactions with SNV inputs are slower but each reaction trace is different which indicate different reaction rate for the SNV inputs. Experiments were performed in 1x TAE with 12.5 mM Mg^{2+} at room temperature.Initial concentrations of probe and input were 10nM and 5nM, respectively. **(D)** Ratio of reaction rates of each SNV input and target input. Reaction rate with SNV1(mutation in toehold) is the slowest. Reaction rate grows as the mutation position moves towards the end of branch migration region and reaction with SNV4 is almost as fast as the reaction with target input.

sink and SNV target only requires one step.

To overcome these issues and create a system that is more easily compared to the model, we next designed a sink that reacts with an input through a similar multi-step reaction pathway as the amplifying probe. Unlike the Probe, the Sink reaction mechanism involves a truncated Fuel species that does not allow repeated cycling of the Target or SNV as a catalyst. Below we will demonstrate that this system not only simplifies comparison with the model but has a major advantage compared to a simpler system.

Position Dependence

So far we have only considered SNV inputs with a mutation in the toehold domain. However, we note that the rate of a strand displacement reaction strongly depends on the exact position of the mutation within the SNV input. Specifically, strand displacement rates are not expected to be sensitive to mutations that occur close to the end of the branch migration region away from the toehold. Once the strand that is being displaced is only

attached to its original binding partner by a few base pairs, these bonds will dissociate spontaneously even if the invading strand cannot replace all the lost base pairs because it carries an SNV. Consequently, because strand displacement is a kinetic process, SNV inputs with the same energy penalty may result in different reaction rate.

In Fig. 3a we compare the reaction rates for the reaction between a reporter complex and four different SNV inputs and experimentally confirm the SNV position dependence of strand displacement kinetics. The four SNV targets are numbered from right (SNV in toehold) to left (SNV at end of branch migration region) and are marked by different colors (blue, green, red, cyan). The SNVs were designed to have the same mutation and nearest neighbors (from CAC to CGC) even thought they occur in different positions within the input. The energy penalties for all I_{SNV}s are therefore the same, and any differences in reaction kinetics should result only from varying the mismatch positions.

Experimental data for the reactions of the different inputs with the probes are shown in Fig. 3b. Experimental traces are shown as solid lines and colored-coded according to the SNV input used as shown in Fig. 3b. We fitted each trace with a simple non-reversible bimolecular rate law to obtain rate constants. The best fit reaction rate constant for target input k_T is $1.2 \cdot 10^6 M^{-1}s^{-1}$ while the rate constants for inputs or SNV1 through SNV4 are $6.3 \cdot 10^5 M^{-1}s^{-1}$, $7.3 \cdot 10^5 M^{-1}s^{-1}$, $8.9 \cdot 10^5 M^{-1}s^{-1}$ and $1.1 \cdot 10^6 M^{-1}s^{-1}$. For comparison, the bimolecular rate constant for the target input is XXXX. The simulation results are shown as dashed lines.

The ratio of reaction rate constants for each SNV input to the rate constant for the target input is shown Fig. 3c. As expected, the rate constant for SNV4 with mismatches by the end of the branch-migration region is almost as fast as the reaction with the target, while reaction rate for SNV1 with mismatches in the toehold is significantly slower than the reaction without mismatch.

Any detection method, such as the competitive reaction using the reporter and sink of

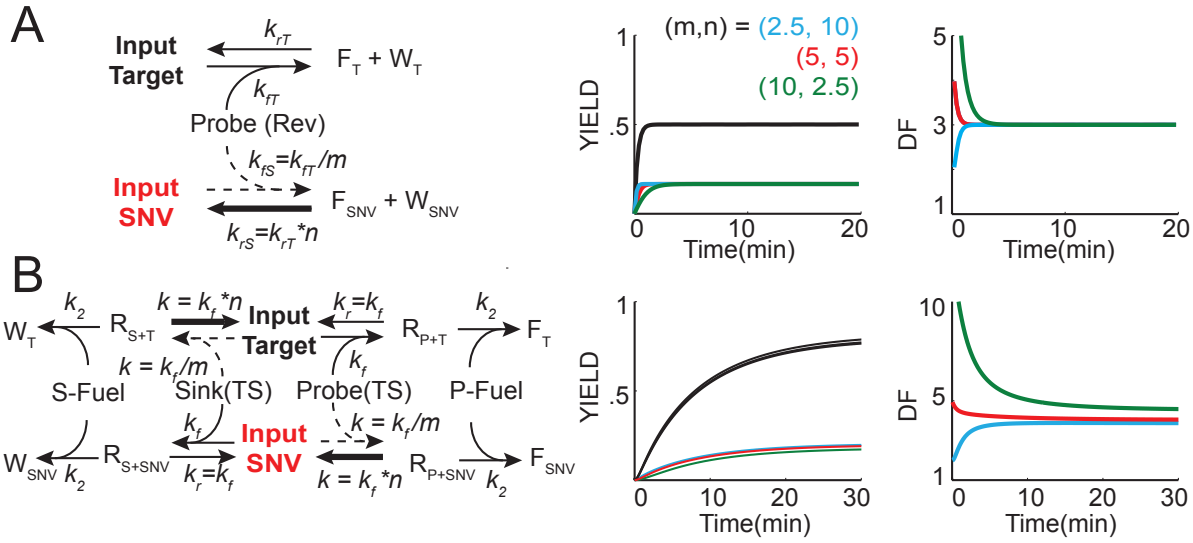

FIG. 4-4: Approaches to reduce position dependence **(A)** A reversible reaction [11]involving a probe that reaches different chemical equilibriums for Target and SNV due to the differential reaction free energy. DF at equilibrium depends only on equilibrium constant but not forward reaction rate difference. **(B)** A new approach to integrate a competitive circuit with reversible reaction to achieve higher discrimination and target yield and preserve the independence of forward reaction rate.

reference XXX, that depends on the ratio on the reaction rate of this non-reversible strand displacement, will lose specificity when there is no difference in reaction rate of the SNV input and target input. Consequently, such an approach cannot distinguish between the target input and input SNV4. Next, we will argue that this issue can be overcome by including a reversible reaction step in the mechanism.

Reversible reaction probe Zhang et al. [11] recently demonstrated an elegant solution to to the problem of position dependence based on toehold exchange. Toehold exchange is a reversible strand displacement reaction where the initially displaced strand can bind back to probe, in turn displacing the target and recreating the original probe. A simple chemical reaction model for this system is given by:

$$I + P_{ToX} \underset{k_-}{\overset{k_+}{\rightleftharpoons}} F + W. \tag{11}$$

Here I is the input strand, P_{ToX} is the toehold exchange probe, F the fluorescent product and W (waste) the non-fluorescent product. This reaction eventually reaches an equilibrium state where the rates for the forward and reverse reaction are balanced:

$$K_{eq} = \frac{[F][W]}{[P_{ToX}][I]} \tag{12}$$

where $k_+/k_- = K_{eq} = e^{-\Delta G/RT}$.

This system functions as a probe because the equilibrium signals will be different for the target and SNV input. To ensure both sensitivity and specificity, we engineer the reaction pathway such that $\Delta \approx 0$ and thus $k_+ \approx k_-$ (13) for the reaction with target input I_P. In practice, this condition can be met by making the toeholds for the forward and reverse reactions equally strong. In this case the yield for this system is $\chi = 0.5$. For reaction with SNV input we have instead $\Delta G_{SNV} = 0 - \Delta\Delta G$ where $\Delta\Delta G$ is the energy penalty for the formation of the mismatch bubble. Importantly, this free energy difference depends only on the identity but not on the position of the SNV.

Next, we derive a closed expression for the discrimination facto $DF = [F_T]_{eq}/[F_{SNV}]_{eq}$. To first find $[F]_{eq}$, we assume that the reaction was initiated with equal amounts of probe and input, $[I]_0 = [P_{ToX}]_0$ and further assume that no products are present initially $[F]_0 = [W]_0 = 0$. It follows the the amounts of probe and input are equal at all times, $[I] = [P_{ToX}] = [I]_0 x$ and that the total amounts of products and reactants should be equal to the initial amounts of reactants, $[W] = [F] = [I]_0(1 - x)$. Substituting these relations into the mass action equilibrium expression and solving for x, we find the following result for the signal at equilibrium as a function of the initial input concentration:

$$[F]_{eq} \;=\; \frac{\sqrt{k_+/k_-}}{\sqrt{k_+/k_-} + 1} * [I]_0. \tag{13}$$

As we noted above, k_+=k_- for the reaction between the probe and the target input and therefore $[F]_{eq} = [I]_0/2$. In contrast, the forward and reverse reaction rate constants for the reaction with the SNV input, k_+^{SNV} and k_-^{SNV}, will vary depending on the location of the SNV. For example, an SNV in the toehold of the input (SNV1) will result in a smaller forward rate constant but will not affect the reverse rate constant. Conversely, a mutation in at the end of the input (SNV4) will not affect the forward reaction but will reduce the rate of the reverse reaction. Still, for the same value of ΔG_{SNV} the ratio of the two rate constants will always have the same value. For the discrimination factor we thus find

$$DF = \frac{[F_T]}{[F_{SNV}]} = \frac{1}{2}\left(1 + \sqrt{\frac{k_-^{SNV}}{k_+^{SNV}}}\right). \tag{14}$$

In the simulation shown in Fig. 4a, we consider three sets of forward and reverse rate constants with the same ratio $k_+^{SNV}/k_-^{SNV} = 25$. Although the different combinations of forward and revere rate constants result in different kinetics traces, their equilibrium states are the same and the discrimination factor at equilibrium is also the same. The discrimination factor calculated from equation is $\frac{1}{2} + \frac{1}{2} * \sqrt{25} = 3$ which exactly agrees with the simulation result.

Our analysis demonstrates that a reversible reaction mechanism can be used to create a highly specific hybridization probe. In fact, Zhang *et al.* [] show that the discrimination can be even better if experiments are performed in a regime where the probe concentration is in large excess of the input concentrations and, furthermore, a large amount of the product species W is added initially to shift the equilibrium towards the reactants. However, this detection method has only very limited sensitivity: in the regime discussed above, the maximals signal that can be achieved is exactly half the input concentration while the signal is even smaller in the regime of Ref. [].

Two step reaction To maintain the position independence we get from reversible

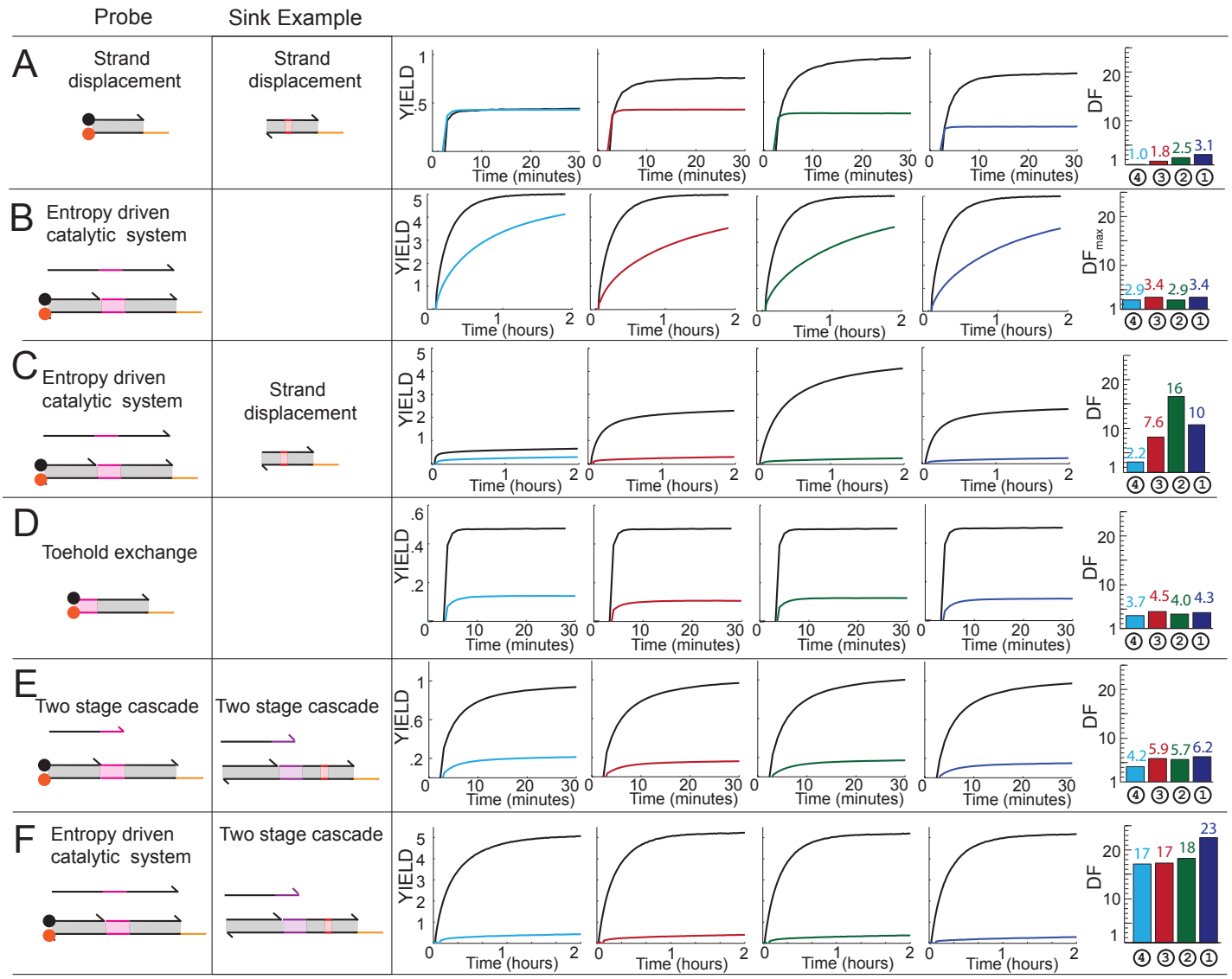

FIG. 4-5: Implementations and time-based fluorescence response for **(A)**The competition circuit exhibits strong DF dependence on the position of the SNV, with SNVs farther from the toehold being more difficult to discriminate. **(B)**Reversible reaction probe do not exhibit significant DF dependence on SNV position. **(C)**Competitive reversible network preserves the position independent property. **(D)**Entropy driven amplification also has a reversible first step reaction, and thus not exhibit significant DF dependence on SNV position. **(E)**competitive amplification circuits achieve higher discrimination for all SNV inputs. DF does not significantly depend on SNV position.

reaction and improve the final yield, we designed a system so that each reaction has two steps: a reversible first step that reaches equilibrium quickly and a slower non-reversible second step that drives the reaction to completion and converts all inputs to products. Combining a probe using this two step reaction mechanism and with a competitive sink using the same mechanism we get the system shown in Fig. 4b where the probe matches the target input, and the sink matches the SNV target. The reactions of the target input can be written as:

$$I_T + P \quad \underset{k_-}{\overset{k_+}{\rightleftharpoons}} \quad R_P + W_1, \;\; R_P + H_P \overset{k_2}{\to} F_T \tag{15}$$

$$I_T + S \quad \underset{k_-^{SNV}}{\overset{k_+^{SNV}}{\rightleftharpoons}} \quad R_S + W_2, \;\; R_S + H_S \overset{k_2}{\to} W_T \tag{16}$$

Here, R_P is a reaction intermediate that can react with the "helper" species H_P to produce the fluorescent signal species. Similarly, R_S is a intermediate for the reaction between the input and the sink and can react with a different helper strand H_S to create a waste product. W_1 and W_2 are strands released in the first, reversible, reaction steps. Finally, we assume that the reaction rates $k_\pm^{SNV}$ for the reactions between target and sink are the same as those for the reactions between SNV input and probe. Below, we will also use that the reactions between target and probe as well as SNV input and sink both occur at rates $k_\pm$.

To obtain the discrimination factor $DF = [F_T]/[F_{SNV}]$ for this system we first derive an expression for $[F_T]$ by approximately solving the differential equation guiding the time evolution of the fluorescent signal,

$$[\dot{F_T}] = k_2[R_P][H_P]. \tag{17}$$

To solve this equation we first need to derive an expression for the reaction intermediate

$[R_P]$ from its equation of motion

$$[\dot{R_{PT}}] = k_+[I_T][P] - k_-[R_P][W_1] - k_2[R_P][H_P] \doteq 0. \tag{18}$$

For the second equation, we made the assumption that the reaction intermediate rapidly reaches a steady, and that the amount of reaction intermediate does not change on time scale of the product formation. This assumption is valid for early reaction time points and is analogous to the assumption made in deriving the Michealis Menten equation for enzyme kinetics. We can solve this equation and find

$$R_{PT} = \frac{k_+[I_T][P]}{k_-[W_1] + k_2[H_P]}. \tag{19}$$

To further simplify this expression and eliminate $[W]$, we note that the following conservation law holds:

$$[W_1] = [F_T] + [R_P] \approx [F_T]. \tag{20}$$

The approximation is valid because we assumed that $[R_P]$ is fixed at a steady state value that will rapidly be exceeded by the amounts of F_T and W_1 since every productive reaction produces one copy of the F_T and W_T species. We can use this relationship to eliminate $[W_1]$ in the expression for $[R_P]$ and substitute into the differential equation of $[F_T]$, so that,

$$[\dot{F_T}] = \frac{k_+k_2[H_P]}{k_-[F_T] + k_2[H_P]}[I_T][P]. \tag{21}$$

If we build a system such that $k_- \gg k_2$ and the concentration of H_P is not very high,

except at the very beginning of the reaction, we have $k_-[F_T] \gg k_2[H_P]$ so that

$$[\dot{F_T}][F_T] = \frac{k_+ k_2[H_P]}{k_-}[I_T][P]. \tag{22}$$

To analyze this expression further, we first note that a completely analogous equation can be derived for $[W_T]$ by considering the differential equations that guide the interaction between the input target and the sink. Specifically, we find that

$$[\dot{W_T}][W_T] = \frac{k_+^{SNV} \cdot k_2[H_S]}{k_-^{SNV}}[I_T][S]. \tag{23}$$

Because $[H_S] = [H_P]$ and $[S] \approx [P]$, we thus have

$$\frac{[\dot{F_T}][F_T]}{[\dot{W_T}][W_T]} = \frac{k_+ k_-^{SNV}}{k_- k_+^{SNV}}. \tag{24}$$

Integration with the initial condition $[F_T]_0 = [W_T]_0 = 0$ yields

$$\frac{[F_T]}{[W_T]} = \sqrt{\frac{k_+ k_-^{SNV}}{k_- k_+^{SNV}}}. \tag{25}$$

Finally we note that at the end of the reaction, all initial input will be converted to either waste $[W_T]$ through reaction with the sink or to $[F_T]$ through reaction with the probe and thus $[I_T]_0 = [F_T] + [W_T]$. Substituting into the equation above, we can solve for $[F_T]$ and obtain

$$[F_T] = \frac{\sqrt{\frac{k_+ k_-^{SNV}}{k_- k_+^{SNV}}}}{1 + \sqrt{\frac{k_+ k_-^{SNV}}{k_- k_+^{SNV}}}}[I_T]_0. \tag{26}$$

An expression for $[F_{SNV}]$ can be derived completely analogously. The result is the same

as that for $[F_T]$ but with the roles of $k_\pm$ and $k_{\pm S}$ interchanged, that is

$$[F_{SNV}] = \frac{1}{1 + \sqrt{\frac{k_+ k_-^{SNV}}{k_- k_+^{SNV}}}} [I_{SNV}]_0. \tag{27}$$

From these results we can finally derive the discrimination factor and find that

$$DF = \sqrt{\frac{k_+ k_-^{SNV}}{k_- k_+^{SNV}}}. \tag{28}$$

So that, in the ideal experimental condition, DF depend only the free energy difference and is independent of the forward reaction rate. Moreover, if we design our system such that $k_+ = k_-$, we find that $DF = \sqrt{k_-^{SNV}/k_+^{SNV}}$. This is result is very similar to the result we found for a fully reversible probe, but we note that the two-step mechanism results in slightly better discrimination than the former. Furthermore, addition of the irreversible second reaction step also results in a higher yield for the reaction.

In the simulation shown in Fig 4b, we tested three cases with same reaction free energy (eg. $m \cdot n$) but different forward and reverse reaction rates for mismatch binding (eg. $(m, n) pairs$). Although DF plot over time shows significant difference at the beginning of the reaction, all traces approach similar values on equilibrium. The DF for reaction with slower forward reaction (eg, larger m) is slightly higher than the other two cases (4.4 compares to 4.0 and 3.9) due to the approximations we took in analysis.

Combining competition with amplification. Next, we will combine a sink based on a two-step mechanism with a competitive amplification reaction. The chemical reactions

for of the target input can be written as:

$$I_T + P \underset{k_-}{\overset{k_+}{\rightleftharpoons}} R_P + W_1, \;\; R_P + H_{Amp} \xrightarrow{k_2} F_T + I_T \tag{29}$$

$$I_T + S \underset{k_-^{SNV}}{\overset{k_+^{SNV}}{\rightleftharpoons}} R_S + W_2, \;\; R_S + H_S \xrightarrow{k_2} W_T \tag{30}$$

These equations are almost identical to the non-amplified case discussed previously, except that the reaction of the input with the probe is now catalytic such that the input is released again in the final reaction step. Furthermore, the helper species for the first reaction, H_{Amp} is modified to enable the catalytic reaction pathway.

We can analyze this system in a similar manner to the analysis we performed for the non-amplifying two-step system. In fact, the derivation of the expression for $[F_T]$ is identical up to Eq. 25. However, instead of the conservation law $[I]_0 = [F_T] + [W_T]$ which applied in the non-catalytic case we here have $[I]_0 = [W_T]$ since an input will be recycled until it is irreversibly bound to the sink. Thus, we find that

$$[F_T] = \sqrt{\frac{k_+ k_-^{SNV}}{k_- k_+^{SNV}}} [I_T]_0. \tag{31}$$

The result for $[F_S NV]$ is identical with the roles of f $k_\pm$ and $k_{\pm S}$ interchanged and $[I_{SNV}]_0$ in place of $[I_T]_0$. Consequently, we find that the discrimination factor is given by

$$DF = \frac{k_+ k_-^{SNV}}{k_- k_+^{SNV}}. \tag{32}$$

Thus, as we found for the simpler one-stage mechanism introduced above, the amplification reaction results in quadratically better discrimination.

Experimental Results of Position Dependence All five approaches to SNV discrimination discussed above were tested experimentally with the four distinct SNV inputs

as shown in Fig 3A. The free energy changes due to the mutation identity are the same, any significant difference in DF depends difference in mutation position.

The discrimination of competition circuit we discussed previously depend only on the forward strand displacement rate. The circuit works best for mutation in the toehold with end discrimination $DF = 3.1$. The DF decreases as the mutation position move towards the end of branch migration region and the system loses specificity (i.e. $DF = 1$) when the mutation happens by the end of strand displacement region (cyan) because there is almost no change in kinetics constant.

The reversible reaction is implemented with toehold exchange probe [11] without any sink. The endpoint discrimination factors range from 3.7 to 4.5 for the four distinct SNVs.

The two step competition circuit is implemented with two stage cascade, where the first reversible step reduces the DF dependence on mutation position. The endpoint DF for this circuit ranges from 4.2 (SNV4) to 6.2 (SNV1). Compare to the simple competition circuit, the position dependence is much reduced.

The simple amplification circuit also has a reversible first step and thus there is no strong DF dependence on mutation position. Because all DF eventually decays to 1, we show the DF_{max} which is the maximum discrimination during the two hours experiment time. The DF_{max} ranges from 3.4 to 2.9 which is close.

In the competitive amplification circuit, either reaction with probe or sink has a reversible first step that reduce the position dependence of discrimination. For all distinct SNVs, DF is significantly larger than and roughly equivalent to ???? the product of the amplification system and two stage competition system.

Let-7 RNA discrimination

So far, we only tested out engineered discrimination system with DNA inputs, but discrimination between single-stranded RNA is of more likely interest for practical applications.

As a proof-of-concept demonstration of RNA detection we designed a system that could distinguish between different members of the let-7 family of microRNAs [**?**]. Let-7 family miRNA have important roles in development and at least eight different family members are found in humans. For our experiments, we used synthetic RNA oligonucleotides with the same sequences as the human miRNA let-7A from let-7C and let-7E. Specifically, we aimed to discriminate between let-7A and the other two sequence which are both only one base change removed from let-7A (Fig. 6A).

We found that a discrimination system combining competition with amplification could distinguish let-7A from both let-7C and let-7E with high specificity (DF$\approx$ 15) and sensitivity. It is particularly encouraging that this experiment did not require any specific modifications to the amplification system or sink, even though DNA-RNA interaction parameters, and thus the strand displacement rate constants, can be fairly different from those measured for DNA-DNA interactions.

Discussion

Here we demonstrate that a rational design approach based on strand displacement reactions can be used to create a sensitive and specific discrimination system. First, we showed that amplification in parallel with competition can result in quadratically better discrimination than a system without amplification, Importantly, because of the built-in amplification step, this system also provided dramatically improved sensitivity. Furthermore, we found that a reaction mechanism involving a reversible first step can result in further specificity improvements. Most importantly, SNVs could be reliably identified independently of their position within a target strand. In contrast, a system based on a single irreversible detection step cannot reliably detect SNV that are far from the toehold.

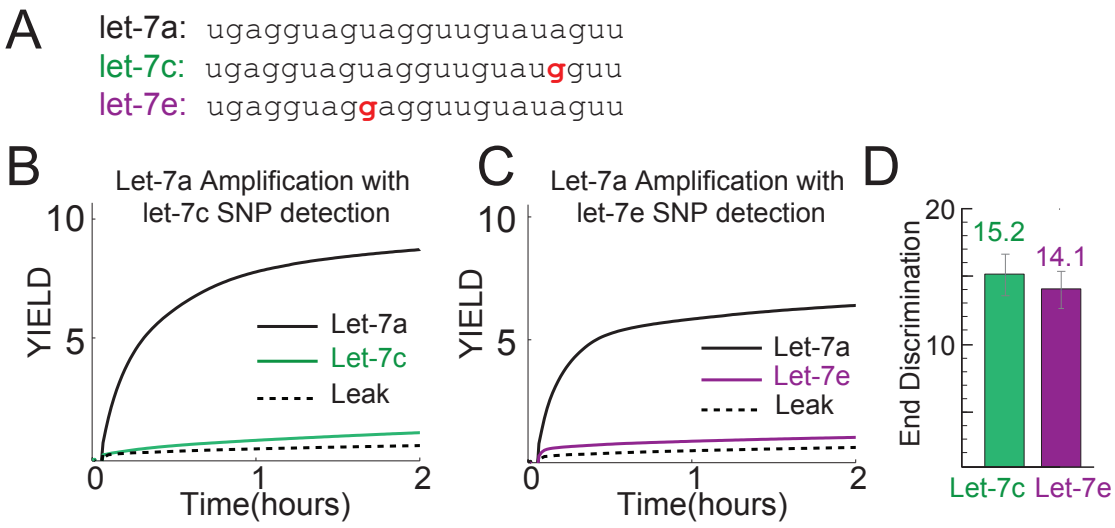

FIG. 4-6: **(A)** Sequences of the let-7a, let-7c, and let-7e microRNA. Both let-7c and let-7e differ from let-7a by only a single nucleotide. **(B)** Time-based fluorescence response of the competitive amplification circuit targeting the let-7a sequence and suppressing the let-7c sequence. **(C)** Time-based fluorescence response of the competitive amplification circuit targeting the let-7a sequence and suppressing the let-7e sequence. Note that because the response due to the let-7a sequence differs from in panel (B) because let-7a interacts differently with the let-7e sink than with the let-7c sink. **(D)** Summary of observed discrimination factor values. Error bars show the standard deviation of the DF across different repeats.

[1] Saiki, R. K., Gelfand, D. H., Stoffel, S., Scharf, S. J., Higuchi, R., Horn, G. T., Mullis, K. B. & Erlich, H. A. Primer-directed enzymatic amplification of DNA with a thermostable DNA polymerase. *Science* **239,** 487-491 (1988).

[2] Kim, S. & Misra A. SNP genotyping: technologies and biomedical applications. *Annu. Rev. Biomed. Eng.* **9,** 289-320 (2007).

[3] Mardis E.R Next-generation DNA sequencing methods*Annu Rev Genomics Hum Genet.* **9**387-402(2008)

[4] Petersen, M. & Wengel, J. LNA: a versatile tool for therapeutics and genomics. *Trends Biotechnol.* **21,** 74-81, (2003).

[5] He, G., Rapireddy, S., Bahal, R., Sahu, B. & Ly, D.H. Strand invasion of extended, mixed-sequence B-DNA by gamma PNAs. *J. Am. Chem. Soc.* **131,** 12088-12090 (2009).

[6] Kierzek, E., Mathews, D. H., Ciesielska, A., Turner, D. H. & Kierzek, R. Nearest neighbor param-

eters for Watson-Crick complementary heteroduplexes formed between 2'-O-methyl RNA and RNA oligonucleotides. *Nucleic Acids Res.* **34,** 3609-3614 (2006).

[7] Tyagi, S. & Kramer, F.R. Molecular beacons: probes that fluoresce upon hybridization. *Nature Biotechnology* **14,** 303-308 (1996).

[8] Tyagi, S., Bratu, D. P., & Kramer, F. R. Multicolor molecular beacons for allele discrimination. *Nature Biotechnology* **16,** 49-53 (1998).

[9] Li, Q., Luan, G., Guo, Q. & Liang, J. A new class of homogeneous nucleic acid probes based on specific displacement hybridization. *Nucleic Acids Res.* **30,** E5 (2002).

[10] Xiao, Y., Plakos, K. J. I., Lou, X., White, R. J., Qian, J., Plaxco, K. W. & Soh, H. T. Fluorescence detection of single-nucleotide polymorphisms with a single, self-complementary, triple-stem DNA probe, *Angew. Chemie Int. Ed.* **48,** 4354-4358 (2009).

[11] Zhang, D.Y., Chen, S. X. & Yin, P. Thermodynamic optimization of nucleic acid hybridization specificity. *Nature Chemistry* **4,** 208-214 (2012).

[12] Zhang, D.Y., Cooperative Hybridization of Oligonucleotides. *Journal of the American Chemical Society* **133,** 1077-1086 (2011)

[13] D. Y. Zhang, E. Winfree, *Nuc. Acid Res.* (2010, pre-published online DOI:10.1093/nar/gkq088).

[14] J. SantaLucia, D. Hicks, *Annu. Rev. Biophys. Biomol. Struct.* **33,** 415 (2004).

[15] D. Y. Zhang, A. J. Turberfield, B. Yurke, E. Winfree, *Science* **318,** 1121 (2007).

Chapter 5: Linear Classification of RNA Single Nucleotide Variants

This work has been experimentally completed and is currently undergoing final proofreading, and describes the construction of a linear classification reaction system that integrates information encoded at the molecular level in RNA species' concentrations. Biological systems are robust to small variations in RNA expression levels, and employ complex networks to robustness communicating information between cells and tissues. The circuit constructed in this work is a first step towards the rational engineering of biomolecular circuits that can sense and regulate nucleic acid environments.

Abstract: Cell state information is encoded across a large number of RNA molecules; biomolecular interpretation of RNA profiles can lead to construction of synthetic biological circuits that are responsive to cell and organism state. Here, we make a first step through the construction of a DNA circuit that performs linear classification on two RNA sequences that differ in sequence by a single nucleotide. This is implemented through two fixed gain amplifier circuits that implement the weighting of the RNA inputs; gain can be tunably

controlled through stoichiometric formulation of two circuit components.

In the past decades, nucleic acids have been used to build logic circuits, amplifiers and single nucleotide polymorphism (SNP) detectors, with the potential for use as scientific analysis tools, point of care diagnostics, or even smart *in vivo* therapeutics. Most of these works have been proof-of-concept, and sought to use biomolecules to mimic electronic computers; consequently, DNA input and output sequences were synthetically designed with little to no secondary structure. As synthetic biology applications of molecular programming emerge, it is necessary to be able to design DNA circuits that act on biologically relevant input sequences. MicroRNAs (miRNA), in particular, as an attractive class of input molecules for sensing biological state, because each microRNA species broadly regulates the expression levels of many different mRNAs. MiRNA profiles have been observed to be significantly different in cancer patients vs. in healthy people.

MiRNAs are broadly expressed but expression levels vary depending on tissue type and disease state. Often, two or more miRNAs regulate the same mRNA, and thus the net effect on a particular targeted mRNA species integrates the effects of these miRNA inputs. Mathematically, we can define this input-output relationship as:

$$[mRNA] = f([miRNA_1], [miRNA_2], ...) \tag{1}$$

where $[mRNA]$, $[miRNA_1]$, $[miRNA_2]$, etc. denote the concentration of RNAs, and $f(\cdot)$ is an arbitrary mapping function. The true form of mapping function in biology is likely complex and varies based on mRNA output species, but a large fraction of the effects may

be captured by a weighted linear combination:

$$[mRNA] = \alpha_1[miRNA_1] + \alpha_2[miRNA_2] \tag{2}$$

where α_1 and α_2 are the weights. From a linear combination input-output relationship, linear classification may be achieved through the use of a thresholding mechanism, e.g. the Notch signalling pathway in developmental biology. Multiple engineered DNA threshold circuits have been demonstrated, but to date linear combination evaluation of input species with arbitrary weights has not been experimentally shown.

Here, we rationally design a biomolecular implementation of a linear combination circuit with tunable weights α (Fig. 1). A test solution will act on a homogeneous sample containing 2 different RNA species, and the resultant fluorescence is the desired linear combination. Fluorescence here serves as a proof of concept; our prior research has shown that conversion of molecular information between different nucleic acid species can be implemented through translator gates [1].

Results

Fixed Gain Amplification. The central component of the linear combination circuit is the fixed gain amplification module, in which the concentration of an RNA input species is converted into another DNA information species at exactly α_1-fold higher concentration. In prior experimental demonstrations of DNA amplification circuits [1–3], the gain (a.k.a. total amplification) of a DNA or RNA input species was primarily determined by oligonucleotide impurity [4] and thus was poorly quantitatively reproduced across different synthesis preparations of the component oligonucleotides.

In principle, combining a catalysis circuit with a sink can implement a fixed gain [5]: in each reaction cycle, there is probability p that an input molecule RNA1 is consumed by the

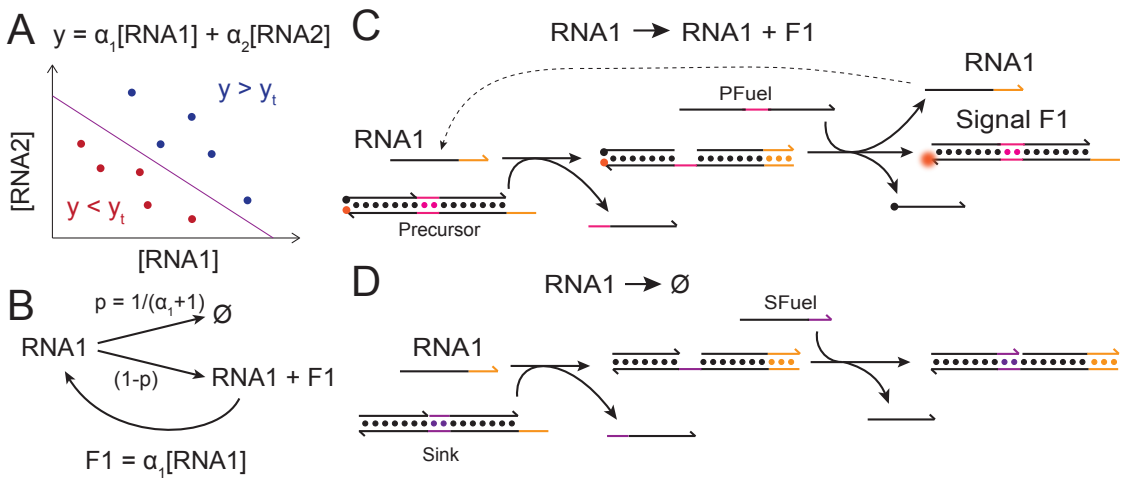

FIG. 5-1: **(A)** Linear classification of two RNA species. The concentrations of RNA1 and RNA2 are weighted by α_1 and α_2 and added to be y. The system is classified as Type 1 (blue) if y exceeds threshold y_t, and Type 2 (red) otherwise. **(B)** Weighting constant α_1 is implemented through a DNA circuit that acts on the RNA1 species. In each reaction cycle, with probability p, RNA1 reacts with a Sink species that consumes RNA1, and with probability $(1-p)$, RNA1 reacts with a catalytic Substrate in a reaction that releases a product molecule while leaving the RNA1 species unchanged. The value of p can be tuned based on both the concentrations of the Sink and the Substrate, and on the relative reaction rate constants. **(C)** Catalysis reaction implementation, based on ref. [2]. The Precursor and Fuel are kinetically inhibited from reaction unless catalyzed by RNA1. Fluorescence increases through the course of the reaction as the quencher on the Precursor is delocalized from the fluorophore. **(C)** Sink reaction implemenetation. The Sink and Fuel are designed so that the Sink reaction maximally resembles the catalysis reaction, so that rate constants are comparable between the two reactions. Catalysis is not possible in this reaction because the shortened Fuel oligonucleotide is unable to displace the RNA1 input.

Sink, and a probability $(1-p)$ that the input molecule instead catalytically releases 1 unit of signal F1. At equilibrium, the total amount of F1 released will be:

$$\begin{aligned}[F1] &= [RNA1] \cdot \sum_{i=1} \infty i p (1-p)^i \\ &= (\frac{1}{p} - 1)[RNA1] \equiv \alpha_1 [RNA1]\end{aligned}$$

Rearranging, we find that $p = \frac{1}{\alpha_1 + 1}$.

Construction of a reaction circuit that properly implements this idea is nontrivial, because the kinetic profiles of the catalysis and sink reactions may be different, resulting in

p values that change over time. We here propose the catalysis and sink systems shown in Fig. 1CD. The catalysis system is adapted from ref. [2], and the sink system is a modified version of the catalyst with a fuel strand that is incapable of displacing the input. Thus, the Sink can be designed with a reaction kinetic profile matching that of the catalyst reaction.

By fixing the concentration ratios $\frac{[\text{PFuel}]}{[\text{Precursor}]}$ and $\frac{[\text{SFuel}]}{[\text{Sink}]}$ to be the same, and the probability p becomes simply dependent on the ratio of the Precursor and Sink concentrations: $p = \frac{[\text{Sink}]}{[\text{Precursor}] + [\text{Sink}]}$. The fixed gain amplification circuit inherently assumes that the Precursor and Sink will not be limiting, that at equilibrium neither Sink nor Precursor is exhausted when RNA1 is converted into α times the Signal.

For two proof-of-concept demonstration of the fixed-gain amplifier circuit, we use let-7a and let-7c, two members of the let-7 family of microRNAs. These two miRNA sequences differ from one another by only one nucleotide and is typically difficult to distinguish by biomolecular circuitry. Fig. 2 shows our individual experimental results on the input-output relationship for the two circuits. The linearity of the output signal with the input concentration indicates that the gain α is conserved for different input concentrations. Triplicate repeats of 2nM input shows that equilibium signal results are repeatable. From our experiments, the best-fit slope is $\alpha_1 = 2.86 \pm 0.06$, and is close to the initial designed value of $\alpha_1 = 3$. Experiments on a fixed-gain amplifier circuit with the let-7c miRNA as input produced a best-fit slope of $\alpha_2 = 3.13 \pm 0.11$, and is also close to the designed value of $\alpha_2 = 3$.

Fig. 3 demonstrates our ability to finely control the gain based on the formulation stoichiometry of Precursor and Sink, Here, the input concentrations are fixed at 2 nM, and the Precursor concentrations are fixed at 30 nM. The concentration of the Sink was adjusted to achieve different designed gains α. Because $\frac{[\text{Precursor}]}{[\text{Input}]} = 15$, the system can tolerate a maximum α of 15 without Precursor being the limiting reagent. The observed α closes matches the designed α for values between 1 and 8 for both circuits based on the let-7a and

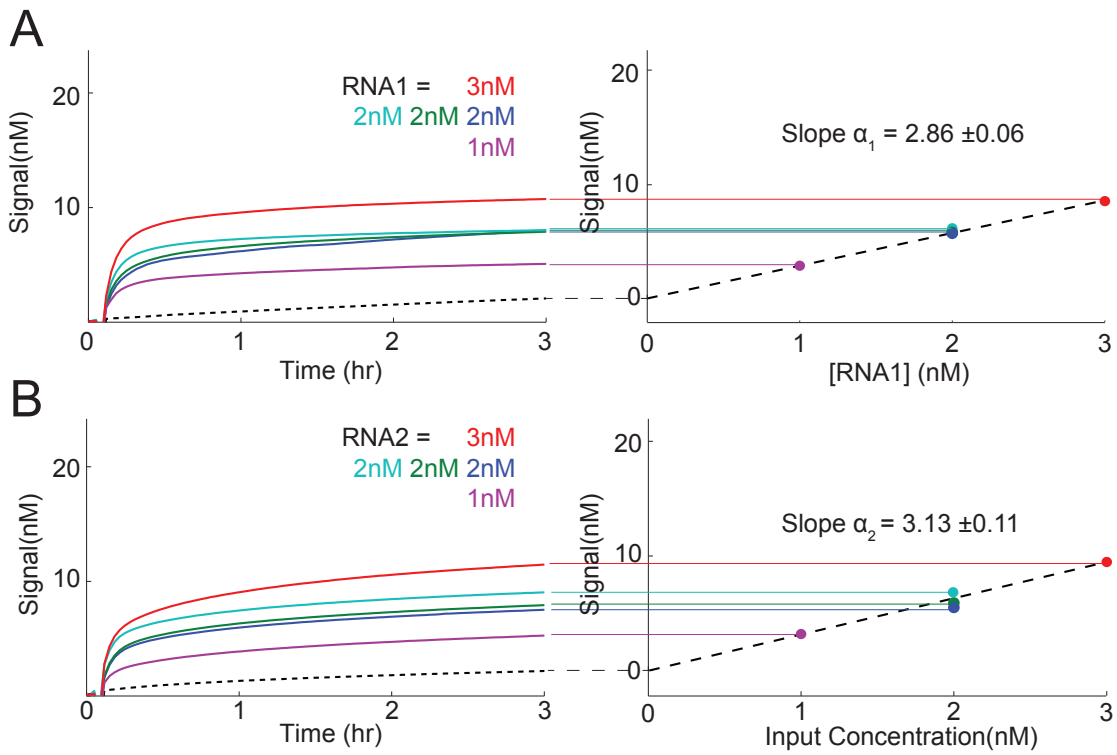

FIG. 5-2: Input-output linearity of fixed-gain circuit. **(A)** A first circuit designed with the let-7a miRNA as the RNA input. Left panel shows kinetic trace; there is slight background signal (dotted line) due to residual uncatalyzed reaction of the Precursor. Gain α_1 was observed to be 2.9 at t = 3hr for [Sink] = 10 nM and [Precursor] = 30 nM, whereas the concentrations suggest designed $\alpha_1 = 3$ if the rate constants of Sink and Precursor were identical. Gain is calculated as the slope of the least-squares fit of the observed fluorescence against the input concentration. **(B)** A second circuit design with the let-7c miRNA as the RNA input, with an observed $\alpha_2 = 3.1$. As in panel (A), [Sink] = 10 nM and [Precursor] = 30 nM.

let-7c inputs.

Linear Combination. A solution containing both sets of fixed-gain amplifier circuits implements the weighted linear combination function. As proof-of-concept, we designed the linear combination circuit with $\alpha_1 = 5.4$ and $\alpha_2 = 3.2$. Fig. 4ab shows the results for 5 combinations of let-7a and let-7c concentrations and their resultant aggregate signal; Fig. 4c shows the concordance between the designed and experimentally observed classifications over a threshold range of 10 to 22 nM.

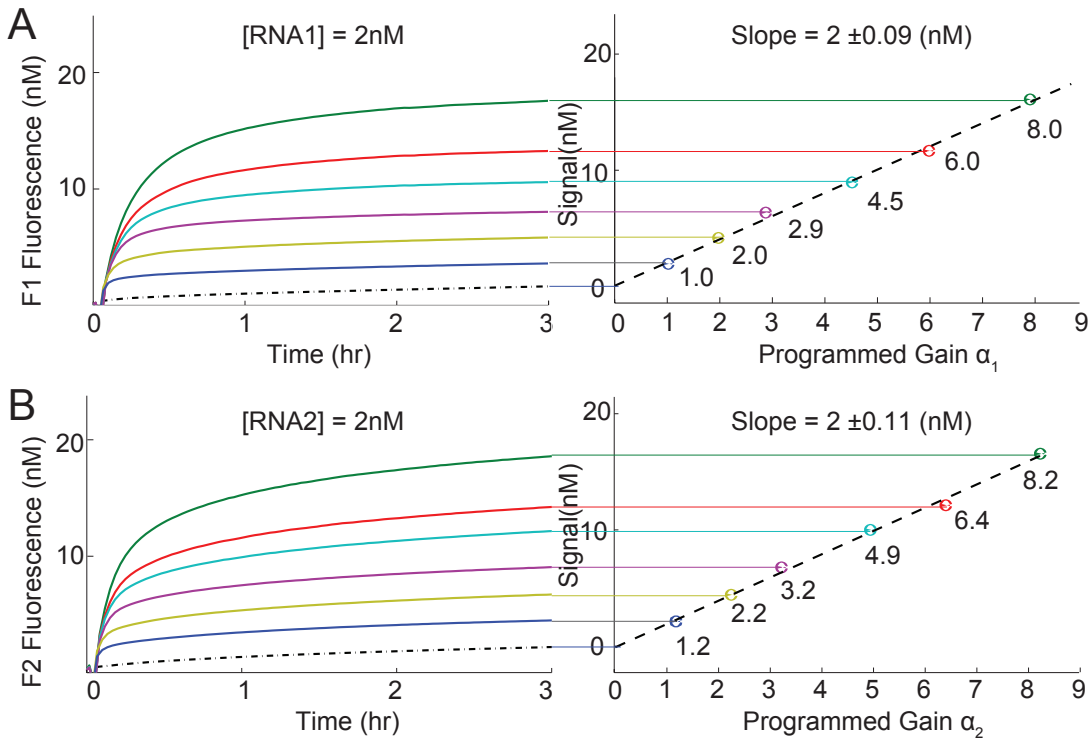

FIG. 5-3: Adjusting gain α. The gain α is expected to be $\frac{[\text{Precursor}]}{[\text{Sink}]}$, assuming that the rate constants of reaction with Precursor and Sink are identical. Shown are predicted vs. observed gains for the circuits with **(A)** let-7a and **(B)** let-7c as inputs. In all experiments, initial Precursor concentration was set at 30 nM, and Sink concentration was determined from desired α.

Discussion

Here we experimentally implemented a linear combination circuit with two inputs. Fixed-gain amplifier circuits were used to implement the weights, with the gain α controlled by the formulation stoichiometry of a catalyst Precursor versus a Sink. A novel Sink architecture was presented to match the kinetics profile of the catalysis reaction and the sink reaction. Used in combination in the same solution, two different fixed-gain amplifier circuits to the let-7a and let-7c microRNA inputs implemented a designed linear weighting function, and experimental results showed high concordance with designed classification.

Combining the linear combination circuit presented here with a threshold circuit will

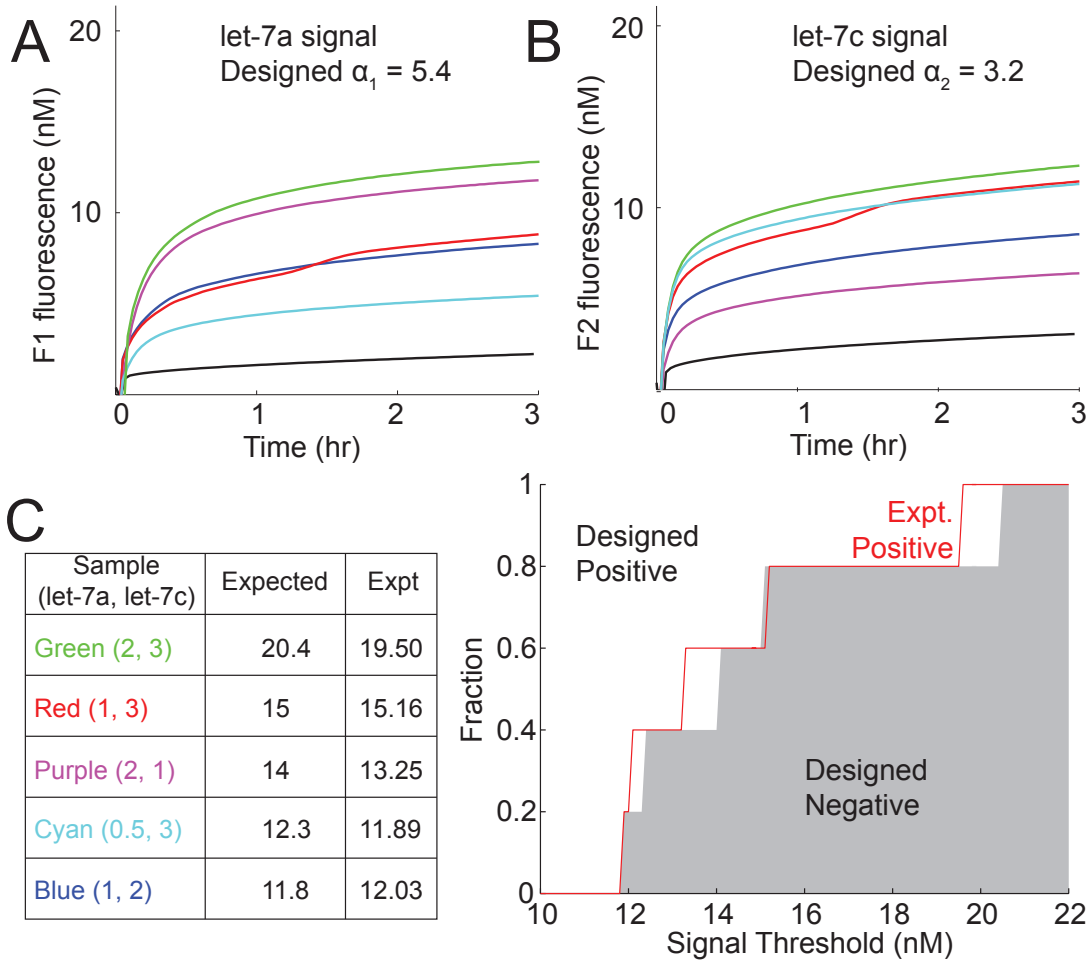

Sample (let-7a, let-7c)	Expected	Expt
Green (2, 3)	20.4	19.50
Red (1, 3)	15	15.16
Purple (2, 1)	14	13.25
Cyan (0.5, 3)	12.3	11.89
Blue (1, 2)	11.8	12.03

FIG. 5-4: Experimental demonstration of linear combination circuit. **(A)** Fixed gain amplification of let-7a with $\alpha_1 = 5.4$ and **(B)** let-7c with $\alpha_2 = 3.2$. **(C)** Summary of observed vs. expected total signal, and classification based on threshold $y_t = 14$ nM.

allow digital linear classification of a nucleic acid sample, and could enable environment-responsive circuits that release one of two different signal or effector molecules depending on the state of the system. Similar DNA circuits have been shown in function inside living organisms, albeit extracellularly in plasma [6]. The expanded capability to meaningfully and robustly sense and classify circulating RNAs in blood may lead to powerful *in vivo* sensors that detect and record abnormal gene expression profile events.

[1] G. Seelig, D. Soloveichik, D. Y. Zhang, E. Winfree, *Science* **314**, 1585 (2006).

[2] D. Y. Zhang, A. J. Turberfield, B. Yurke, E. Winfree, *Science* **318**, 1121 (2007).

[3] Qian, L. & Winfree, E. Scaling up digital circuit computation with DNA strand displacement cascades. *Science* **332**, 1196(2011).

[4] D. Y. Zhang, E. Winfree, *Nuc. Acid Res.* **38(12)** 4182(2010).

[5] G. Seelig, D. Soloveichik, E. Winfree, 107, 5393 (2010) *Proc. Nat. Acad. Sci. USA* **107(12)** 5393 (2010).

[6] Y. Amir, E.B. Ishay, D. Levner, S. Ittah, A. A. Horowitz, I. Bachelet *Nature Nanotechnology* **9**, 353 (2014).